5-2015

Unraveling Controls on Fracture Stratigraphy in Carbonates: The Influence of Regional Stress, Mechanical Properties, and Diagenesis

Matthew H. Peppers
University of Nebraska-Lincoln, matthew.peppers@huskers.unl.edu

Unraveling Controls on Fracture Stratigraphy in Carbonates: The Influence of Regional Stress, Mechanical Properties, and Diagenesis

by

Matthew H. Peppers

A THESIS

Presented to the Faculty of

The Graduate College at the University of Nebraska

In Partial Fulfillment of Requirements

For the Degree of Master of Science

Major: Earth and Atmospheric Sciences

Under the Supervision of Professor Caroline M. Burberry

Lincoln, Nebraska

May 2015

Unraveling Controls on Fracture Stratigraphy in Carbonates: The Influence of Regional Stress, Mechanical Properties, and Diagenesis

Matthew H. Peppers, M.S.

University of Nebraska, 2015

Advisor: Caroline M. Burberry

Fracture characteristics analyzed from outcrops provide key insights into the migration pathways of subsurface hydrocarbons, and allow for a detailed understanding of the tectonic history in an area. This study looks to assess the impacts that various controlling factors have on the development of fracture characteristics. To complete this objective, a succession of Ordovician to Mississippian rocks was examined. The logged section includes the Cotter Dolomite, Chattanooga Shale, St. Joe Formation, and the Boone Formation (subdivided into informal Upper and Lower members). Located in northwestern Arkansas and southwestern Missouri, data were collected from roadcut exposures along Highway 71. Collected fracture orientation data were used to determine the evolution of regional stress affecting the area of interest. Using hardness data measured from outcrops via a Schmidt Hammer, a generated mechanical stratigraphy was compared to lithology and diagenetic alteration. Photographs taken of fractures from the field were used to determine Fracture Intensity (FI) values, and used to ascertain the effect that bed thickness and mechanical property variation had on the development of FI.

Fracture orientations indicate 4 main deformation events: 1) folding of the Ordovician strata, 2) oblique compression and indentation during the Ouachita Orogeny, 3) effect of far-field stresses from Ancestral Rocky Mountain uplifts, and 4) far-field

stresses as a result of the late stage of the Alleghanian Orogeny. FI varies with mechanical contrasts, but is not constrained by bed boundaries. The mechanical stratigraphy observed in the studied succession is a direct result of lithological changes, with minor impact from diagenetic chert within some units. This work indicates that in this study area, regional stresses exert the primary control over fracture orientation, while large-scale mechanical variations control the FI. These findings contribute to the development of a suite of "best practices" for future studies by demonstrating that a thorough regional stress investigation and careful mechanical stratigraphy analysis are critical to understanding fracture development.

Dedication

This thesis is dedicated first to my parents, Nick and Laura. Throughout my academic career, you have always pushed me to achieve my best, and provided unwavering support in my decisions and endeavors. The opportunities you have afforded me in both school and in life have made me who I am today, and I hope to make you proud in my future pursuits.

My work is also dedicated to two women who have been incredible mentors to me throughout my education in the sciences. Mrs. Young, you taught me how science could be fun, exciting, and beautiful. Dr. Judge, your enthusiasm for geology was contagious, and the level of attention and care you showed when advising students was inspiring. You helped give students confidence to pursue and understand individual research, and prepared me for the rigors of graduate school.

Acknowledgements

I would like to acknowledge the various people who have contributed to make this research possible. First and foremost I thank my advisor, Dr. Caroline Burberry, for her guidance and mentorship on this project. Her knowledge, patience, and advice helped push my work to where it is. I would also like to acknowledge Dr. Chris Fielding and Dr. Tracy Frank for serving on my committee. . Lily Christman provided invaluable assistance for this project by helping to collect field data with me, and by keeping me sane and on track during this project. For their emotional support I would like to thank Tom Baldvins, Kat Chen, and Nicole Pierson, who always found ways to provide a dose of comedic relief. Lastly, I would like to thank the UNL Department of Earth and Atmospheric Sciences for their financial support, the GSA Foundation, "Graduate Student Research Grant" and the AAPG Grants-in-Aid, "J. Elmer Thomas Past-Presidents Memorial Grant" for generous contributions toward my research goals, and numerous other students in the department and in the UNL AAPG Student Chapter for their support and friendship. Thank you.

Table of Contents

List of Figure

1. Introduction

Examining and interpreting fracture patterns allows for a detailed understanding of the local tectonic history of an area. Additionally, fractures studies are critical to understanding hydrocarbon migration and preservation in tight reservoirs. Approximately 60% of the world's hydrocarbon reservoirs are carbonates, and of those, nearly 85% are naturally fractured (Lamarche et al., 2012). Detailed fracture patterns can aid in the structural interpretations of complex areas (Bellahsen et al., 2006), and outcrop-scale fractures can be used as analogs for subsurface fracture patterns (Ghosh and Mitra, 2009). Outcrop studies of fracture development are critical because most fracture networks exist at a smaller resolution than current seismic data can resolve (Lamarche et al., 2012). Interpreting regional patterns of subsurface fractures is important as they can 1) serve as primary pathways for groundwater flow (Brusseau, 1994; Caine and Tomusiak, 2003; Billi, 2005; Cooke et. al., 2006) and 2) function as pathways for hydrocarbon migration (Narr and Currie, 1982; Dholakia et al., 1998; Barbier et al., 2012).

Fracture interpretation is typically achieved by the creation of a mechanical stratigraphy (defined as the division of a rock sequence based on the mechanical properties of the layers) and a fracture stratigraphy (defined as the division of the rock sequence based on fracture characteristics, such as orientation and intensity) (Laubach et al., 2009). Because the mechanical stratigraphy of a sequence can vary between the time of deposition and the present day, the two do not always correspond, which is why it is necessary to construct each one individually before comparing the two and looking for a correlation (Laubach, et al., 2009). A fracture study is particularly useful in carbonate successions, where the mechanical properties of the rock are more likely to control

critical fracture characteristics than other structural processes such as folding or faulting (Cooke et al., 2006). These concepts will be addressed in more detail in the following section.

This research will help elucidate the tectonic history of NW Arkansas during the Mississippian and Pennsylvanian by creating a record of the multiple phases of deformation in the local area, compared to the regional framework developed by Hudson (2000) and Cox (2009). In addition, furthering the understanding of how natural fractures are developed and organized within carbonate reservoirs will promote improved reservoir characterization during hydrocarbon exploration.

To achieve the overarching goal of understanding natural fractures, this work has 3 detailed objectives: 1) Develop a mechanical stratigraphy and a fracture stratigraphy for a succession of Ordovician to Mississippian (485-330 Ma) carbonate rocks in the southern Ozark Plateau (NW Arkansas) using field observations. 2) Interpret the mechanical stratigraphy and fracture stratigraphy data to elucidate the structural and tectonic history of the field area during the Mississippian to Pennsylvanian. 3) Develop a set of best practices for creating and interpreting mechanical and fracture stratigraphies that are applicable to other carbonate sequences. To achieve these objectives, the study area (NW Arkansas, Fig. 1) was chosen based on a number of factors. First, it contains relatively good exposure of outcrops analogous to other naturally fractured carbonate reservoirs in the United States (e.g. the Mississippi Lime plays of the Mid-Continent). Second, it records a history of multiple deformation events that have been recently explored in the literature, but is not intensely thrusted. The lack of complex folding and faulting removes the influence that these features would have on the observed fractures.

2. Background

2.1 Mechanical Stratigraphy

One of the primary concepts impacting this research is the development of a "fracture stratigraphy" for a series of rocks, and the relationship that this concept has with the mechanical properties of the rocks, known as a "mechanical stratigraphy," as defined in Section 1. The concept of a mechanical stratigraphy has been noted in literature for some time. One of the primary papers to address this is by Erickson (1996), who pioneered the idea that it is possible to predict, model, and understand rock deformation if the mechanical properties of successive rock layers are known. In particular, he looked at the influence of the mechanical strengths of different rocks on the possibility of rocks either folding or faulting. This work developed three-layer models of varying rock thickness and strength, and determined that when a succession has high strength contrasts and a weak decollement layer, folding is favored over faulting (Erickson, 1996). Using outcrop-scale mechanical stratigraphies to evaluate fracture networks has been utilized successfully in a number of additional studies (Corbett et al., 1987; Morettini et al., 2005; Laubach et al., 2009). These studies have shown that fracture networks are often controlled by variations in mechanical properties at an outcrop scale, and that the outcrop analogs can be used to predict fracture patterns in the subsurface.

Mechanical controls, such as rock properties, the thickness of beds, and the interface controls between beds can all impact fracture development, intensity, and orientation (Shackleton et al., 2005; Olson et al., 2007; Laubach et al., 2009; Barbier et al., 2012). Previous work has shown that there is some stratigraphic control on fractures (Bai and Pollard, 2000; Underwood et al., 2003; Cooke et al., 2006; Wennberg et al.,

2006), and that diagenetic processes can also affect how fractures develop (Eberli et al., 2003; Morettini et al., 2005; Ahmadahdi et al., 2008; Laubach et al., 2009). Finally, as seen in Erickson (1996), mechanical layer thickness and strength can impart strong controls on how large-scale deformation develops. However, until the paper by Laubach et al. (2009), investigations into characterizing mechanical properties and characterizing fracture properties were treated as similar concepts. As Laubach et al. (2009) asserts, the two concepts are distinct and need to be treated separately and compared to gain a better understanding of deformation.

Mechanical properties are not always constant; rather, they are time-dependent characteristics that evolve from deposition to present day (Laubach et al., 2009). Thus, the mechanical properties observed today are not necessarily the same ones that existed at the time of fracture formation. Through diagenesis and burial, rocks can change mechanical characteristics (Marin et al., 1993; Dvorkin et al., 1994; Rijken et al., 2002; Shackleton et al., 2005; Laubach et al., 2009). As such, it becomes necessary to develop two separate stratigraphies when undertaking a fracture study: first is a mechanical stratigraphy, whereby the relative mechanical properties of rock units are recorded and compared, and second is a fracture stratigraphy, whereby rock units that share similar fracture attributes are identified.

During data collection and analysis, important mechanical properties to note are things such as rock hardness, rock unit thickness, and any diagenetic alteration the rock may have undergone (Underwood et al., 2003; Wennberg et al., 2006; Laubach et al., 2009). Fracture attributes of particular interest are fracture orientation, intensity (the number of fractures in a given unit area), and fracture abutting relationships and bed

boundary relationships (Barbier et al., 2012; Morretini et al., 2005; Wennberg et al., 2006).

2.2 Fracture Attributes

For the purposes of this study, a “fracture” refers to opening mode (Mode I) planar discontinuities in a rock surface (Engelder, 1982, 1987; Hancock, 1985; Pollard and Aydin, 1988; Aydin, 2000). These extension fractures form parallel to the maximum imposed stress (Hmax) or Sigma 1 (Hancock, 1985).

Collecting various fracture attribute data is helpful for a more complete understanding of subsurface fracture patterns. Different fracture attribute measurements (orientation, intensity, and abutting relationships) are of varying importance for an overall interpretation, and so deciding which attributes are most useful for a project’s overall goal is paramount. Projects focused on tectonic interpretation and reservoir characterization will place emphasis on analyzing fracture orientation data, abutting relationships, fracture intensity, and the influence of large-scale structural features.

Fracture orientation is a primary characteristic that provides a representation of a regional stress regime and its evolution throughout time (Engelder, 1987; Pollard and Aydin, 1988). When identifying fractures related to a regional or local stress regime, emphasis is placed on identifying fractures with similar preferred orientation in a systematic set (Holst and Foote, 1981; Verbeek and Grout; 1983; Warpinski and Teufel, 1989). A systematic set shares a common orientation across a wide area that represents a regional stress direction (Stearns and Friedman, 1972; Hancock and Bevan, 1987). Systematic fracture sets propagate parallel to the direction of maximum compressive stress, or perpendicular to the maximum tensile stress (assuming excess fluid pressure

does not drive fracturing) (Pollard and Segall, 1987; Pollard and Aydin, 1988). Additionally, fracture orientation also plays a role in reservoir characterization. A major concern in recovering hydrocarbons from carbonate reservoirs is the efficient use of natural fractures (Barbier et al., 2012). Horizontal drilling (commonly undertaken in tight and unconventional reservoirs) is enhanced by utilizing the existing fracture networks, by drilling perpendicular to the strike direction of the planes, so as to intersect as many as possible (Engelder et al., 2009). This is particularly critical in carbonate reservoirs, in which fractures are an important contributor to reservoir porosity and permeability (Lucia, 1995).

Fracture relationships to bed boundary surfaces are also important for determining regional deformational history and potential hydrocarbon movement. Fracture sets can be characterized based on their relationships to bed boundaries when observed in outcrops (Hooker et al., 2013). This also aids in the prediction of how different fracture sets will behave in the subsurface (Hooker et al., 2013).

Abutting and crosscutting relationships between fractures allow the determination of relative age of distinct fracture sets. This is a key practice in evaluating successive and overlapping deformation events, as shown in the schematic example in Fig. 2. The referenced figure shows two hypothetical tectonic compression events, with the arrows showing the direction of compression. The older event (red) created a series of systematic fractures across the representative rock. The younger set (blue) is a less systematic set that abuts against the existing fracture set. Younger fractures cannot propagate across an open existing fracture, so this relationship is only available when the fracture sets are

open. If the older set was filled when the younger set began to form, the younger set would cross-cut the existing fractures.

When looking to relate this study to hydrocarbon recovery and reservoir characterization, fracture spacing and intensity are important attributes. Fracture spacing and intensity are essentially inverse values: fracture spacing records the space between individual fractures, while fracture intensity (FI) records the number of fractures within a given area, generally per linear meter (Corbett et al., 1987; Wennberg et al., 2006). FI can be determined for an entire fracture population, or for individual fracture sets (Wennberg et al., 2006). These attributes are commonly collected via a scan line across an outcrop exposure (Wennberg et al., 2006), but can also be collected from photographs of the outcrop in cross-section as demonstrated in Section 4. However, because the scan line is only oriented in one direction, there are some sampling biases for this method relative to fracture orientation. The best option is to attempt to choose a scan line perpendicular to the most dominant sets, but the directional bias can be corrected on a fracture-by-fracture basis (Wennberg et al., 2006), or by integrating photographs of the cross-sectional and plan view (bedding plane) exposures. FI is a common attribute used for fracture density prediction because it is possible to identify a relationship between it and various other factors specific to carbonates. FI is generally primarily controlled by either bed thickness or mechanical unit thickness (Ladeira and Price, 1981; Narr and Suppe, 1991; Gross and Engelder, 1995; Pascal et al, 1997; Bai and Pollard, 2000). In carbonates, it also is affected by texture (Dunham, 1962), dolomite cement content, facies distribution, and other sedimentary features (Nelson, 1985; Wennberg et al., 2006). As found in the papers cited, FI generally increases (spacing decreases) in thinner layers, and increases (spacing

decreases) in thicker layers. Opening mode fractures are often confined by bed boundaries with spacing proportional to the layer thickness (Bai et al., 2000). This control on spacing is driven by the "stress shadow" that develops around existing fractures (Bai et al., 2000). A stress shadow is formed when tensile stress within a rock is reduced around existing fractures, and so prevents the formation of additional extensional fractures in the near vicinity (Gross et al., 1995; Bai et al., 2000). The lateral extent of this stress shadow is proportional to the height of the fracture, which is often controlled by bed thickness (Gross et al., 1995).

2.3 The Effects of Multiple Deformation Events

Groups of planes of weakness (referred to as fractures or faults) act as records of tectonic events that have impacted an area throughout time. Particularly in highly deformed areas or in older rocks, multiple sets of faults and fractures can exist with varying orientation, as a result of different tectonic events and stresses affecting the area throughout geologic history (Nieto-Samiengo and Alvarez, 1997). A challenging and critical task is differentiating the physical representations of the individual deformation events.

There are four major possibilities that result in multiple overprinted fault/fracture patterns: 1) one or more discreet deformation events with changes in the orientation of maximum stress; 2) the reactivation of pre-existing planes of weaknesses; 3) a three-dimensional strain event following a "slip model" (forming an orthorhombic four-fault pattern and two slickenline sets in a single strain event); or 4) multiple events that follow a model wherein faults interact in a hypothetical block (Nieto-Samaniego and Alaniz-Alvarez, 1997). In the case of this study area, the first possibility (one or more discreet

events with changes in the orientation of maximum stress) is believed to be the dominant mode of deformation based on previous literature (Hudson, 2002; Cox, 2009). This allows the use of abutting relationships to distinguish the age relationships of the fractures related to the various tectonic events (known as tectonic fractures). Tectonic fractures are discussed more in Section 2.4.

2.4 Tectonic Fractures vs Unroofing Fractures

A critical component of a fracture study like this is distinguishing between fractures that are tectonic in origin and those that are a product of unroofing, that is, fractures created during strain release as overlying layers of rocks are removed during erosion, also known as neotectonic joints (Hancock and Engelder, 1989). Tectonic fractures are typically systematic in nature, and can be grouped by distinct patterns in orientation (Engelder, 1987; Pollard and Aydin, 1988). They are planar features, roughly parallel to each other, and are usually horizontally and vertically through-going (are not constrained by bed boundaries) (Bellahsen et al., 2006). Unroofing fractures are formed primarily near the surface of the uplifted rocks, and are formed when the compressive stress is released along pre-existing weaknesses, or perpendicular to the regional direction of tectonic compression, generally resulting in uniform orientation distributions (Davis et al., 2012). A final concern is identifying fractures of human origin (such as blasting zones in road-cuts). These fractures are found directly around the preserved drill hole traces in outcrops, in a radial pattern, and may be confused with the pre-existing natural fractures in the rock.

3. Geologic Setting

3.1 Regional Tectonics of the Ozark Plateau

The field area is located in the Ozark Plateau of northwestern Arkansas and southwestern Missouri. The area is a topographic high, with road-cut exposures along Highway 71 north of Bentonville, AR (Fig. 1). The most active part of the tectonic history of this study area is during the Late Paleozoic in the Pennsylvanian, between 330-300 Ma (Hale-Erlich and Coleman, 1993; Hudson, 2000). Some studies detail uplift of the Ozark Plateau as early as the Devonian (e.g. Koenig, 1967; Cox, 2009) perhaps related to the Taconic and Acadian orogenies (roughly 450-375 Ma), but the most significant uplift occurred as a result of the Ouachita, Alleghanian, and Ancestral Rocky Mountain (ARM) orogenies in the Pennsylvanian (Cox, 2009).

The Ozark Plateau has remained a relative structural high throughout the entire sedimentation of the midcontinent (Cox, 2009). Theories as to the formation of the Ozark Plateau primarily cite flexure of the Laurentian plate in response to thrust loading during the Ouachita and Alleghanian Orogenies (Cox, 2009). In this model, the Ozark Plateau is thought to be the location of the forebulge related to these orogenies.

Previous work has used the characterization of large-scale features within the Ozark Plateau to gain a better understanding of the multiple phases of tectonic deformation (Cox, 2009). In general, mesoscale structures such as faults and folds indicate 4 main tectonic events (Fig. 3) that affected the Ozark Plateau as a whole during the Paleozoic (Cox, 2009). Deformation in the Early Mississippian (Fig. 3a) records the oblique movement of the Ouachita microplate after its initial collision with the North American craton, generating NW-directed compression that is expressed as northwest

trending fractures (Cox, 2009). During the Late Mississippian (Fig. 3b), the dominant orientation of fractures in the southern Ozark Plateau was north to northwest, and was created as the Ouachita microplate began to indent into the North American continent (Cox, 2009). Thrust sheet loading in the hinterland and indentation of the Ouachita microplate into the continental land mass resulted in outer arc extension across the forebulge, generating normal faults oriented approximately west (Cox, 2009). Early Pennsylvanian deformation (Fig. 3c) then caused dominantly reverse faults oriented northwest across the Ozark Plateau (Cox, 2009). This change was potentially due to the compression related to the Ancestral Rocky Mountain Orogeny in the late Paleozoic (Cox, 2009). The final deformation event (Fig. 3d) demonstrated a return to northwest trending fractures that are concentrated mostly in the northern and eastern parts of the Ozark Plateau (Cox, 2009). This was most likely related to northwest compression along the Alleghanian front, located to the southeast of the study area (Cox, 2009). These tectonic events are also shown in the tectonostratigraphic column below (Fig. 4). This figure also details the stratigraphic succession (Section 3.4.1), and the depositional environment of the studied rocks according to previous literature within the area of interest (3.4.2).

3.2 Detailed Tectonics of the Study Area

Recent work (Hudson, 2000) has confirmed that the tectonic setting in NW Arkansas is a complex system (Fig. 5), and not a simple south-dipping homocline, as has been previously reported (Croneis, 1930). In general, the southern edge of the Ozark Plateau (NW Arkansas) is currently known to show a combination of normal faults, oblique reverse faults, and monoclinal folds that accommodated north-south extension

and east-west shortening that may be related to the flexure of the Ouachita Orogeny foreland (Hudson, 2000).

Figure 6 is modified from Cox (2009) to show the inferred Hmax (horizontal maximum stress direction) in the study area. Deformation Event 1 was E-W to NW-SE directed shortening that is variable across the local study area in response to oblique compression during the Ouachita Orogeny (Fig. 3a). Deformation Event 2 was strongly NNW directed, and may be related to the indentation of the Ouachita microplate (Hudson, 2002) (Fig. 3b). Event 3 was a NE-SW to ENE-WSW directed shortening, recorded by prominent jointing (Gibbons, 1962) and calcite twinning (Chinn and Konig, 1973) that may be related to the ARM deformation described by Cox (2009) (Fig. 3c). The final Event 4 was a return to E-W directed deformation, likely tied to Alleghanian deformation (Fig. 3d).

3.3 Stratigraphy

In the Ozark Plateau of NW Arkansas, the strata are Ordovician to Pennsylvanian in age (Fig. 7), and generally dip gently to the south (McFarland, 2004). The exposed rocks are the product of marine depositional environments, and show multiple unconformities due to changes in sea level throughout the Paleozoic (McFarland, 2004). Stratigraphic terms for the Lower Mississippian units are variable across state lines, as shown in Fig. 8 from Manger et al. (1988). The logged section includes the Cotter Dolomite, Chattanooga Shale, St. Joe Formation, and the Boone Formation (subdivided into informal Upper and Lower members). The terms used in this study (the St. Joe Formation, and the subdivision of the Boone Formation into informal Upper and Lower untis) are the ones utilized in studies of Arkansas stratigraphy.

Within the stratigraphic sequence, the Devonian Chattanooga Shale likely acts as a regional detachment surface during deformation. A more local detachment may separate the brittle Mississippian units studied here from the underlying Devonian ductile unit.

Precambrian aged rocks in the midcontinent region are largely buried far beneath Phanerozoic sedimentary layers, and so geophysical analyses or samples from deep drilling are the only key to the nature of the basement complexes (Bickford et al., 1986). What little data are available suggests that the basement of NW Arkansas is granite-rhyolite that is around 1340-1400 Ma, using U-Pb Zircon dating (Bickford et al., 1986).

3.3.1 Lithological Descriptions

Formations within the scope of this study are described below. Lithological descriptions from various literature sources (Sullivan and Boss, 2002; Hudson and Cox, 2003; McFarland, 2004; Dowell et al., 2005; Chandler and Ausbrooks, 2010) are supplemented by field observations and data collected for this study.

<u>*Cotter Dolomite*</u> (Early Ordovician – 485-470 Ma)

> The Cotter Dolomite consists of a massive medium-grained dolostone that is light tan, but turns to dark grey when weathered. There are local beds of shale, with an abundance of chert. Rare fossils are found in the formation, including gastropods, cephalopods, and some algae. The lower contact of this unit is not exposed in Arkansas. The thickness of this formation is thought to be between 340 and 500 feet.

Clifty Formation (Middle Devonian Period – 395-385 Ma)

The Clifty Formation was first described as sandy limestone at its type location at Little Clifty Creek in Carroll County, but other localities have shown it to be sandstone. It is not exposed in northwestern Arkansas or southwestern Missouri, thus was not observed in this study. The thickness of the Clifty Formation is usually around 4 feet, but can be thinner in some areas.

Chattanooga Shale (Late Devonian – 384-360 Ma)

The Chattanooga Shale is a black shale that is prominently jointed. The lower member of the unit, the Sylamore Sandstone Member, dominates the Chattanooga Shale in some areas. The Sylamore Sandstone Member is fine-grained grayish-white phosophatic quartz sandstone. In places where it does not occur, the upper part of the Chattanooga Shale is slightly sandy and has abundant pyrite formation. The Chattanooga Shale has been shown to preserve conodonts and brachiopods, and ranges in thickness from 0 to 85 feet, including the Sylamore Sandstone Member.

St. Joe Limestone (Early Mississippian – 358-346 Ma)

The St. Joe Limestone is fine-grained, crinoidal, and generally lacks chert nodules. It is a fossiliferous unit, and crinoids, brachiopods, bryozoans, conodonts, blastoids, ostracods, and rugose corals have all been recovered from the St. Joe. The base of the unit is considered disconformable on the Chattanooga Shale by most workers, and its thickness ranges from 0 to 110 feet.

Boone Formation (Early and Middle Mississippian – 358-330 Ma)

The Boone Formation is the most prominently exposed unit in much of NW Arkansas. It is a gray, fine to coarse grained, fossiliferous limestone. It is interbedded with chert, and displays karstic dissolution features. There are a variety of fossils contained within the Boone Formation, but crinoids are by far the most abundant. The lower contact of the unit is generally conformable with the St. Joe Formation. The thickness is typically 300 to 350 feet, but can be as much as 390 feet in some locations. The Boone Formation is informally divided into Upper and Lower Units, generally separated just before the occurrence of a zone of tripolitic chert within the rock.

3.3.2 Depositional Environments

The Cotter Dolomite, although relatively understudied, is thought to have been deposited in intertidal and supratidal settings (Young et al., 1972; Ethington et al., 2012). In the area of interest, the Cotter Dolomite is unconformably overlain by the Chattanooga Shale, which was deposited in a deep marine basin. The Mississippian carbonate rocks were deposited within a shallow marine shelf slope/margin setting as a broad carbonate platform, known as the Burlington Shelf (Gutschick and Sandberg, 1983). The abundance of crinoid fossils (Fig. 9) in the units of interest indicates that the depositional setting is concentrated in the upper slope of the marine shelf (Lane and DeKeyser, 1980). This is also supported by a regional mid-continent paleo-depositional map (Fig. 10), which shows that the study area falls close to the boundary between the shelf margin and the main shallow shelf environment. Deposition in the shelf margin area occurred in a high-energy environment, with depositional dips of approximately 1-5° (Gutschick and

Sandberg, 1983). The Burlington Shelf is classified as a passive shelf margin, prior to the onset of the Ouachita Orogeny and represents prograding carbonate material (Gutschick and Sandberg, 1986).

4. Methods

Field data were collected from 17 outcrop locations along Highway 71 in Arkansas and Missouri (Fig 11). First, 33 oriented hand samples were collected from key lithologies throughout the sequence, and were characterized using the Dunham classification scheme (Dunham, 1962). The collected samples were then made into thin sections for further petrographic analysis. Using an Olympus BH-2 microscope and camera and a Nikon Eclipse Ci microscope with a Nikon Y-TV55 camera, the thin sections were observed under PPL and XPL light, and then half of the slide was stained using Alizarin Red S and Potassium Ferricyanide in order to better identify the carbonate minerals present. The Alizarin Red S stains calcium carbonate red, while the Potassium Ferricyanide allows for the identification of Fe-poor calcite (red-pink), Fe-rich dolomite/siderite (blue), dolomite (no stain), and Fe-rich calcite (purple). Once stained, the thin sections were observed under cathololuminescence using a CITL (Cambridge Image Technology Ltd.) Cathodoluminescence Mk5-2 Instrument, in order to qualitatively assess the diagenesis of the rocks (Boggs and Krinsley, 2006). The presence of manganese-enriched calcite (shown by stimulated luminescence) generally indicates reducing conditions associated with early to intermediate stages of diagenesis (Scholle and Ulmer-Scholle, 2003). A nonluminescent response usually occurs in oxidizing environments, and dull response occurs where there is a lower Mn/Fe ratio that formed during intermediate to late diagenesis with the addition of Fe (Scholle and Ulmer-

Scholle, 2003). Using the lithological and diagenetic observations, a full lithological description and stratigraphic column was generated for the studied succession.

A structural cross section was generated from NNW to SSE along Highway 71 through the study area (A-A' in Fig. 11). Outcrop lithology and bedding dips were used to identify major structures in the area, and the interpretation made in this study was compared to other structural cross-sections generated throughout NW Arkansas (Croneis, 1930). The generated cross-section was used to identify places where local modification of the stress field (i.e. around faults or folds) might have overridden the more regional tectonic stresses and affected the fracture systems formed.

731 fracture orientation measurements (Appendix A) were collected using a Brunton compass, along with information on abutting relationships between fracture sets and fracture fill characteristics. Photographs of the outcrops were taken in order to determine fracture spacing and intensity relationships, as well as the relationship of fractures to mechanical and lithological boundaries. The measured fractures were plotted onto stereonet diagrams using OSXStereonet 3.4 (Allemdinger et al., 2012) and separated by their outcrop and stratigraphic level (full stereonet suite shown in Appendix B). These stereonets allowed the identification of discrete fracture sets by orientation, and could be used to link the present fracture sets to known regional or local tectonic events. In areas where there were known structural features (i.e. folds or faults), fractures were rotated to account for changes in orientation. The fracture data were used to construct a fracture stratigraphy through the sequence, where zones of similar fracture properties were grouped based on shared characteristics.

Finally, a Proceq SilverSchmidt Type N Hammer® was utilized to collect mechanical hardness data from major rock beds in the exposed outcrops. The hammer measures the rebound velocity value (Q) of the rock interface, and is used in accordance with ASTM D5873 for use of the Schmidt Hammer when testing rock hardness.

The typical value for measuring hardness is the R (rebound) value. However, this measurement is affected by friction of the measuring tools and by gravity. The Q value is achieved by measuring the velocity of impact and rebound immediately before and after the impact occurs, resulting in the physical rebound coefficient. This measurement is essentially free of the errors associated with the traditional R value (calculated by Proceq). For this research, a series of 10 measurements was collected per bed (full measurement suite shown in Appendix C). In places where bed thickness permitted, multiple measurement series were taken, and averaged together. The mean value of these rebound measurements was calculated, as was the standard deviation. This provides a representation of the general mechanical strength of the measured rock bed.

A fracture stratigraphy was developed based on the measured orientation and intensity data, in order to characterize the fracture attributes throughout the measured sequence. The mechanical data were compiled, and a mechanical stratigraphy was then developed for the sequence. Q values were used to identify areas of relatively competent beds and relatively incompetent beds. Q values were then compared to lithological variations throughout the sequence, as well as diagenetic alteration, in order to establish whether those factors have impacted the mechanical stratigraphy. The established fracture stratigraphy was then compared to the created mechanical stratigraphy, to identify whether the mechanical units exhibited any relationship to the fractures within

the studied sequence. Additionally, the fracture orientation data were used to interpret any tectonic events that have affected the region, in order to gain a more thorough understanding of the tectonic history experienced by the study area.

5. Results

5.1 Lithology and Diagenesis

Field observations, hand sample characterization, and thin section analysis allowed for the creation of a detailed stratigraphic column for the study area (Fig. 12). The column was compared to literature descriptions of the region to confirm accuracy. The logged section includes the Cotter Dolomite, Chattanooga Shale, St. Joe Formation, and the Boone Formation (subdivided into informal Upper and Lower members) (Sullivan and Boss, 2002; Hudson and Cox, 2003; McFarland, 2004; Dowell et al., 2005; Chandler and Ausbrooks, 2010). Within the stratigraphic succession, petrographic work identified 6 major lithologies present. A medium-grained dolostone (Fig.13a) makes up the Cotter Dolomite at the base of the measured section. The Chattanooga Shale is a thick layer of black shale that includes minor amounts of pyrite. The St. Joe Formation is dominantly a crinoidal packstone/grainstone (Fig. 13b), which passes into the bioclastic wackestones (Fig. 13c) and bioclastic packstones (Fig. 13d) of the Lower Boone Formation. Within the St. Joe and Lower Boone Formations, there are also rare intervals of mudstone/wackestone (Fig. 13e) that separate the more competent lithologies. The Upper Boone Formation is primarily composed of crinoidal packstones similar to those in the St. Joe Formation (Fig. 13b) as well as more bioclastic packstones and grainstones (Fig. 13f).

Cathodoluminescence investigation indicates that multiple phases of diagenesis have affected this succession, beginning with the dolomitization of the Cotter Dolomite (Fig. 14a). Additionally, some samples in the upper part of the sequence (Fig. 14b/14c) show a luminescent response that likely shows a period of diagenesis resulting from the infiltration of meteoric water during subaerial exposure.

However, in the Mississippian carbonates, diagenesis is dominated by chert formation. Chert nodules are commonly found throughout the sequence within the studied Formations. This suggests that a silica-rich fluid infiltrated along bedding planes, and allowed the formation of the nodules to begin around asperities and heterogeneities within the rock, such as fossil fragments (Fig. 15a; Maliva and Siever, 1989). Chert nodules are the most prevalent in the Lower Boone and Upper Boone Formations, but are also present in rare instances in the upper portion of the St. Joe Formation and within the Cotter Dolomite. In addition to the development of chert nodules, some intervals contain chert that is not localized into nodules (Fig. 15b), and a significant interval within the Upper Boone Formation is composed of tripolitic chert (Fig. 15c). In this interval, the silica is pervasive, as most of the original carbonate material has dissolved away, leaving only the pre-existing silicic material. This chert interval has been subsequently weathered, suggesting some period of subaerial exposure (Mazzullo and Wilhite, 2010). Potential sources of silica for this chert are sponge spicules, volcanic ash, and pre-existing silica-rich rocks, although the last origin is unlikely, as these would be quartz instead of amorphous SiO_2 (Rogers, 2001). While previous literature investigations of Mississippian tripolitic chert in Kansas and Oklahoma resulted in the identification of spicule-rich rocks (suggesting the chert is derived from that source), the tripolitic chert

found in southwestern Missouri and northwestern Arkansas (this study area) is generally spicule-poor (Mazzullo and Wilhite, 2010).

Many of the observed bed boundaries are heavily stylolitized (Fig. 15d), as deposition of further carbonate material and subsidence caused pressure dissolution (Bathurst, 1987). Lastly, the entire succession is capped by a heavily oxidized regolith (Fig. 15e) that is poorly documented across northwestern Arkansas.

5.2 Cross-Section

As seen in the cross section (Fig. 16), most of the study area is relatively undeformed. Near site 006, however, measured dips and existing literature (e.g. Evans et al., 2013) indicate that there is a fault-related fold in the Formations underneath the Chattanooga Shale unconformity. This structure has uplifted the Cotter Dolomite directly beneath the Chattanooga Shale, and has slightly displaced the overlying formations, creating subtle dips and very minor folding to the north and south of the feature. Previous work indicates that large structural features (such as faults and folds) impart a strong control on the development of nearby fractures (Harris et al., 1960; Friedman, 1969; Engelder et al., 1997; Peacock, 2001; Hennings et al., 2007). As such, the presence of this fold in the Cotter Dolomite necessitated that fracture measurements taken from all locations nearby were rotated to account for the bedding dip and minor folding observed. Fractures that return to vertical when rotated to account for dip are formed prior to the development of structural folding.

5.3 Fracture Orientations

From the fracture orientation measurements, 4 distinct fracture sets were identified (Fig. 17a). This was accomplished by comparing all fracture measurements

from individual locations to one another, as well as by analyzing all fracture orientations plotted together on a single rose diagram (Fig. 17b). Figure 17b also allowed for the determination of major regional fracture orientations that were the most prevalent across all studied outcrops. Set 1 strikes approximately N-S and is one of the dominant regional sets from Figure 17b; Set 2 is slightly variable E-W and is the second regional set from Figure 17b; Set 3 strikes NE-SW, and Set 4 is variable to the NW-SE.

Fracture orientation variations throughout the studied sequence are shown in Fig. 18. Set 1 is dominant in the Cotter Dolomite, with only a minor representation of Set 2. Fractures here are not constrained by bed boundaries, and show no fill. Set 2 is then dominant throughout the Chattanooga Shale and the St. Joe Formation, with Set 1 as a minor component. However, abutting relationships show that while Set 1 is older than Set 2 in the Cotter Dolomite, the relationship is reversed in the Chattanooga Shale and St. Joe Formation, with Set 2 being the oldest and Set 1 being younger (Fig. 18). Set 1 is confined to individual bed boundaries in the upper part of the St. Joe Formation, and no fractures have fill. Transitioning into the Lower Boone Formation, fracture Sets 3 and 4 are present in the first part of the formation (with Set 4 cutting across all bed boundaries and showing some calcite fill), but further up the sequence fracture Sets 2 and 4 are present (Fig. 18). The base of the Upper Boone Formation sees the return of Set 1 again, along with increased variability in orientation. The Upper Boone Formation contains Sets 1, 2, 3, and 4, but Sets 1, 3, and 4 appear the most often (Fig. 18). Fractures are generally not constrained by bed boundaries, and numerous fractures show some degree of fill.

The variation within the Lower Boone Formation may be due to subtle changes in lithology up the Lower Boone Formation. The variable nature of the fractures within the

Upper Boone Formation is likely a result of the increased asperities noted in this section. Crinoids and other fossil fragments heavily dominate lithology in the Upper Boone Formation, presenting an increased number of nucleation points for fracture generation, and causing deviations in the pathway of fracture generation (Van de Steen et al., 2002).

The observed fracture orientations show different phases of tectonic deformation affecting the area, as demonstrated by the examples in Fig. 18, and represent a distinct large-scale fracture stratigraphy. Fracture sets are generally consistent within a given major unit of the studied sequence. All identified sets are systematic or near systematic, and so likely represent regional tectonic forces. The change in systematic fracture orientation throughout the sequence can be observed and tracked, allowing an interpretation of how the regional tectonic forces impacting the area vary throughout time. This will be addressed in more detail in Section 6.1.

5.4 Fracture Intensity

Fracture Intensity (FI) values (fractures/linear meter) were calculated for selected outcrops within the sequence. Outcrops were chosen for their clear exposure and the lack of any blasting fractures. Differentiating blasting fractures from tectonic fractures, while relatively easy in the field, proved more difficult when using photographs. The presence of blasting zones presented a greater challenge in obtaining correct fracture measurements. Because of this constraint, only a few outcrops were deemed appropriate for use in the measurement of FI. The FI values measured from outcrop photographs were plotted against bed thickness and labeled by outcrop (Fig. 19). The outcrops also represent different lithologies. The data indicate that FI does not show a relationship to the thickness of the bed it was measured from, regardless of outcrop location. From all

data, most of the beds measured are less than 1 meter in height, but FI varies from 1.2 to 8 in that interval.

To further examine the controls on FI, fracture intensity was qualitatively compared to varying lithology and mechanical contrasts. FI values did not exhibit much change across boundaries of similar mechanical contrast or across boundaries of similar lithologies. However, as seen in the annotated photo (Fig. 20), where a significant contrast in mechanical property or lithology was encountered, FI changed. In the example shown in Figure 20, FI is higher in the softer mudstone/wackestone and much lower in the more competent crinoidal packstone/grainstone.

If bed thickness was the controlling factor for FI in this instance, the intensity would be higher in the thin crinoidal packstone/grainstone, and lower in the thicker mudstone/wackestone. Although one result from this study (a higher FI is obtained from a softer lithology) is similar to that described by Barbier et al. (2012), which also noted higher FI in softer lithologies, there are several key differences. Barbier et al. (2012) indicated a higher FI in dolomite than in carbonate, which is not seen in this succession. Additionally, that study noted that bed boundaries often defined mechanical units, and that there was no straightforward relationship between mechanical unit thickness and FI. Lastly, the investigations of Barbier et al. (2012) were in an area with strong structural control on fracture development, while the area in this study is relatively undeformed. In this succession, the more competent lithologies act as large-scale mechanical units, as bed boundaries do not provide enough contrast to partition it into smaller mechanical units. The less competent lithology, however, is a smaller separate mechanical unity, and so has

a higher FI when compared to the more competent unit. Thus, the mechanical behavior can override bed thickness controls when examining FI.

5.5 Mechanical Stratigraphy

Q values obtained from the Schmidt Hammer were used to make a mechanical stratigraphy for the sequence (Fig. 21). Most of the Q values obtained were confined to the 40-60 range, with some measurements in the 10-30 range, and only 3 values in the 60+ plus range.

The mechanical stratigraphy was then compared to a lithological interpretation of the sequence (Fig. 22). The lower range Q values coincide with the softer shales and mudstones within the succession. Overall, the values within the larger dolomite and carbonate sequences show little systematic variation. However, when comparing subtle changes in lithology (such as wackestone to packstone to grainstone), the Q values show a slight difference, with the more competent grainstones having marginally higher Q values than the less competent wackestones as shown in Fig. 22.

The observed relationship between the mechanical stratigraphy and lithology demonstrate that the mechanical stratigraphy of this sequence is fundamentally related to the large-scale contrasts between the softer lithologies and the much more competent lithologies. The lack of any noticeable trend within the competent limestones and dolostones demonstrates that variation in texture or diagenetic alteration is not significant enough to enhance or weaken the inherent mechanical properties of carbonate units, with the exception of the tripolite unit. Dissolution of the carbonate material in the tripolitic unit has left a significant and extensive layer of chert. Development of chert nodules and recrystallization of the carbonate cement was neither pervasive nor dramatic enough to

enhance or impact major differences in the properties of the carbonate units. Overall, the mechanical stratigraphy observed shows only very subtle variation throughout the sequence, and that alteration can largely be correlated with changes in lithology. This suggests that the mechanical stratigraphy is the sum of all diagenetic processes on the succession, occurring early in the lithification process, and pre-dating fracture formation. The mechanical stratigraphy generally mimicking the measured lithological succession is a similar result to other work, including Ferrill et al. (2014). A key difference between this work and that of Ferrill et al. (2014) is that this work looked at less substantial lithological contrasts, indicating that carbonate lithologies vary on a fine scale in terms of mechanical strength, and that even subtle changes in mechanical strength can affect fracture intensity.

6. Interpretation of Mechanical and Fracture Stratigraphy

Based on the results of this study, a mechanical stratigraphy and a fracture stratigraphy were developed for the sequence of Ordovician-Mississippian carbonates in NW Arkansas. The fracture stratigraphy primarily utilizes fracture orientation directions to establish a comprehensive characterization of the sequence. Fracture orientations show a distinct evolution throughout the measured sequence, shown in Figure 18, and described below. The observed sets are systematic, generally are not constrained by bed boundaries, and show preferred orientation, indicating that they are a result of tectonic deformation (Engelder, 1987; Pollard and Aydin, 1988). Because of this, they provide a record of the multiple deformation events that have impacted the study area post-deposition. The Cotter Dolomite records the first deformation event affecting the study area (Fig.18). The N-S striking Set 1 that dominates this Formation is likely a result of

the fault-related folding undergone by this Formation. Previous literature indicates that the N-S trending fold apex underlies the study area in this investigation (Evans et al., 2013). Structural control on fracture pattern development indicates that dominant fracture orientation would be parallel to the trend of the fold apex, resulting in the N-S striking fracture sets observed. The younger Set 2 fractures in the Cotter Dolomite record the beginning of the second phase of deformation seen in the Chattanooga Shale and the St. Joe Formation (Fig.18). This second phase of deformation records primarily N-S forebulge outerarc extension and slight E-W compression expressed as the Set 2 fractures in these formations, accompanied by the re-emergence of a younger N-S striking set of Set 1 fractures. This shift in deformation direction from E-W to N-S is likely related to the Events 1 and 2 (Fig. 3 & Fig. 4). The oblique movement of the indentor during the Ouachita orogeny records shifting compression directions in the study area from E-W to NNW-SSE (Fig. 6a/6b). The fracture sets in the Lower Boone Formation record the third phase of deformation in the study area. Set 3 records the NE-SW compression of the Ancestral Rocky Mountain (ARM) uplift detailed in Event 3 (Fig. 3 & Fig. 4) while Set 4 likely results from the re-activation of underlying shear zones (seen in Fig. 6 as faint gray lines). The NW-SE fractures of Set 4 are the surface expression of the shear zone activity during this time period. The fracture sets observed in the Lower Boone Formation appear to change from Set 3 and Set 4 in the bottom of the interval to Set 2 and Set 4 toward the top. This apparent change in orientation may record shifting tectonic forces during the ARM uplift and shear zone reactivation, or it may record the influence of differing mechanical contrasts and changes in granular structure (along with increased asperities), causing the fracture orientation to deflect as they move into slightly more heterogeneous

strata (Van de Steen et al., 2002). The final phase of deformation in this area is recorded in the Upper Boone Formation by a return of Set 1 and Set 2, with minor complements of Set 4. This interval houses a much more diverse suite of fracture orientations than the lower units. This may have been the result of shifting forces from the Appalachian orogeny to the southeast of the study area, but is also likely enhanced by the numerous asperities in this interval that provide nucleation points for additional tectonic fractures and for unroofing fractures. As a whole, this sequence has been subjected to a number of far-field stresses from various orogenic events throughout the Mississippian and Pennsylvanian that have defined the fracture stratigraphy. Fracture intensity values show no relationship to the bed thicknesses measured, suggesting a different control on their patterns. In the case of this study, FI is altered by major interface changes in lithology and mechanical contrast (i.e. between mudstone and packstone).

The mechanical stratigraphy was created using hardness rebound (Q) values obtained from the outcrop examples within this sequence. Q values were primarily concentrated in the 40-60 range, with few values in the 0-30 range, and even fewer in the 60+ range, indicating no major variations in mechanical properties throughout the succession. Based on the results obtained, the mechanical stratigraphy is heavily dependent on lithology. Units of similar lithologies (crinoidal packstones/wackestones) behave as one mechanical unit, while less competent lithologies (mudstones and shales) behave as different units. This is especially apparent in Fig. 22, which shows how the Q values vary with high lithological contrast, but show very little variation between small changes in lithology. Diagenesis, which can exert an influence on mechanical stratigraphy (Wennberg et al., 2012), has a mixed effect on this sequence. The

development of chert nodules within the bedding planes is not pervasive enough to have any noticeable impact on the mechanical strengths of the observed units. The development of carbonate cement related to the diagenesis from meteoric water is also not significant enough to impact mechanical strength, as it presents similar mechanical properties to the original carbonate material it has surrounded. However, the tripolitic chert unit does show that diagenesis can impact a mechanical stratigraphy when it occurs on a large enough scale. The near complete replacement of an entire interval of carbonate material with chert that has been significantly weathered by meteoric fluids to develop large amounts of porosity was enough to bring the Q value down into the lower ranges (Fig.22). Additionally, layers of significant chert that have not been altered plot toward the higher end of the scale of Q values, as seen in Fig. 22, Layer 3a.

The development and comparison of the mechanical and fracture stratigraphies has accomplished Objectives 1 and 2 of this study. When comparing the fracture stratigraphy to the mechanical stratigraphy, it becomes apparent that there is no strong relationship between fracture orientation and mechanical properties (Fig. 23). Orientations within the 4 fracture units were consistent, regardless of mechanical variation, and numerous fracture sets were not generally constrained by bed boundaries. A potential exception occurs in the Lower Boone Formation, where orientation data shows slight variation up-section. However, this could also be related to the lithological variations as the interval becomes more fossiliferous upward. The reason for the lack of mechanical control on fracture orientation may be because the mechanical contrasts are not significant enough to impact fracture characteristics that are controlled by large-scale tectonic forces. The Q values measured from the succession are similar among the

carbonate lithologies, and are only significantly variable across strong lithological contrasts, such as shales to limestones. Instead, fracture orientation is dominantly a product of the multiple phases of tectonic deformation that have impacted the area, as represented throughout the different aged units in the sequence.

FI values, however, appear to be influenced by the developed mechanical stratigraphy. Bed thickness showed no relationship to measured FI values, but contrasts in mechanical and lithological properties did show a control on the measurement, similar to the findings in previous cited literature. This indicates that the mechanical stratigraphy influences fracture intensity in this study area. The relationship between FI and mechanical layers indicates that the present-day mechanical stratigraphy was the same one that existed when fracture formation began (Laubach et al., 2009).

Finally, the mechanical stratigraphy is the sum of all diagenetic processes on the succession, occurring early in the lithification process, and pre-dating fracture formation. This indicates that in the studied area, diagenesis does not exert a significant control on the fracture stratigraphy.

7. Impact of This Study and Future Work

This study underscores the findings of previous literature, which necessitate the separate treatment of fracture and mechanical stratigraphies when a fracture study is undertaken. A significant result of this thesis is that unlike the findings of earlier work stating that fracture intensity is dominantly controlled by bed thickness, fracture intensity is extremely sensitive to mechanical contrast, rather than to bed thickness without any contrast. In the completion of Objectives 1 and 2, this study has effectively used the mechanical and fracture stratigraphies to better understand the structural and tectonic

history of the study area, and has allowed for the fulfillment of Objective 3: making recommendations for future fracture studies in carbonate sequences worldwide. Mechanical stratigraphy cannot only vary throughout time, but can also have subtle effects on certain fracture properties. Fractures must be analyzed within a broader tectonic context, as the deformation history is shown to be the key controlling factor for fracture orientations. Additionally, the tectonic forces impacting an area, both regional and local, may override small-scale variations in mechanical competency, bed spacing or geometry, and lithology. Because tectonic forces are so dominant in their control over fracture orientation, they are a critical point of understanding when attempting to characterize tight or unconventional reservoir for horizontal drilling. Knowing the orientation of the major tectonic fractures is necessary to target drill routes, as production can be optimized from some unconventional reservoirs when penetrating systematic fracture sets perpendicularly (Engelder et al., 2009).

Intensity, another important component for characterizing reservoirs, is shown here to not always be controlled by bed thickness. Instead, a thorough understanding of high mechanical and lithological contrasts may be the key to predicting subsurface zones of high fracture intensity. The zones of high FI found in softer lithologies and thinner mechanical units present the most likely chance of producing economically viable hydrocarbons from tight carbonate reservoirs. Targeting softer or thinner units for greater economic recovery is not an intuitive result. Overall, this study presents an opportunity to further the understanding and characterization of carbonate reservoirs using a detailed fracture and mechanical stratigraphic analysis. As shown in this study, high hydrocarbon productivity zones in carbonate reservoirs may actually be constrained

to narrow intervals of mudstone within a shelf sequence, given the higher observed FI. Given the lack of connectivity between mechanical units, reservoir exploitation must not only be accomplished through drilling in the correct orientation, but must also target the correct high-fracture-permeability zones. Because of these observed constraints, a useful addition to analyzing drilled core would be to include a strength test in order to better characterize the small-scale sequence stratigraphy of the target interval.

Looking forward, continued acquisition of fracture orientation data will allow for a refinement of the existing tectonic framework interpretation of the study area. While a large scale comparison exists from previous literature such as Hudson (2000) and Cox (2009), collected fracture orientation data will enhance the understanding of more local tectonic forces and modification of regional forces. Additional information on abutting relationships will enable a more strict understanding of the timing of the fracture sets. This study uses relative timing relationships to infer origin from previously discussed tectonic events, but a more detailed timing study would give a much more concrete genetic history of the established fractures. Fracture intensity was only briefly examined in this study, and in largely a qualitative sense. This fracture characteristic is the one most often controlled or altered by the mechanical stratigraphy, so a dedicated project examining bed boundary relationships and fracture intensity values would allow for a more detailed interpretation of fracture density in carbonate rocks. Some studies (Eberli et al., 2003; Underwood et al., 2003; Morettini et al., 2005) have shown that fracture stratigraphy varies with carbonate facies changes. A detailed facies analysis would supplement the lithological observations, and provide an additional potential control on the observed fracture patterns. Lastly, the sequence has seen a complex but subtle history

of diagenesis that largely appears to have no effect on the mechanical stratigraphy. Further work with cathodoluminescence, and investigations into the origin and characteristics of the chert, may provide a better understanding of the impact diagenesis has on the fracture stratigraphy and mechanical stratigraphy of the sequence, as it was not the main focus of this study.

8. Conclusions

This work has developed a fracture stratigraphy with 4 main orientation sets: N-S (Set 1), E-W (Set 2), NE-SW (Set 3), and NW-SE (Set 4). These 4 identified fracture sets represent 4 episodes of regional stress affecting the study area: a) Folding of the underlying Cotter Dolomite (potentially related to the uplift of the Ozark Plateau) generating an older Set 1; b) Oblique closure and indentation of the Ouachita Orogeny resulting in Set 2 and a younger Set 1; c) ARM deformation combined with the re-activation of subsurface shear zones creating Sets 3 and 4; d) Possible influence of far field stress of the Appalachian orogeny combined with unroofing fractures to create younger Sets 1,3, and 4. Additionally, an investigation into fracture intensity reveals that FI is controlled by variations in the mechanical stratigraphy rather than by strict bed thickness, with thinner mechanical layers (most often the softer lithologies) having a higher FI than the thicker mechanical layers.

The mechanical stratigraphy of the sequence is directly related to lithological variations. Higher hardness (Q) values occur in the more competent lithologies such as packstones and grainstones, while lower Q values are confined to mudstone and shale lithologies. Diagenesis only appears to have an impact on mechanical variations when it is pervasive and on a large scale. Chert nodules do not impact the mechanical

stratigraphy, but wide units of chert replacement, such as in the tripolitic unit, do impact the mechanical properties.

Regional stresses are the primary control on fracture orientation. Although changes in large-scale mechanical stratigraphy may subtly influence orientation, it is not a dominant influence. FI in this study is related to mechanical package thickness, rather than bed thickness. Softer mechanical units (such as mudstones/shales) show higher FI values than the more mechanically competent layers. The mechanically competent packages are thicker in this sequence than the softer packages, so the competent packages behave as a massive sequence in regards to FI values, overriding bed boundary controls.

The fact that FI values are sensitive to changes in mechanical competency suggests that the large-scale mechanical stratigraphy (related to lithology) was developed before fracture formation occurred. More subtle variations in the mechanical stratigraphy, such as those brought about by diagenesis likely developed after the fracture stratigraphy, although more work is needed to better demonstrate that relationship.

Given the wide range of controls and heterogeneities that influence fracture development in carbonates, future studies on the subject must be prepared to attempt a multi-disciplinary approach to the subject. Fracture orientations are largely controlled by regional structural influences and pre-existing structural trends and faults. FI is influenced by mechanical variations, which are in turn a product of both lithology and diagenesis. Although facies relationships are not explored in this study, they may also be a controlling factor on fracture and mechanical variations. Additionally, these types of studies must be addressed at multiple scales. Many of the described controls, such as diagenesis and lithology, influence fractures on a smaller scale than the regional tectonic

stresses. For that reason, hydrocarbon evaluations of carbonate reservoirs must account for both the large scale and the small scale investigations into fracture characteristic controls. Because of this, outcrop evaluations are of critical importance to properly assess characteristics that are challenging to recover from conventional subsurface datasets such as core and seismic reflection volumes.

FIGURES

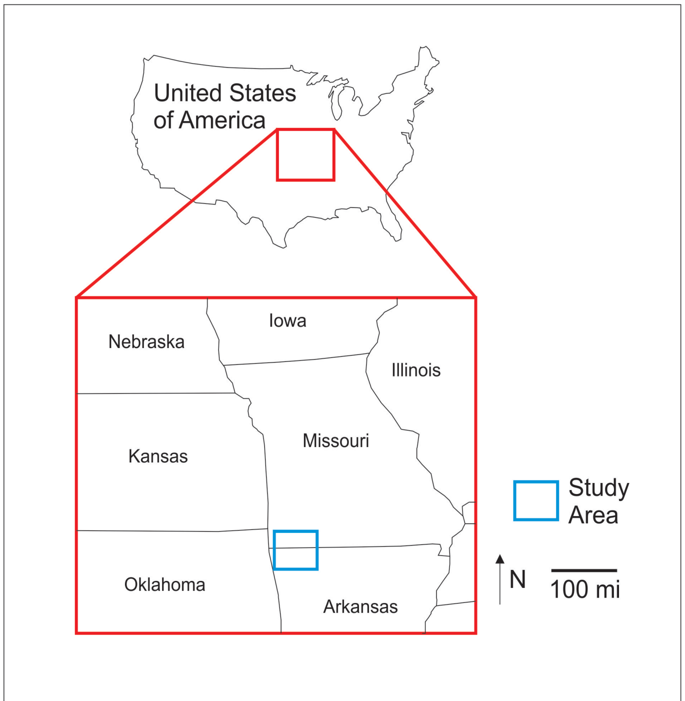

Fig. 1: Map showing the location of the study area within the Mid-Continent of the United States. The blue box also sits within the Ozark Plateau Region of Arkansas and Missouri.

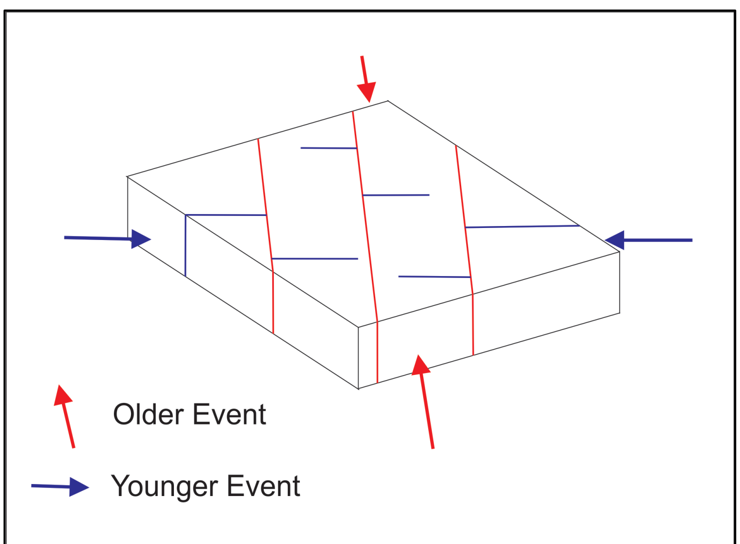

Fig. 2: Schematic representation of fracture abutting relationships. Older set is shown in red, younger set is shown in blue. The younger set was unable to propagate through the existing fractures, allowing for relative ages of deformation to be determined.

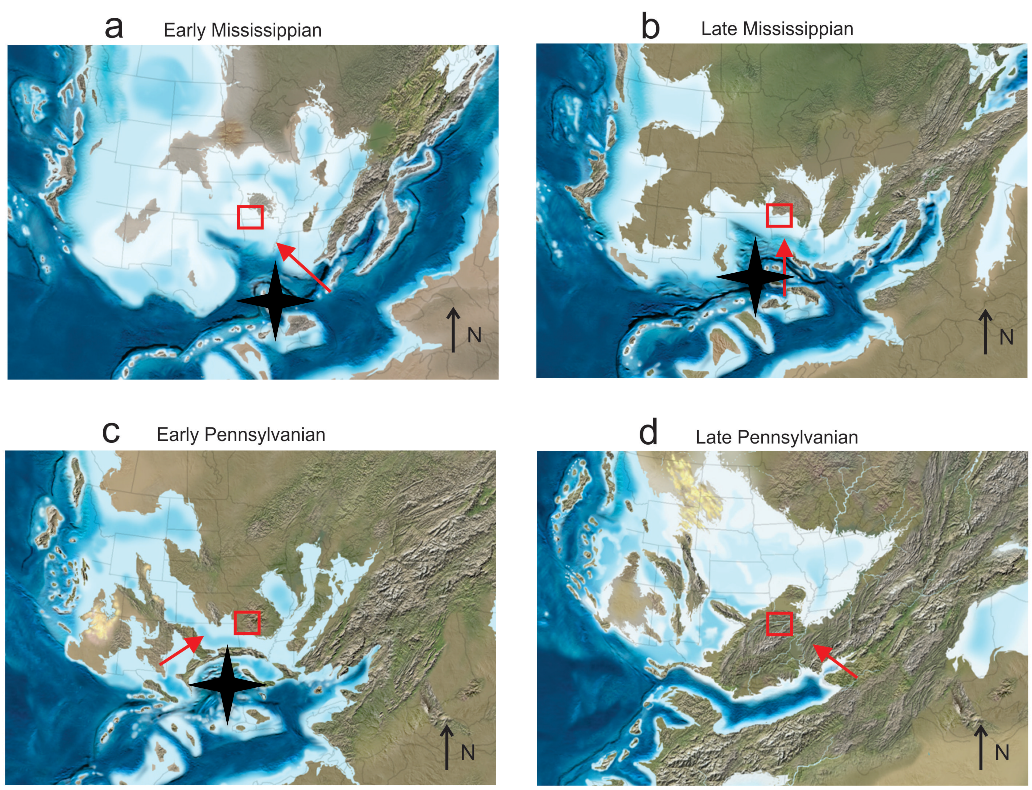

Fig. 3: Paleo-geography maps showing the major tectonic events impacting the study area (red box). Red arrows indicate direction of maximum horizontal stress (Hmax) resulting from regional scale tectonic forces in the Mississippian to Pennsylvanian. Black star indicates location of the Ouachita microplate. Maps modified from: https://www2.nau.edu/rcb7/nam.html.

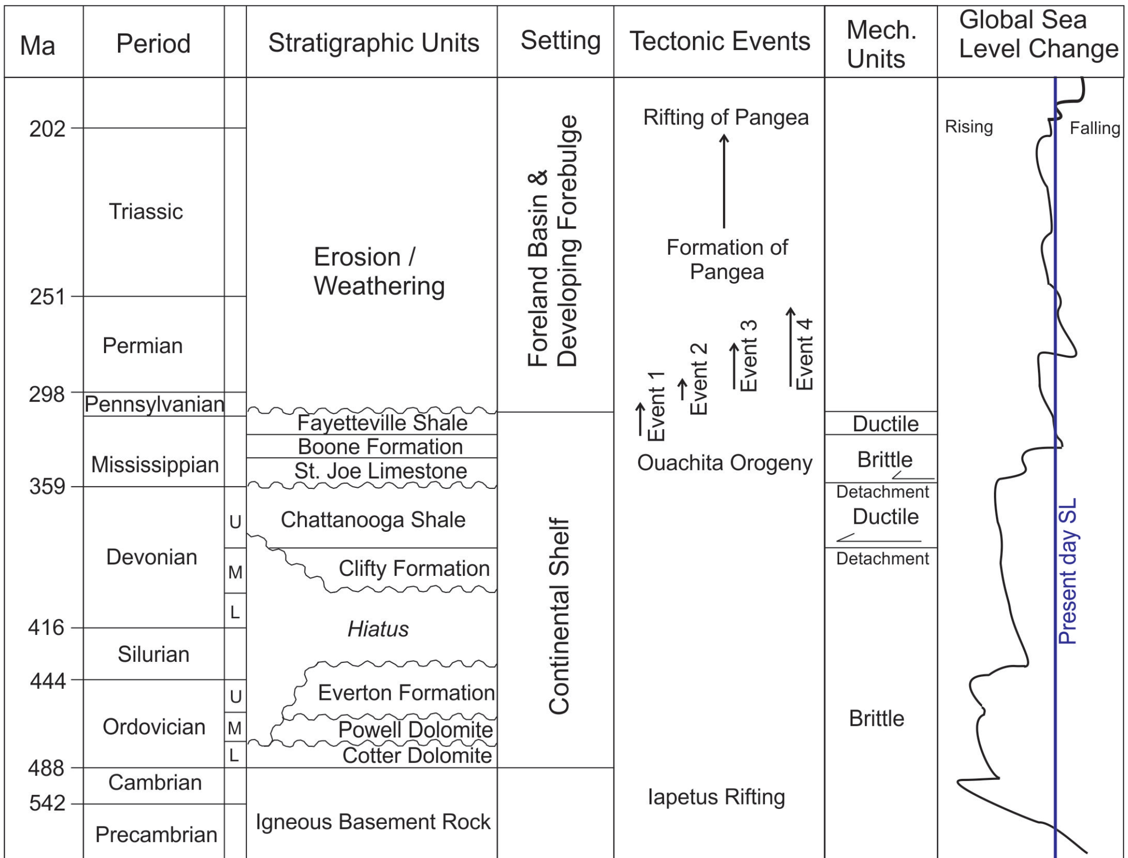

Fig. 4: Tectonostratigraphic column for NW Arkansas from the Precambrian to Permian. Sea level curve shows global relative rise and fall from present day levels. Sea Level Curve from: (http://higheredbcs.wiley.com/legacy/college/levin/0470000201/chap_tutorial/ch12/chapter12-03.html.

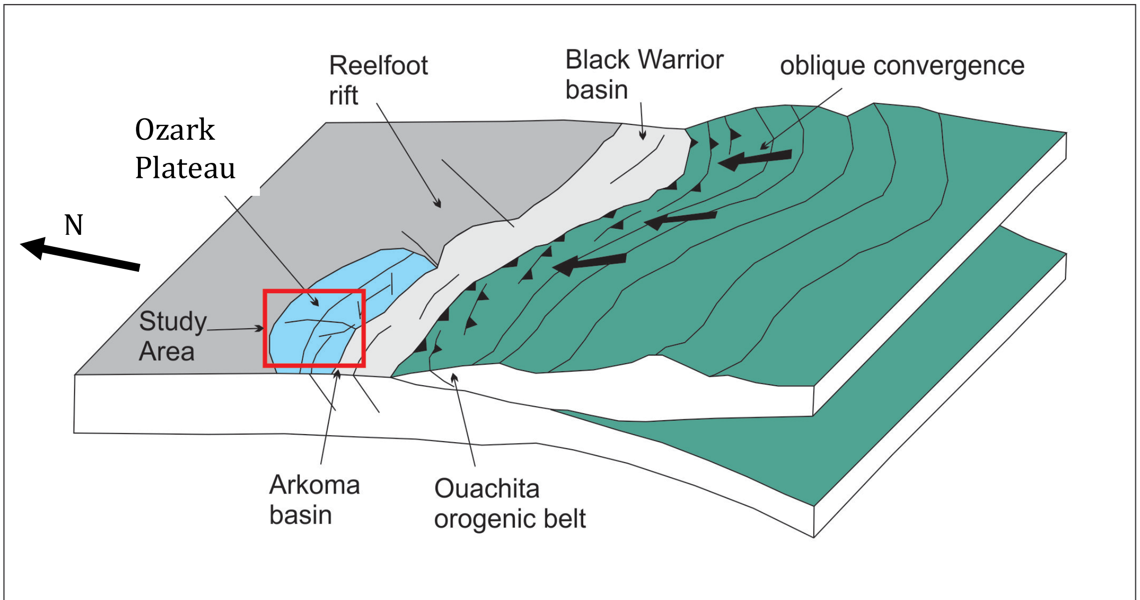

Figure 5: Diagram showing the tectonic setting of the southern Ozark Plateau (light blue) in the foreland basin (light gray). Study area outlined in red, and is on the forebulge of a pro-foreland basin. Figure modified from Hudson (2000), Fig. 4.

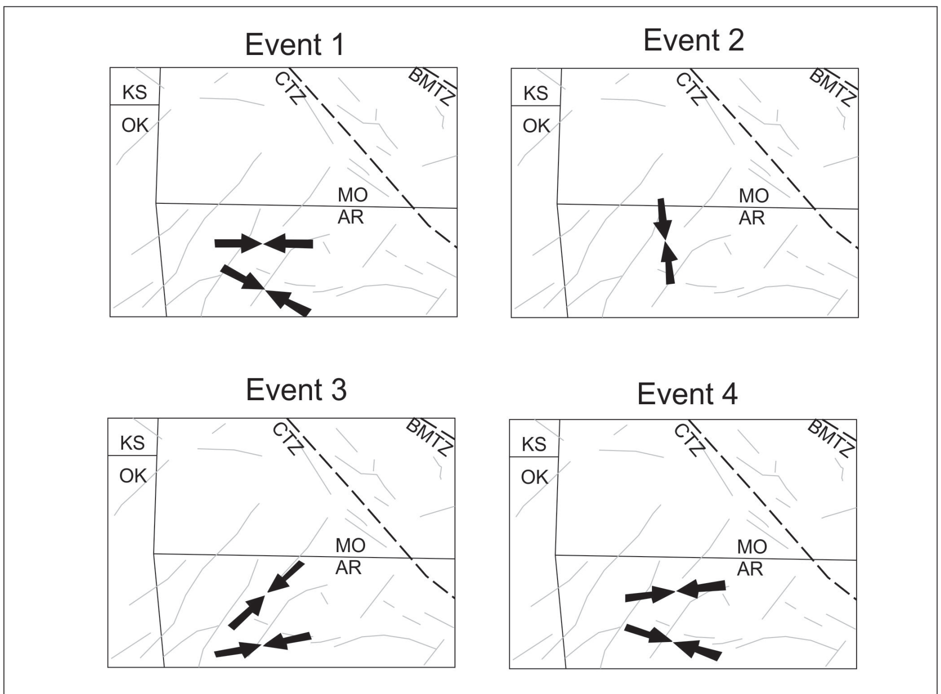

Fig 6: Arrows show maximum horizontal stress directions (Hmax) in the study area (box outline). Hmax varies from E-W in Event 1, to N-S in event 2, Nw-SE in Event 3 and returns to E-W in Event 4. Light gray lines denote major lineaments. CTZ = Chesapeake Tectonic Zone, BMTZ = Bolivar-Mansfield Tectonic Zone. Figure modified from Cox (2009), Fig. 2.

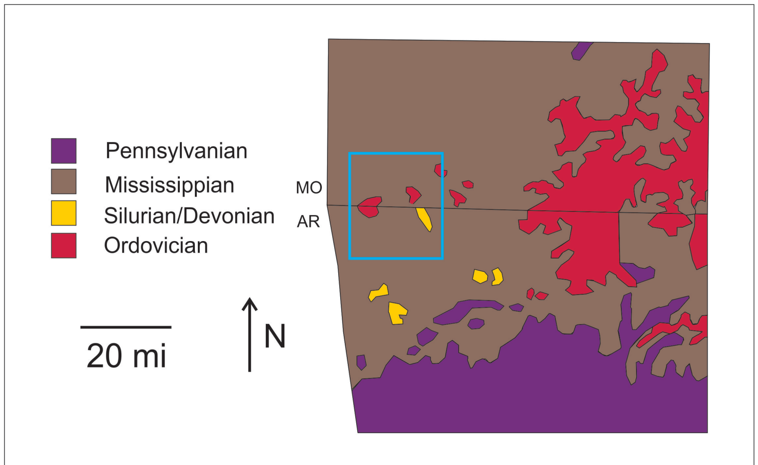

Fig. 7: Geologic map showing ages of units present within the study area of Arkansas and Missouri (blue box). Figure modified from Missouri Department of Natural Resources (1990) and Arkansas Geological Survey (2015).

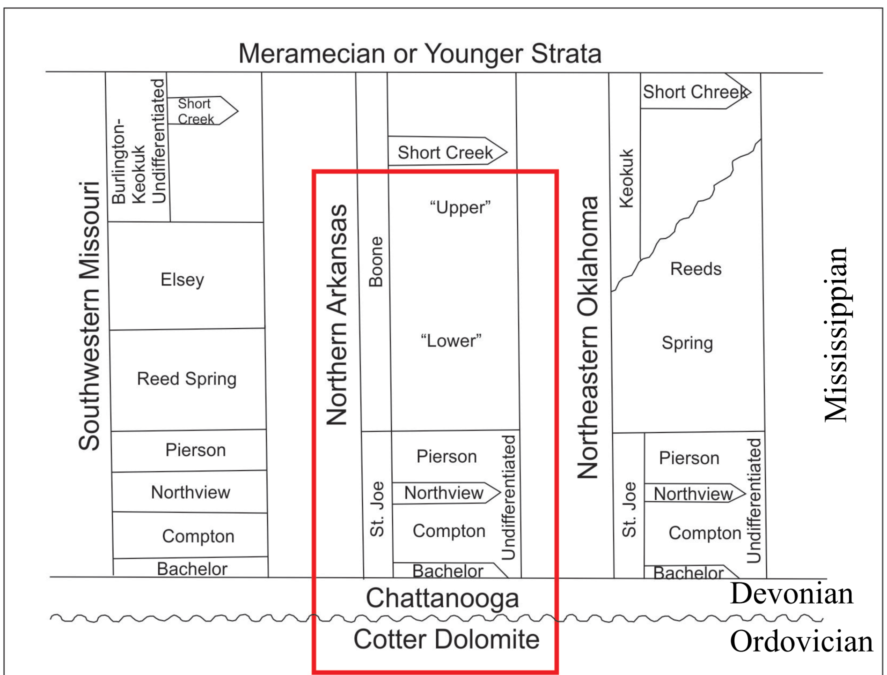

Fig. 8: Stratigraphic columns showing differences in terminology across the state lines of Missiouri, Arkansas, and Oklahoma. Red box outlines units of interest in the study area. Figure modified from Manger et al., (1998).

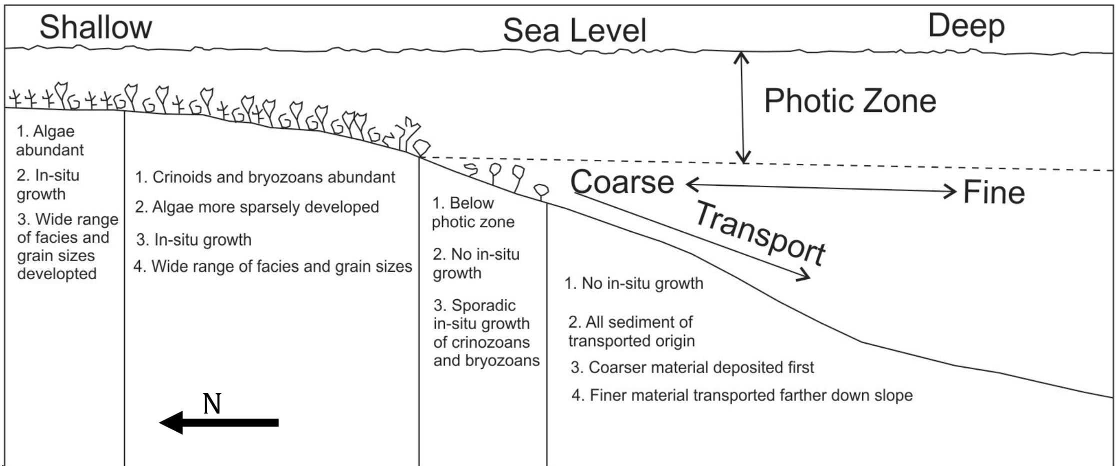

Fig. 9: Schematic representation of the depositional environment of carbonates in NW Arkansas. The presence of crinoids indicates that the studied succession comes from the intertidal to supratidal zone. Figure modified from Shelby (1986).

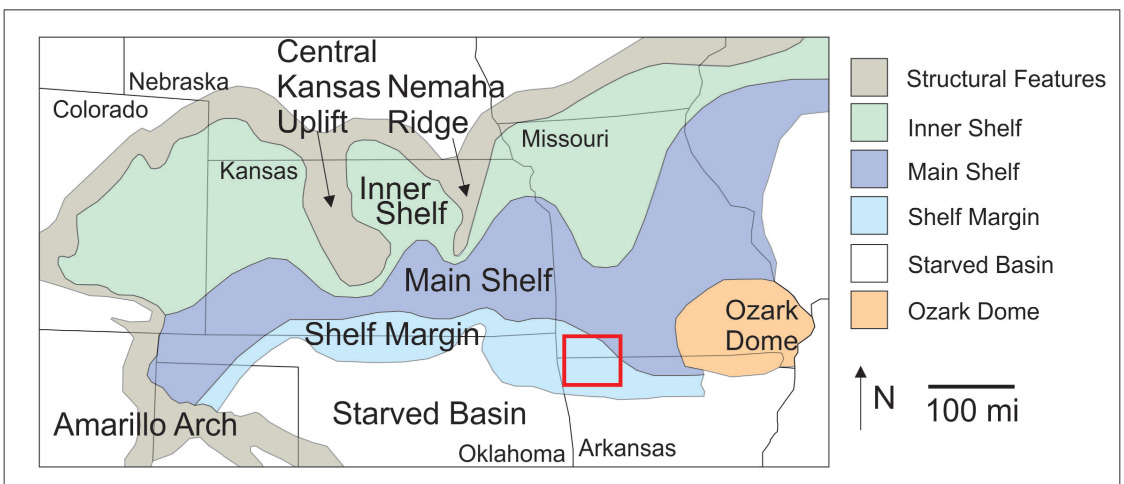

Fig. 10: Mississippian depositional environments across the Mid-Continent region of the United States indicating the study area formed as part of a shelf margin. Study area outlined by red box. Figure modified from Lane and DeKeyser, 1980, Fig. 8.

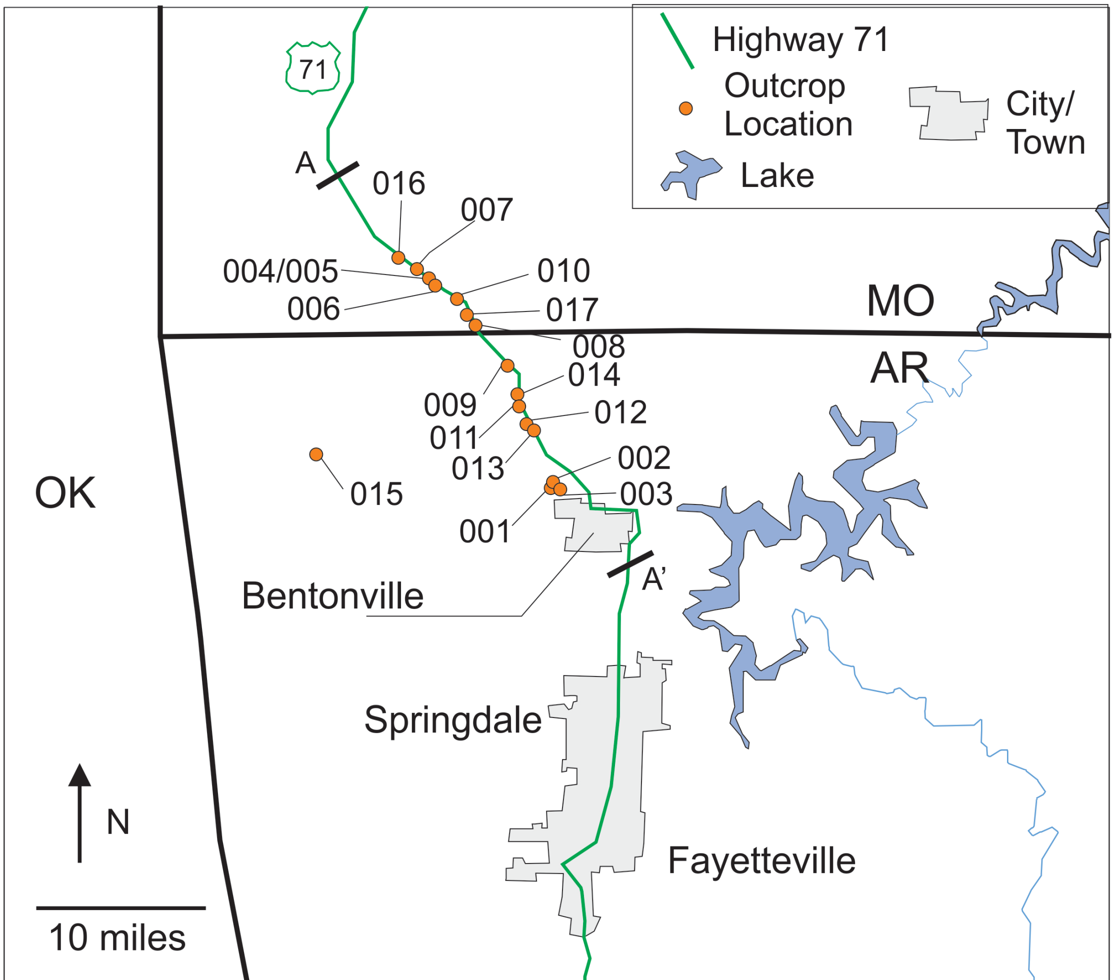

Fig. 11: Map showing the location of the measured outcrops (orange dots) within the study area. Most exposures fall along Highway 71 (green line) which runs through northwest Arkansas and southwest Missouri. Created cross section runs along Highway 71 from A to A'.

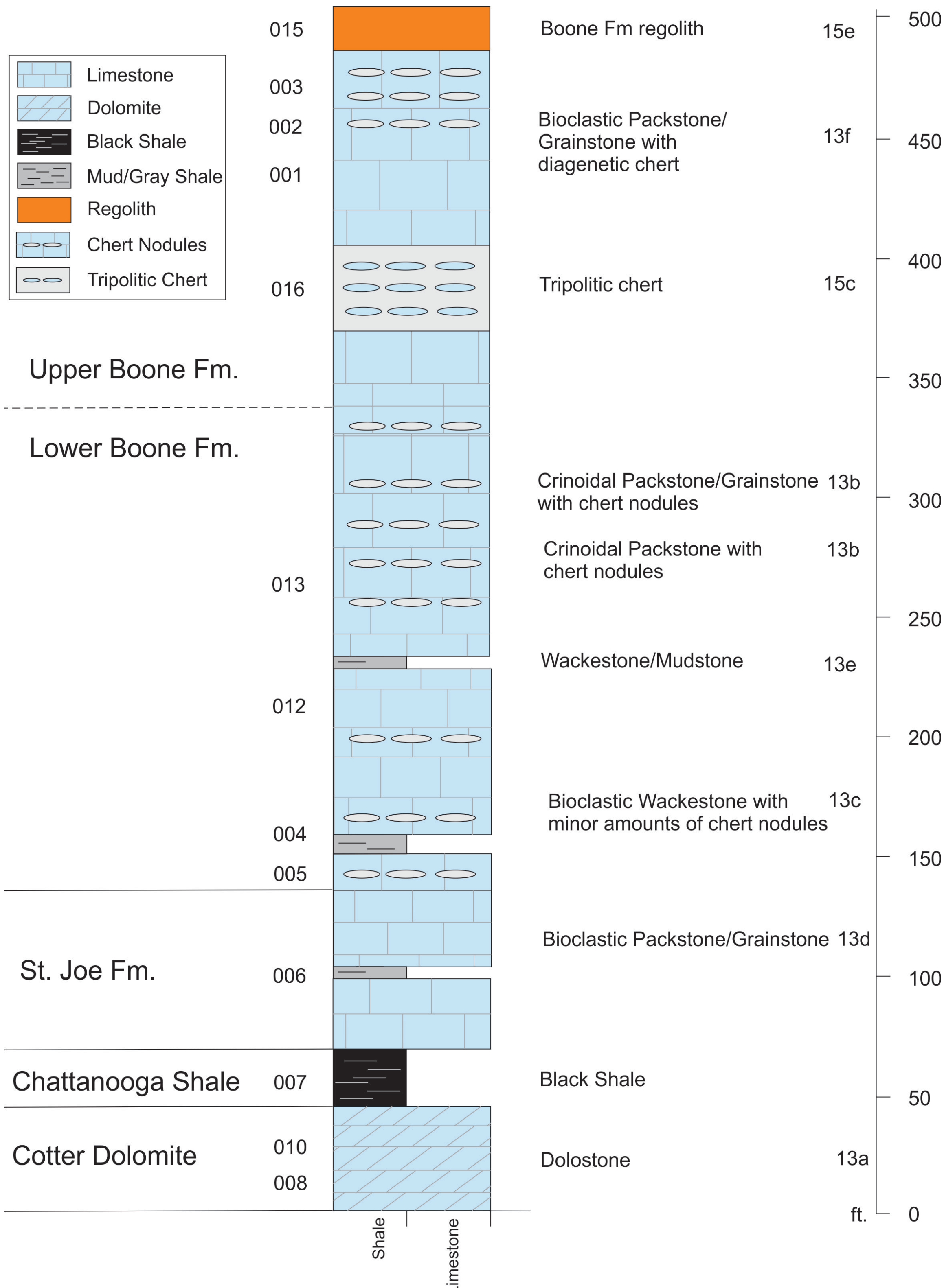

Fig. 12: Stratigraphic column showing the major lithologies present within the primary units of the sequence. Photographs of the identified lithologies/diagenetic areas are labeled along the right side of the column. Numbers on the left are outcrops where lithological data was collected.

Lithology	Example Photomicrograph	Formation Name	Depositional Environment
Dolostone	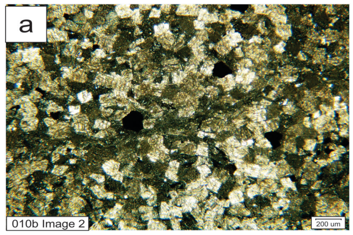	Cotter Dolomite	Intertidal/ Supratidal
Crinoidal Packstone/ Grainstone	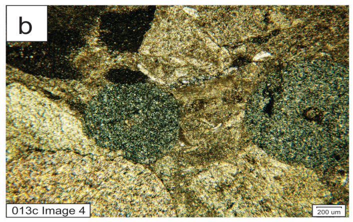	Lower Boone Formation	Shallow Marine
Bioclastic Wackestone	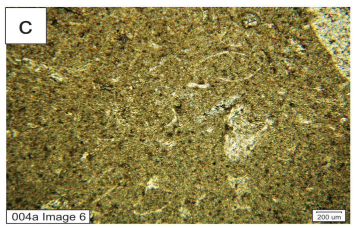	Lower Boone Formation	Shallow Marine
Bioclastic Packstone	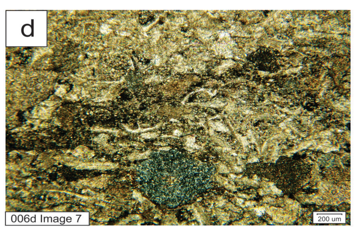	Lower Boone Formation	Shallow Marine
Wackestone/ Mudstone with Pyrite	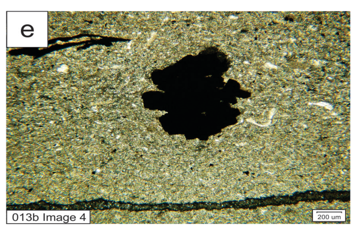	Lower Boone Formation	Shallow Marine
Bioclastic Packstone/ Grainstone	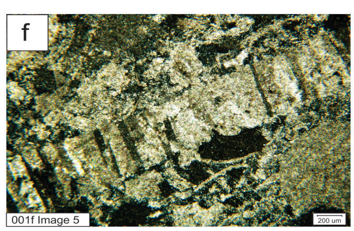	Upper Boone Formation	Shallow Marine

Fig. 13: Example photomicrographs of the major lithologies within the studied succession. Lithology name is in the first column, representative photomicrographs are in the second, column, formation of the example lithology is in the third column, and the fourth column indicates the broad depositional environment.

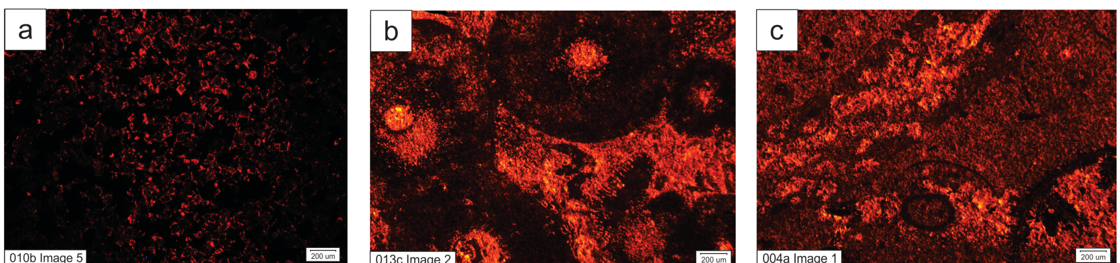

Fig. 14: Cathodoluminescence photos showing different phases of diagenesis within the sequence. a) dolomitization (Cotter Dolomite). b) nonluminescent crinoids (preserved original cement) surrounded by luminescent cementation. c) bryozoan fragment and crinoids showing diagenetic alteration by high-Mn calcite in a muddy matrix.

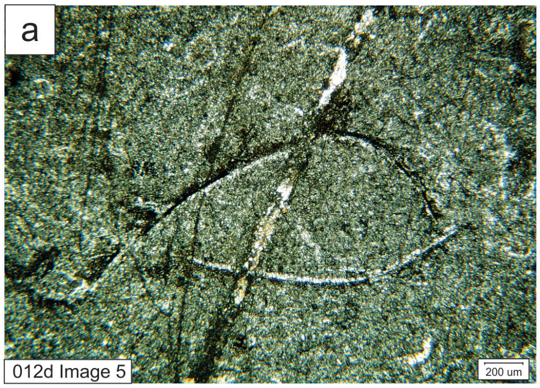

Chert Nodule with Fracture and Shell Fragment in Bioclastic Wackestone

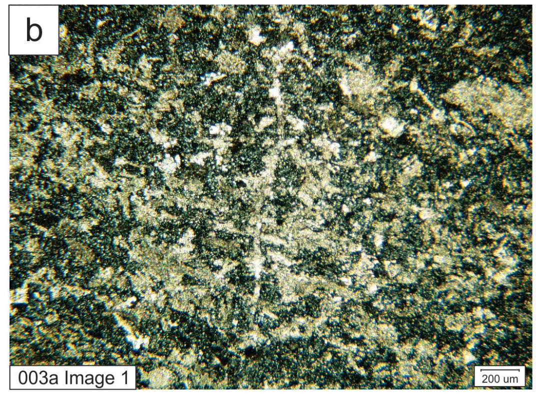

Diagenetic Chert in Wackestone

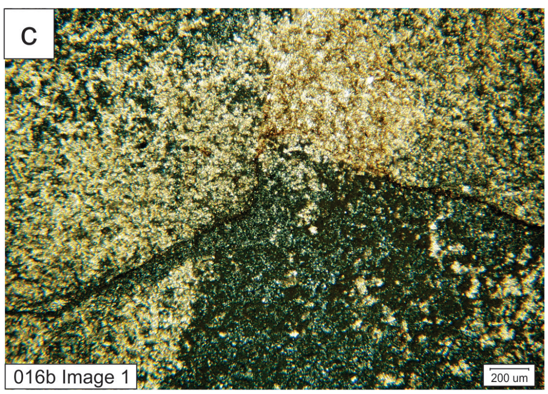

Tripolitic Chert with Stylolite

Stylolitized Bedding Plane

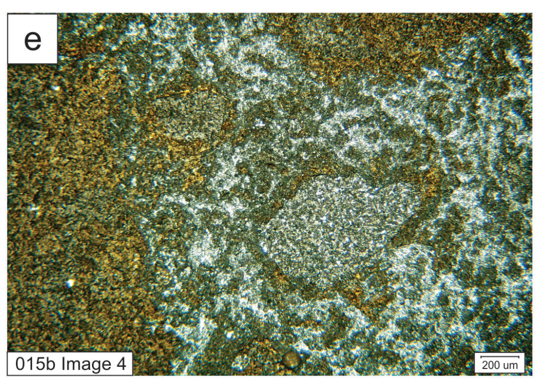

Oxidized Regolith

Fig. 15: Thin section photographs showing the various forms of chert diagenesis (a-c) within the studied sequence, an example of a stylolitized bed boundary (d) as well as the oxidized regolith at the top of the sequence (e).

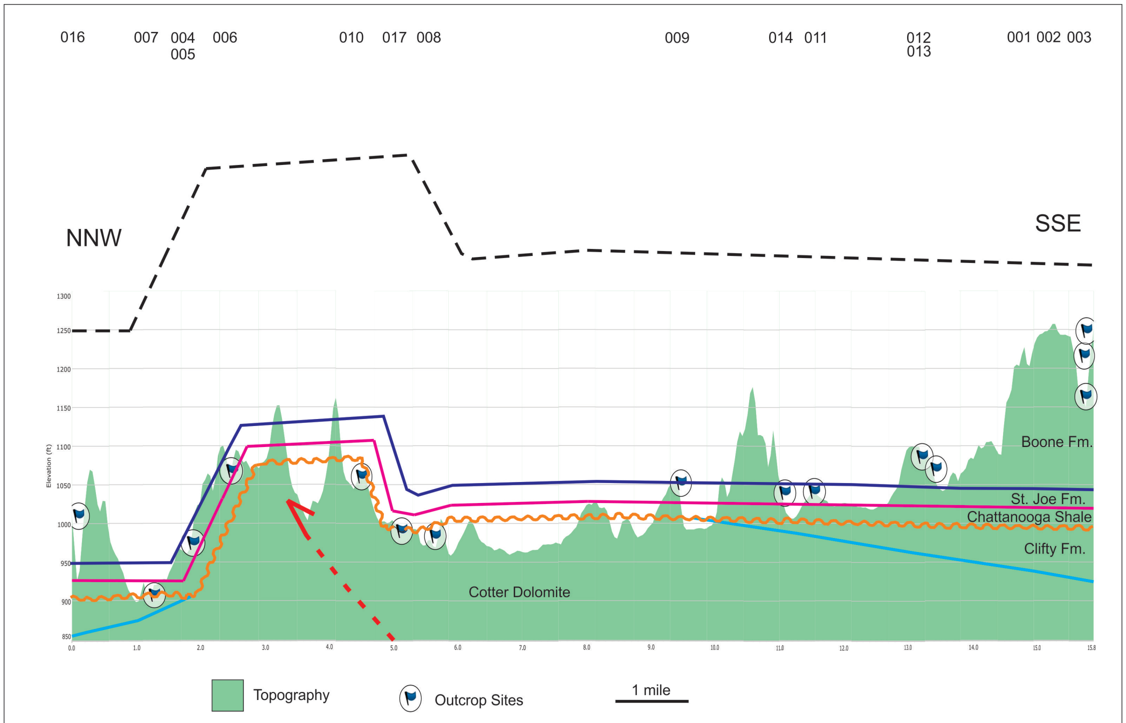

Fig. 16: Cross section of the studied outcrops along Highway 71 showing the presence of a fault related fold in the Cotter Dolomite. Green color is the topographic surface, red dashed line shows interpreted fault location, flags indicate outcrop locations (labeled at top of section), and units are labeled (dashed black line is inferred top of Boone Fm). Vertical Exaggeration is 60x.

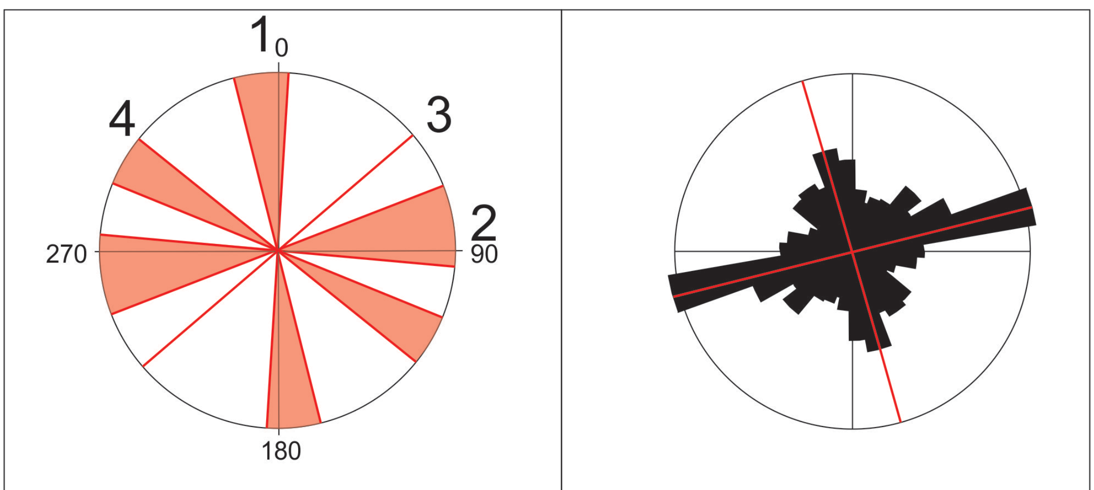

Fig. 17: a) Rose diagram showing the 4 identified fracture sets in the study area oriented N-S, E-W, NE-SW, and NW-SE. Light red color indicates variability in each set. b) Rose diagram of all (731) measured fracture orientations identifying the dominant regional fracture orientations: N-S and E-W.

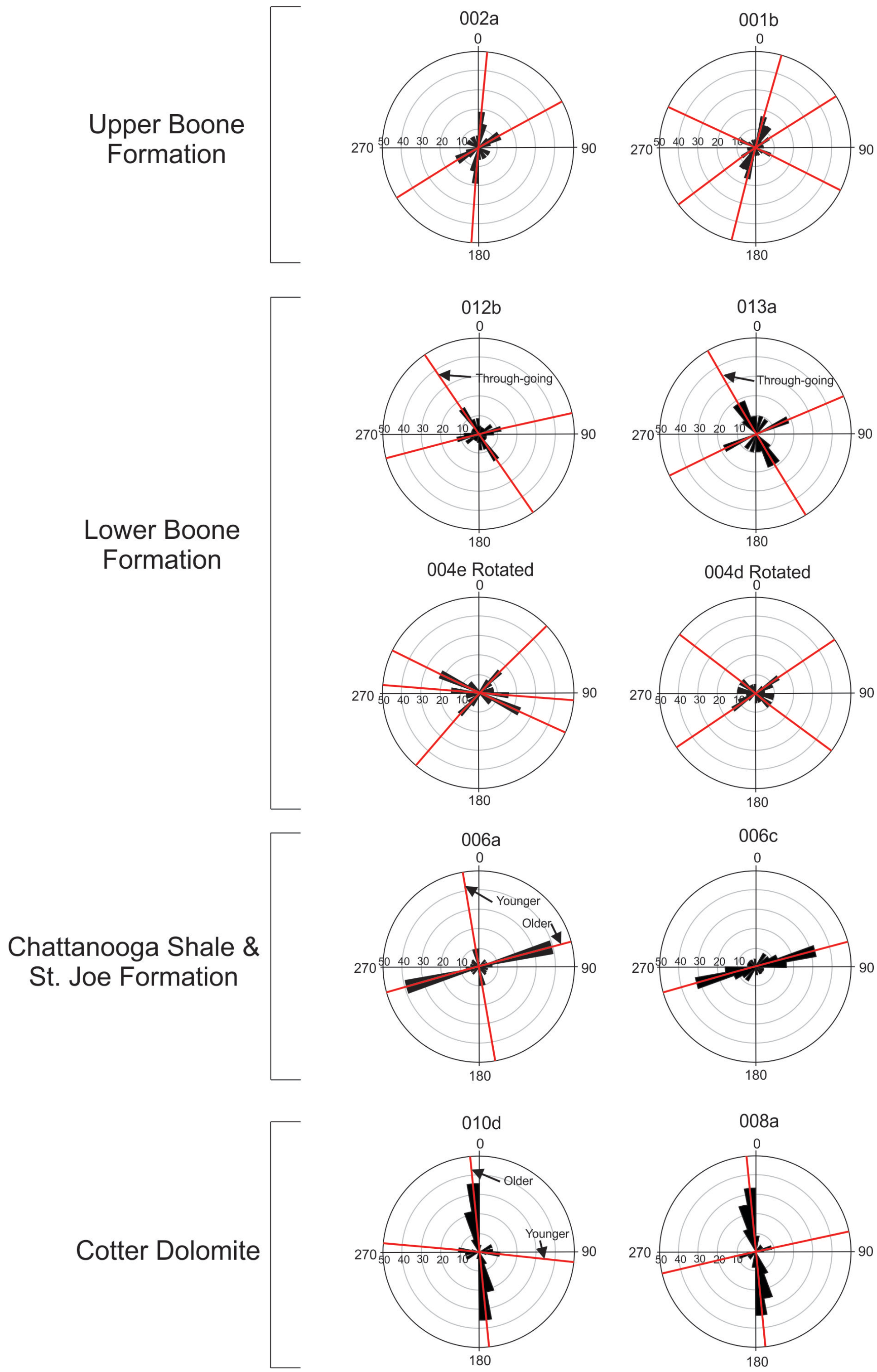

Fig. 18: Representative stereonets showing the fracture stratigraphy up sequence, characterized by orientation. Red lines emphasize major orientation directions. Where possible, age relationships are labeled. Locations of the representative stereonets within the stratigraphic sequence are labeled to the left of the diagrams.

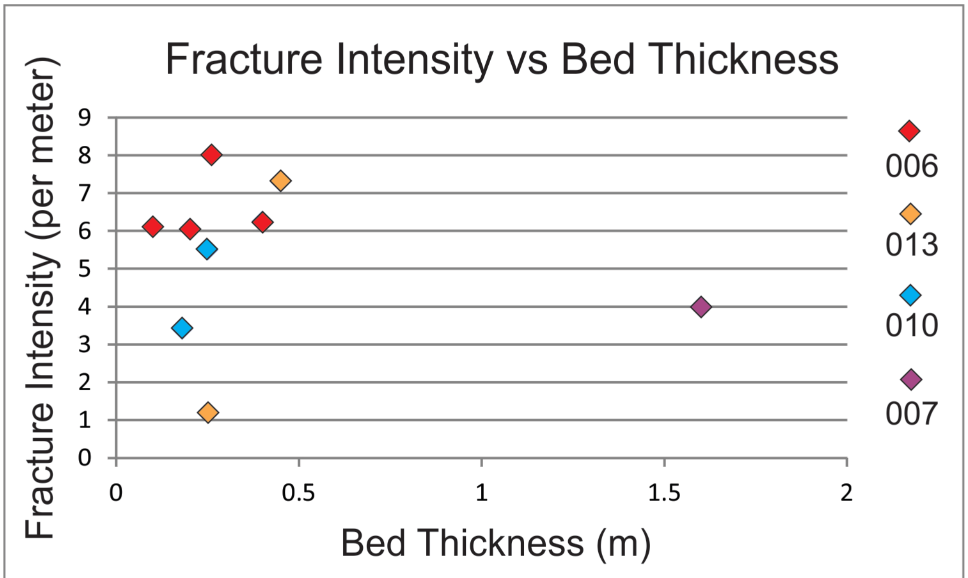

Fig. 19: Graph comparing FI and Bed Thickness. Each point represents an individual bed, showing little relationship between FI and Bed Thickness. Measurements are color coded based on the outcrop each was taken from. 007 (purple) = shale; 010 (blue) = dolostone; 013 (orange) = mudstone /crinoidal grainstone; 006 (red) = crinoidal packstone.

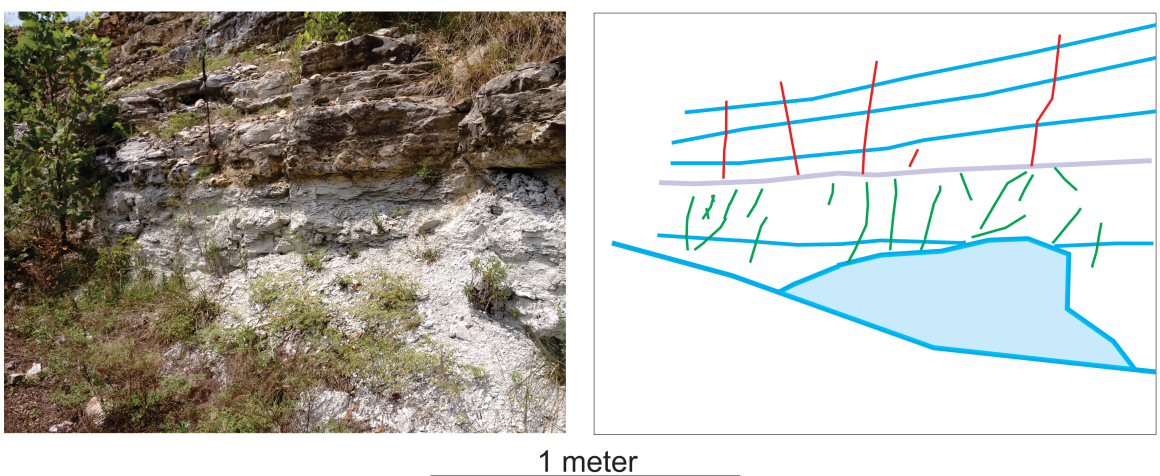

Fig. 20: Annotated photograph showing contrast between FI of two rock units with differing mechanical and lithological properties. Bed boundaries are in light blue, with covered section in pale blue. FI 1 in green (mudstone lithology), FI 2 in red (crinoidal packstone lithology). Purple line shows boundary between mechanical units. FI is not influenced by bed thickness, but is altered by mechanical layer thickness.

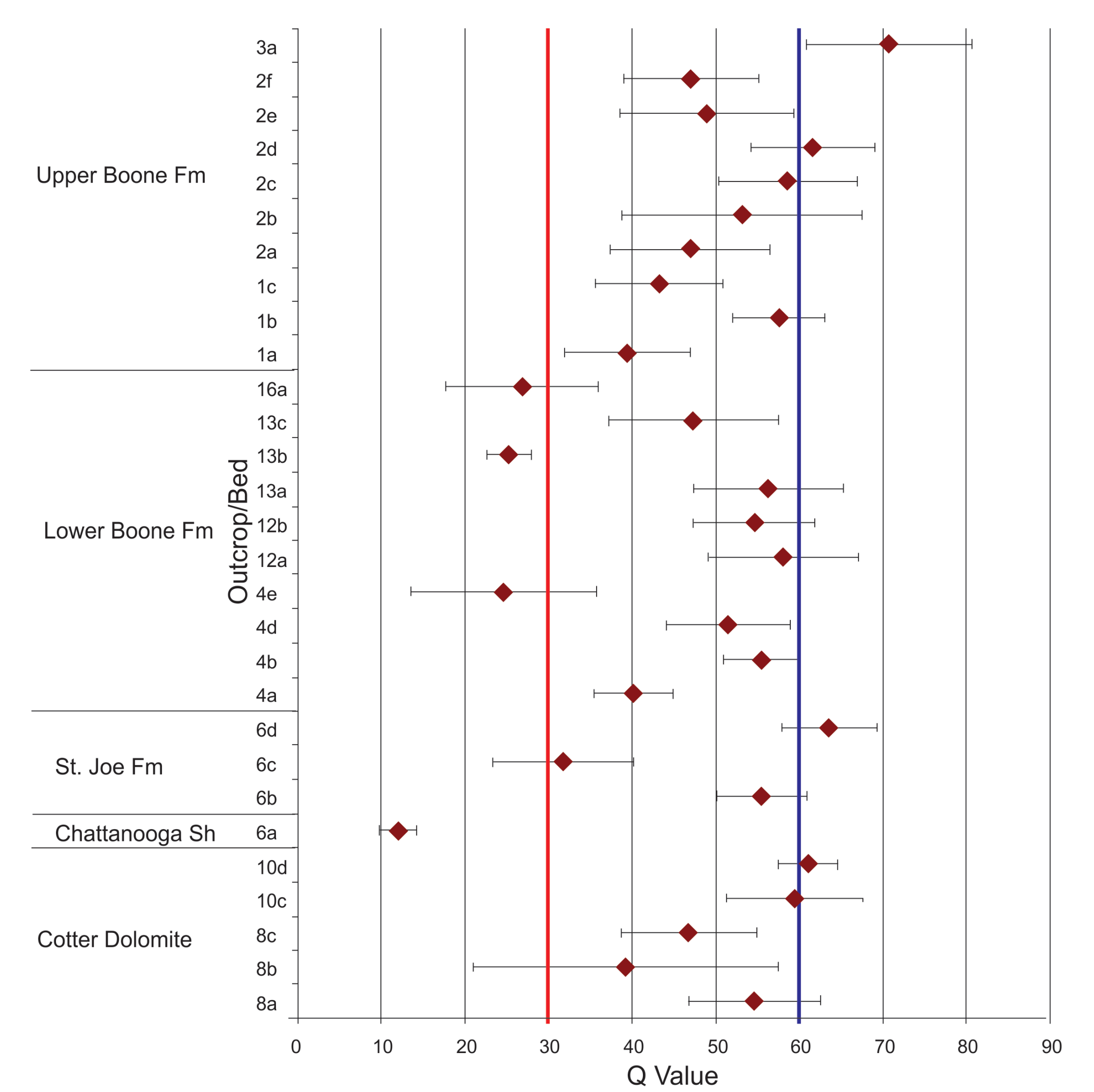

Fig. 21: Graph showing Q values (and standard deviations) taken from the measured sequence. Chart is organized from low stratigraphic position at the bottom to high stratigraphic position at the top. Red line separates the 0-30 Q value and 30-60 Q value range, while the blue line separates the 30-60 Q value and the 60+ Q value range. Formation thicknesses not to scale.

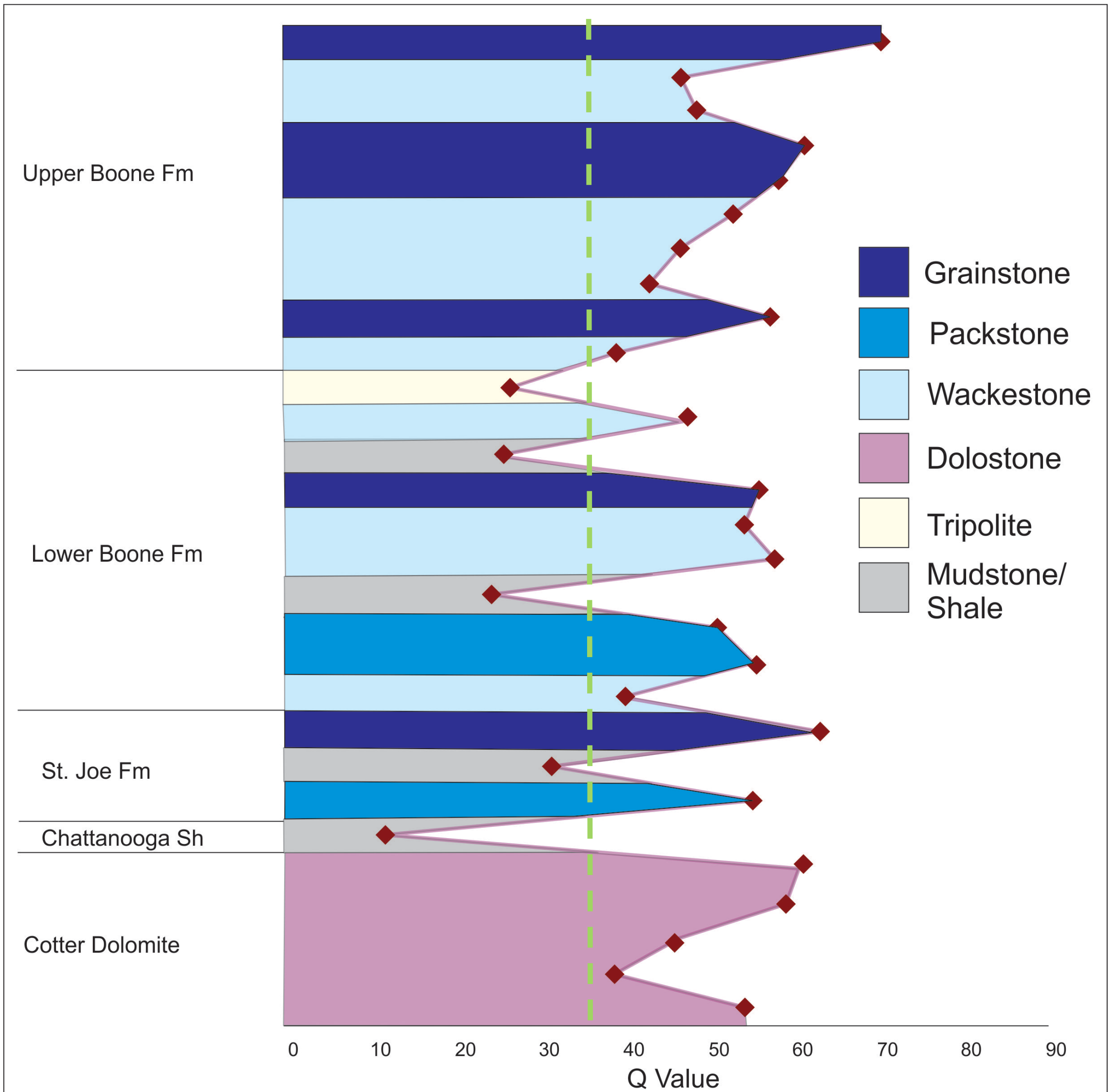

Fig. 22: Image shows Q values from Fig. 21 related to lithology (colored). Stratigraphic units are labeled from lowest position at bottom to highest position at top. The variations in mechanical values are related to the differences in lithology throughout the sequence. Dashed green line indicates approximate cutoff for softer lithologies vs harder lithologies. Formation thicknesses not to scale.

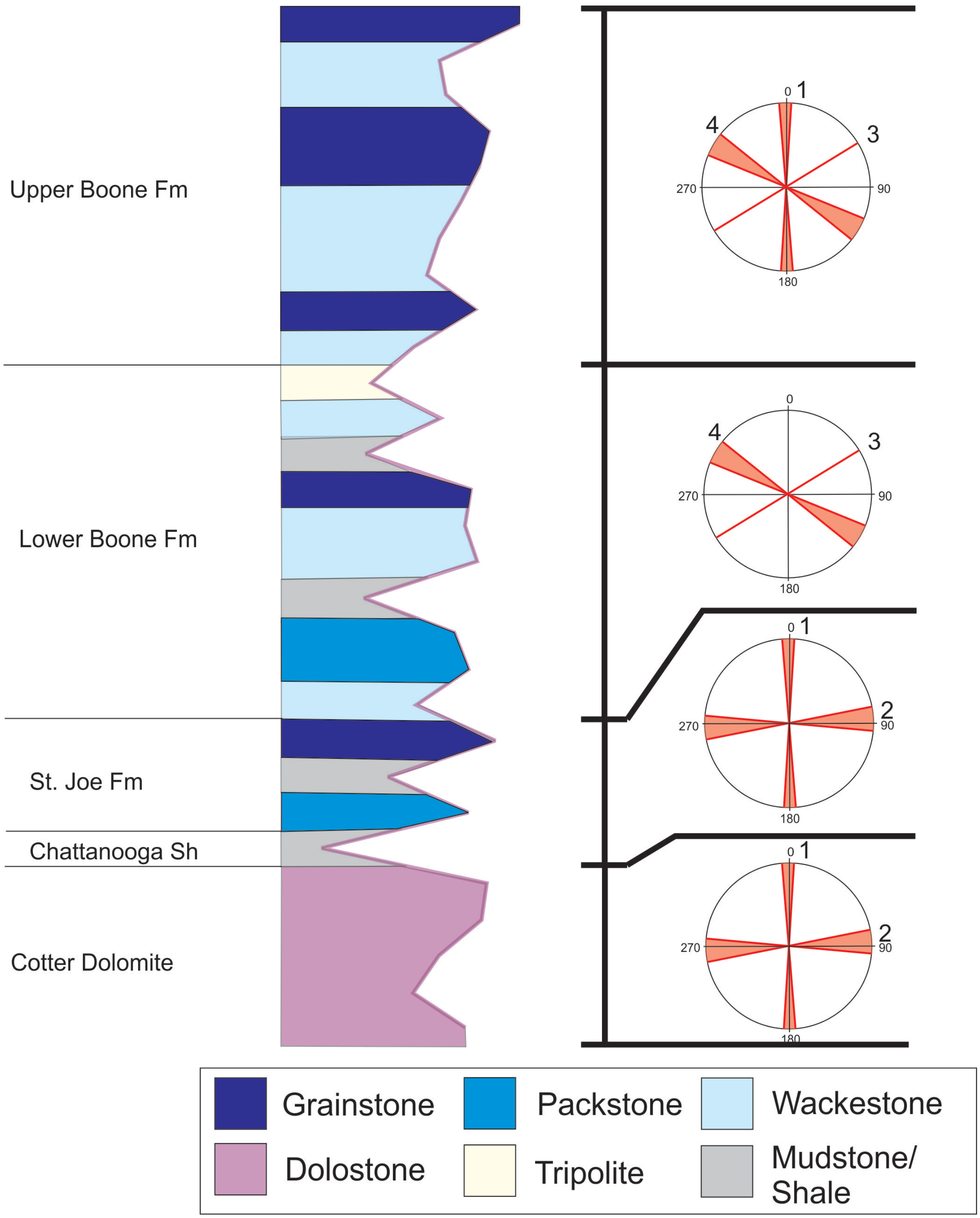

Fig. 23: Diagram comparing the mechanical stratigraphy (Fig. 22) to the fracture stratigraphy (orientation data). No clear relationship exists between the observed fracture sets and the changes in mechanical data. Formation thicknesses not to scale.

References

Ahmadahdi, F., Daniel, J.M., Azzizadeh, M., Lacombe, O., 2008, Evidence for pre-folding vein development in the Oligo-Miocene Asmari formation in the central Zagros fold-belt, Iran. Tectonics 27.doi:10.1029/2006TC001978 TC1016.

Allmendinger, R. W., N. Cardozo, and D. M. Fisher, 2012, Structural geology algorithms. Vectors and tensors:Cambridge, Cambridge University Press, 304 p.

ASTM D5873-14, Standard test method for determination of rock hardness by rebound hammer method.

Aydin, A., 2000, Fractures, faults, and hydrocarbon entrapment, migration and flow: Marine and Petroleum Geology, v. 17, no. 7, p. 797–814, doi:10.1016/S0264-8172(00)00020-9.

Bai, T., and Pollard, D.D., 2000, Fracture spacing in layered rocks: a new exploration based on the stress reduction. Journal of Structural Geology, v. 22, p. 43-57.

Bai, T., Pollard, D.D., and Gao, H., 2000, Explanation for fracture spacing in layered materials. Letters to Nature, v. 403, p. 753-756.

Barbier, M., Hamon, Y., Callot, J.P., Floquet, M., and Daniel, J.M., 2012, Sedimentary and diagenetic controls on the multiscale fracturing pattern of a carbonate reservoir: The Madison Formation (Sheep Mountain, Wyoming, USA). Marine and Petroleum Geology, v. 29, p. 50-67.

Bathurst, R.G.C., 1987, Diagenetically enhanced bedding in argillaceous platform limestones: stratified cementation and selective compactions. Sedimentology, v. 34, p. 749-778.

Bellahsen, N., Fiore, P., and Pollard, D.D., 2006, The role of fractures in the structural interpretation of Sheep Mountain Anticline, Wyoming. Journal of Structural Geology, v. 28, p. 850-867.

Bickford, M.E., Van Schmus, W.R., and Zietz, I., 1986, Proterozoic history of the midcontinent region of North America. Geology, v. 14, p. 492-496.

Billi, A., 2005, Attributes and influence on fluid flow of fractures in foreland carbonates of southern Italy. Journal of Structural Geology, v. 27, p. 1630-1643.

Boggs, S., and D. Krinsley, 2006, Application of cathodoluminescence imaging to the study of sedimentary rocks: New York, Cambridge University Press, 176 p.

Brusseau, M.L., 1994, Transport of reactive contaminants in heterogeneous porous media. Reviews of Geophysics v. 32, p. 285–313.

Caine, J.S., Tomusiak, S.R.A., 2003, Brittle structures and their role in controlling porosity and permeability in a complex Precambrian crystalline-rock aquifer system in the Colorado Rocky Mountain Front Range. Geological Society of America Bulletin v. 115, p. 1410–1424.

Caplan, W.M., 1957, Subsurface Geology of Northwestern Arkansas. Arkansas Geological Survey Information Circular, v. 19, p. 1-14.

Chandler, A., and Ausbrooks, S., 2010, Geology of the Pea Ridge and Garfield Quadrangles, Benton County, Arkansas. Arkansas Geological Survey Information Circular, v. 41, p. 1-23.

Chinn, A.A., and Konig, R.H., 1973, Stress inferred from calcite twin lamellae in relation to regional structure of Northwest Arkansas. Geological Society of America Bulletin, v. 84, p. 3731-3736.

Cooke, M.L., Simo, J.A., Underwood, C.A., and Rijken, P., 2006, Mechanical and stratigraphic controls on fracture patterns within carbonates and implications for groundwater flow. Sedimentary Geology, v. 184, p. 225-239.

Corbett, K., Friedman, M., and Spang, J., 1987, Fracture development and mechanical stratigraphy of Austin Chalk, Texas. American Association of Petroleum Geologists Bulletin, v. 71, p. 17-28.

Cox, R.T., 2009, Ouachita, Appalachian, and Ancestral Rockies deformation recorded in mesoscale structures on the foreland Ozark plateaus. Tectonophysics, v. 474, p. 674-683.

Croneis, C., 1930, Geology of the Arkansas Paleozoic area, with special reference to oil and gas possibilities. Arkansas Geological Survey Bulletin, v. 3, 457 p.

Davis, G.H., Reynolds, S.J., and Kluth, C., 2012, Structural Geology of Rocks and Regions (3rd ed.). John Wiley and Sons, Inc., New York, New York, 884 p.

Dholakia, S.K., Aydin, A., Pollard, D.D., Zoback, M.D., 1998, Fault controlled hydrocarbon pathways in the Monterey Formation, CA. American Association of Petroleum Geologists Bulletin, v. 82, p. 1551–1574.

Dvorkin, J., Nur, A., and Yin, H., 1994, Effective properties of cemented granular materials. Mechanics of Materials, v. 18, p. 351-366.

Dowell, J.C., Hutchinson, C.M., and Boss, S.K., 2005, Bedrock geology of Rogers Quadrangle, Benton County, Arkansas. Journal of the Arkansas Academy of Science, v. 59, p. 56-64.

Dunham, R. J., 1962, Classification of carbonate rocks according to depositional texture, in W. E. Ham, ed., Classification of carbonate rocks: AAPG Memoir 1, p. 108–121.

Eberli, G.P., Smith, L.B., Morettini, E., Al-Kharusi, L., 2003, Porosity partitioning in sedimentary cycles: implications for reservoir modeling. American Association of Petroleum Geologists Annual Meeting, Salt Lake City.

Engelder, T., 1982, Is there a genetic relationship between selected regional joints and contemporary stress within the lithosphere of North America? Tectonics, v. 1, no. 2, p. 161–177, doi:10.1029/TC001i002p00161.

Engelder, T., 1987, Joints and shear fractures in rock, in B. K. Atkinson, ed., Fracture mechanics of rock: London, Academic Press Inc., p. 27–69.

Engelder, T., Gross, M.R., Paul, P., 1997, An analysis of joint development in thick sandstone beds of the Elk Basin anticline, Montana-Wyoming. In: Hoak, T.E., Kalwitter, A.L., BLomquist, P.K. (Eds.), Fractured Reservoirs: Characterization and Modeling. Rocky Mountain Association of Geologists, Denver, Colorado, p. 1-18.

Engelder, T., Lash, G.G., and Uzcategui, R.S., 2009, Joint sets that enhance production from Middle and Upper Devonian gas shales of the Appalachian Basin. American Association of Petroleum Geologists Bulletin, v. 93, p. 857-889.

Erickson, S.G., 1996, Influence of mechanical stratigraphy on folding vs. faulting. Journal of Structural Geology, v. 18, p. 443-450.

Ethington, R.L., John, E.R., and James, R.D., 2012, Ordovician of the Saulk Megasequence in the Ozark Region of Northern Arkansas and parts of Missiouri and adjacent states. *in* J. R. Derby, R. D. Fritz, S. A. Longacre, W. A. Morgan, and C. A. Sternbach, eds., The great American carbonate bank: The geology and economic resources of the Cambrian–Ordovician Sauk megasequence of Laurentia: AAPG Memoir 98, p. 275–300.

Evans, K.R., Bassett, D.J., Mickus, K.L., Miller, J.F., Ethington, R.L., and Manger, W.L., 2013, Pre-Ouachita tectonism of the Ozarks. Geological Society of America North Central Section Presentation. May 2, 2013, Kalamazoo, Michigan.

Ferrill, D.A., McGinnis, R.N., Morris, A.P., Smart, K.J., Sickmann, Z.T., Bentz, M., Lehrmann, D., and Evans, M.A., 2014, Control of mechanical stratigraphy on bed-restricted jointing and normal faulting: Eagle Ford Formation, south-central Texas. American Association of Petroleum Geologists Bulletin, v. 98, p. 2477-2506.

Friedman, 1969, Structural analysis of fractures in cores from Saticoy field, Ventura county, California. American Association of Petroleum Geologists Bulletin, v. 53, p. 367-389.

Geologic Map of Missiouri, 1990, Missouri Department of Natural Resources, Division of Geology and Land Survey (now Geological Survey and Resource Assessment Division).

Geologic Map of Arkansas, http://www.geology.ar.gov/educational/geology_resources.htm. Accessed April 2015.

Gibbons, J., 1962, Shear and tension fracture patterns of northwest Arkansas. Arkansas Academy of Science Proceedings, v. 16, p. 19-22.

Ghosh, K., and Mitra, S., 2009, Structural controls of fracture orientations, intensity, and connectivity, Teton Anticline, Sawtooth Range, Montana. The American Association of Petroleum Geologists Bulletin, v. 93, p. 995-1014.

Gross, M.R., and Engelder, T., 1995, Strain accommodated by brittle failure in adjacent units of the Monterey Formation, U.S.A.: Scale effects and evidence for uniform displacement boundary conditions. Journal of Structural Geology, v. 17, p. 1303-1318.

Gross, M.R., Fischer, M.P., Engelder, T., and Greenfield, R.J., 1995, Factors controlling joint spacing in interbedded sedimentary rocks: integrating numerical models with field observations from the Monterey Formation, USA. In: Ameen, M.S., (ed.), 1995, Fractography: fracture topography as a tool in fracture mechanics and stress analysis. Geological Society Special Publication, v. 92, p. 215-233.

Hale-Erlich, W.S., and Coleman, J.L., 1993, Ouachita-Appalachian Juncture: a Paleozoic transpressional zone in the southeastern U.S.A. The American Association of Petroleum Geologists Bulletin, v. 77, p. 552-568.

Hancock, P. L., 1985, Brittle microtectonics: Principles and practice: Journal of Structural Geology, v. 7, no. 3–4, p. 437–457.

Hancock, P.L., and Bevan, T.G., 1987, Brittle modes of foreland deformation. In: Coward, M.P., Dewey, J.F., and Hancock, P.L. (eds.), Continental extension tectonics. Geological Society Special Publication, v. 28, p. 127-137.

Hancock, P.L., and Engelder, T., 1989, Neotectonic joints, Geological Society of America Bulletin, v. 101, p. 1197-1208.

Harris, J.F., Taylor, G.L., Walper, J.L., 1960, Relation of deformational fractures in sedimentary rocks to regional and local structures. American Association of Petroleum Geologists Bulletin, v. 4, p. 1853-1873.

Holst, T.B., and Foote, G.R., 1981, Joint orientation in Devonian rocks in the northern portion of the lower peninsula of Michican. Geological Society of America Bulletin, v. 92, p. 163-177.

Hudson, M.R., 2000, Coordinated strike-slip and normal faulting in the southern Ozark dome of northern Arkansas: deformation in a late Paleozoic foreland. Geology, v. 28, p. 511-514.

Hudson, M.R., 2002, Three-phase late Paleozoic deformation of the southern Ozark Dome, western Buffalo River region, northern Arkansas. Abstracts with Programs – Geological Society of America, v. 34, p. 79 (Abstract Only).

Hudson, M.R., and Cox, R.T., 2003, Late Paleozoic tectonics of the southern Ozark dome: Field trip guidebook for Joint South-Central and Southeastern Sections, Geological Society of America, Tennessee Division of Geology Report of Investigations 51, p. 15-32.

Koenig, J.W., 1967, The Ozark uplift and midcontinent Silurian and Devonian stratigraphy. Tulsa Geological Society Digest, v. 35, p. 119-147.

Ladeira, F.L., and Price, N.J., 1981, Relationship between fracture spacing and bed thickness. Journal of Structural Geology, v. 3, p. 179-183.

Lamarche, J., Lavenu, A.P., Gauthier, B.D., Guglielmi, Y., and Jayet, O., 2012, Relationships between fracture patterns, geodynamics and mechanical stratigraphy in Carbonates (South-East Basin, France). Tectonophysics, v. 581, p. 231-245.

Lane, H.R., and DeKeyser, T.L., 1980, Paleogeography of the late Early Mississippian (Tournaisian 3) in the central and southwestern United States; in, Paleozoic Paleogeography of West-central United States, T.D. Fouch and E.R. Magathan, eds.: Society of Economic Paleontologists and Mineralogists, Rocky Mountain Section, p. 149-159.

Laubach, S.E., Olson, J.E., and Gross, M.R., 2009, Mechanical and fracture stratigraphy. The American Association of Petroleum Geologists Bulletin, v. 93, p. 1413-1426.

Lucia, F.J., 1995, Rock-fabric/petrophysical classification of carbonate pore space for reservoir characterization. American Association of Petroleum Geologists Bulletin, v. 79, p. 1275-1300.

Manger, W.L, Shelby, P.R., Farris, S.G., 1988, Devonian-Lower Mississippian lithostratigraphy, northwestern Arkansas. The Compass, v. 65, no.4: Sigma Gamma Epsilon, Norman, Oklahoma.

Maliva, R.G., and Siever, R., 1989, Nodular chert formation in carbonate rocks. The Journal of Geology, v. 97, p. 421-433.

Marin, B.A., Clift, S.J., Hamlin, H.S., and Laubach, S.E., 1993, Natural fractures in Sonora Canyon sandstones, Sonora and Sawyer fields, Sutton County, Texas. Society of Petroleum Engineers Paper No. 25895, p. 523-531.

Mazzullo, S.J., and Wilhite, B.W., 2010, Chert, tripolite, spiculite, chat: What's in a name? Kansas Geological Society Bulletin, v. 85, p. 21-24.

McFarland, J.D., 2004, Stratigraphic summary of Arkansas. Arkansas Geological Survey Information Circular, v. 36, p. 1-38.

Morettini, E., Thompson, A., Eberli, G.P., Rawnsley, K., Wenche, A., Christman, P., Cortis, T., Foster, K., Hitchings, V.H., Kolkman, W., Konijenburg, J.H., 2005, Combining high-resolution sequence stratigraphy and mechanical stratigraphy for improved reservoir characterization in the Fahud field of Oman. GeoArabia, v. 10, P. 17-44.

Narr, W., Currie, J.B., 1982, Origin of fracture porosity—example from Altamont Field, Utah. American Association of Petroleum Geologists Bulletin, v. 66, p. 1231–1247.

Narr, W., and Suppe, J., 1991, Joint spacing in sedimentary rocks. Journal of Structural Geology, v. 13, p. 1037-1048. \

Nelson, R.A., 1985, Geologic analysis of naturally fractured reservoirs. Houston, Gulf Publishing, 320 p.

Nieto-Samaniego, Á.F., Alaniz- Álvarez, S.A., 1997, Origin and tectonic interpretation of multiple fault patterns. Tectonophysics, v. 270, p.197-206.

Olson, J.E., Laubach, S.E., Lander, R.L., 2007, Combining diagenesis and mechanics to quantify fracture aperture, distributions, and fracture pattern permeability. In: Lonergan, L., Jolley, R.J., Sanderson, D.J., Rawnsley, K., (Eds.), Fracture Reservoirs, v. 270. Geological Society, London, p. 97-112. Special Publication.

Pascal. C., Angelier, J., Cacas, M.C., and Hancock, P.L., 1997, Distribution of joints: Probabilistic modeling and case study near Cardiff (Wales, U.K.). Journal of Structural Geology, v. 19, p. 1273-1274.

Peacock, D.C.P., 2001, The temporal relationship between joints and faults. Journal of Structural Geology, v. 23, p. 329-341.

Pollard, D. D., and A. Aydin, 1988, Progress in understanding jointing over the past century: Geological Society of America Bulletin, v. 100, p. 1181–1204.

Pollard, D.D., and Segall, P., 1987, Theoretical displacements and stresses near fractures in rocks: with applications to faults, joints, veins, dikes and solution surfaces. In: Atkinson, B.K. (ed.), Fracture Mechanics of Rock, Academic Press, London (1987), p. 277-349.

Proceq Literature, "Rebound Hammer- 'Q'-Value," www.silverschmidt.com/home/home.html. Accessed March, 2015.

Rogers, M.R., 2001, Deposition and diagenesis of Mississippian chat reservoirs, north-central Oklahoma. American Association of Petroleum Geologists Bulletin, v. 85, p. 115-129.

Shackleton, J.R., Cooke, M.L., Sussman, A.J., 2005, Evidence for temporally changing mechanical stratigraphy and effects on vein-network architecture. Geology, v. 33, p. 101-104.

Shelby, P.R., 1986, Depositional history of the St. Joe-Boone formations in northern Arkansas. [M.S. Thesis]. Department of Geology, University of Arkansas, Fayetteville, Arkansas. 92 pp.

Stearns, D.W., and Friedman, M., 1972, Reservoirs in fractured rock. In: King, R.E. (ed.), Stratigraphic oil and gas fields – classification, exploration methods, and case histories. American Association of Petroleum Geologists Memoir, v. 16, p. 82-106.

Sullivan, R.A., and Boss, S.K., 2002, Revised bedrock geology of War Eagle Quadrangle, Benton County, Arkansas. Journal of the Arkansas Academy of Science, v. 56, p. 2002.

Underwood, C.A., Cooke, M.L., Simo, J.A., Muldoon, M.A., 2003, Stratigraphic controls on vertical fracture patterns in Silurian dolomite, northeastern Wisconsin. American Association of Petroleum Geologists Bulletin, v. 87, p. 121-142.

Van de Steen, B., Vervoort, A., and Sahin, K., 2002, Influence of internal structure of crinoidal limestone on fracture paths. Engineering Geology, v. 67, p. 109-125.

Verbeek, E.R., and Grout, M.A., 1983, Fracture history of the northern Piceance Creek basin, northwestern Colorado. In: J.H., Gary (ed.), Proceedings of the 16th Oil Shale Symposium, p. 26-44.

Warpinski, N.R., and Teufel, L.W., 1989, In situ stresses in low permeability, nonmarine rocks. Journal of Petroleum Technology, v. 41, p. 405-414.

Wennberg, O.P., Svana, T., Azizzadeh, M., Aqrawi, A.M.M., Brockbank, P., Lyslo, K.B., and Ogilvie, S., 2006, Fracture intensity vs. mechanical stratigraphy in platform top carbonates: the Aquitanian of the Asmari Formation, Khaviz Anticline, Zagros, SW Iran. Petroleum Geology, v. 12, p. 235-245.

Young, L. M., L. C. Fiddler, and R. W. Jones, 1972, Carbonate facies in Ordovician of northern Arkansas. AAPG Bulletin, v. 56, p. 68–80.

APPENDIX A

FRACTURE ORIENTATION DATA

Strike	Dip	Direction
001a		
186	74	N
324	79	NE
9	62	ESE
120	89	SW
39	87	SE
9	82	E
320	88	SW
304	89	SW
4	90	
001b		
202	69	W
151	65	W
191	86	W
198	68	WNW
292	89	SW
13	81	SE
296	90	
35	80	SE
235	90	
192	90	
120	90	
211	90	
208	88	SE
230	90	
200	90	
301	90	
192	84	NW
19	80	SE
254	90	
260	90	
173	90	
30	90	
32	90	
48	90	
001c		
8	90	
72	90	
13	90	
16	90	
4	64	E
65	78	SE
20	90	
290	90	
348	90	
65	78	SE
89	90	
92	90	
260	90	
255	90	
002a		
179	55	W
189	64	W
58	90	
190	76	W
118	90	
193	90	
144	87	W
71	90	
64	90	
53	90	
186	73	W
182	90	
152	90	
121	90	
63	90	
41	90	
002b		
91	90	
11	90	
3	90	
6	90	
64	90	
86	90	
135	60	
75	60	
65	90	
122	90	
94	60	
74	90	
79	90	
20	90	
104	90	
10	90	
46	90	
31	90	
63	76	E
15	90	
14	90	
002c		
64	70	S
10	88	E
15	90	
240	90	
230	90	
245	75	SE
174	90	
242	90	
204	90	
002d		
203	90	
310	90	
310	90	
19	90	
76	75	W
141	90	
162	90	
32	90	
45	90	
315	90	
40	90	
19	90	
141	88	SW
28	90	
002e		
21	90	

66	90	
44	90	
140	90	
124	90	
94	70	SW
129	90	
230	90	
130	90	
209	90	
200	90	
40	80	SE
8	89	SW
41	90	
65	90	
88	90	
24	90	
002f		
43	90	
44	90	
6	90	
275	90	
105	90	
31	90	
42	75	NW
24	90	
49	90	
35	90	
50	90	
22	90	
5	90	
7	90	
23	90	
2	90	
31	90	
18	90	
350	90	
22	85	NW
26	86	NW
22	76	NW

003a		
36	90	
31	90	
326	90	
45	90	
320	90	
25	90	
320	90	
305	90	
330	90	
329	90	
26	90	
35	90	
22	90	
004a		
46	44	NE
35	43	NE
92	35	N
98	40	N
106	75	N
70	90	
80	90	
79	77	SE
50	72	SE
004b		
78	71	NW
94	86	NE
76	68	N
102	82	NE
111	84	N
29	46	NW
110	74	N
349	74	E
76	70	NW
47	78	SE
40	85	SE
004d		
71	78	NW
109	90	

98	90	
140	90	
57	90	
136	90	
42	81	SE
126	90	
130	90	
120	90	
84	80	SE
62	70	NW
160	90	
58	85	SE
110	75	N
68	89	N
59	72	NW
95	90	
356	70	W
335	80	NW
100	63	N
339	82	NW
004e		
94	90	
80	82	N
75	90	
45	71	NW
41	90	
135	90	
90	90	
129	90	
50	90	
30	85	SE
110	75	N
115	80	NE
110	82	NE
46	72	NW
006a		
70	72	SE
66	74	SE
341	80	SW

72	54	SE
344	80	SW
359	90	
350	78	SE
352	75	SE
341	68	SE
2	75	SW
75	70	SE
310	90	
50	80	SE
45	55	SW
46	72	SE
85	70	SE
82	69	SE
316	45	E
70	90	
78	90	
80	90	
65	90	
73	90	
72	90	
75	90	
74	90	
344	90	
72	90	
350	90	
105	90	
95	90	
120	90	
131	90	
129	90	
72	90	
76	90	
104	90	
75	90	
78	90	
130	90	
74	90	
74	90	

76	90	
006b		
90	80	S
100	90	
104	90	
71	70	SE
52	90	
11	84	E
70	90	
79	90	
352	90	
25	90	
64	90	
331	90	
58	90	
66	90	
341	90	
60	90	
79	90	
006c		
80	78	SE
74	82	SE
73	90	
78	90	
66	90	
81	90	
78	90	
354	90	
84	89	SE
109	90	
74	80	SE
79	79	SE
55	90	
128	90	
298	90	
327	90	
74	82	SE
30	90	
80	90	

55	90	
119	90	
62	90	
69	90	
32	90	
76	85	SE
006d		
76	90	
136	90	
98	90	
326	90	
294	90	
298	90	
346	90	
286	90	
344	90	
11	90	
56	90	
108	90	
288	90	
325	90	
262	90	
349	90	
292	90	
199	90	
170	90	
164	90	
75	89	SW
72	88	SW
70	90	
336	90	
81	86	SW
40	90	
81	90	
341	90	
36	90	
347	90	
349	90	
68	84	SW

45	80	SW
49	90	
46	90	
40	90	
70	90	
007a		
72	89	SE
68	90	
304	75	NE
61	82	NNE
335	90	
65	80	SE
79	90	
72	86	SE
52	85	SE
70	88	SE
286	75	N
68	90	
322	90	
330	90	
70	72	SE
69	90	
328	90	
75	72	SE
61	90	
72	90	
41	65	SE
356	90	
298	59	N
59	80	NW
345	90	
55	72	NW
008a		
158	80	NE
160	80	NE
157	90	
89	90	
160	90	
72	90	

170	90	
177	90	
168	82	NE
160	90	
45	90	
175	90	
57	84	NNE
157	90	
164	90	
75	78	NE
172	90	
179	90	
180	90	
175	90	
179	90	
175	90	
182	90	
169	90	
008b		
190	90	
200	90	
212	90	
185	90	
183	90	
233	90	
174	90	
244	90	
179	90	
170	90	
180	90	
60	90	
179	90	
58	90	
199	90	
180	90	
65	90	
70	90	
008c		
354	90	

52	90	
334	90	
347	90	
346	90	
77	90	
4	90	
95	90	
353	90	
347	90	
350	90	
332	90	
37	90	
92	90	
84	90	
354	90	
79	90	
349	90	
350	90	
84	90	
346	90	
349	90	
346	90	
344	90	
350	90	
009a		
75	90	
59	90	
71	90	
72	90	
69	90	
64	90	
74	90	
60	90	
65	90	
88	90	
345	90	
40	90	
25	90	
60	90	

40	90	
40	90	
76	55	NE
72	73	N
82	60	N
55	60	N
009c		
70	90	
66	90	
31	90	
010c		
174	90	
153	90	
180	90	
181	90	
165	90	
154	90	
163	75	E
150	90	
170	90	
139	90	
141	90	
222	90	
166	90	
120	90	
60	70	SE
162	90	
143	80	NE
177	90	
145	80	NE
010d		
331	90	
349	90	
354	90	
350	90	
0	90	
84	90	
357	90	
69	90	

344	90	
358	90	
355	90	
84	90	
92	90	
347	90	
350	90	
340	90	
344	90	
93	90	
100	90	
354	90	
77	90	
351	90	
354	90	
352	90	
347	90	
64	90	
98	90	
332	90	
61	90	
011a		
136	90	
31	90	
92	75	SE
214	84	N
195	44	N
210	90	
112	90	
100	90	
208	72	NW
310	90	
275	90	
314	90	
210	75	NW
200	75	NW
320	90	
220	75	NW
314	90	

318	90	
315	90	
205	61	NW
136	90	
135	90	
135	90	
58	90	
68	76	NW
318	90	
315	90	
142	90	
139	90	
320	90	
200	50	N
310	90	
235	69	N
238	90	
315	90	
10	48	N
239	90	
315	90	
228	68	N
240	90	
315	90	
202	85	N
210	90	
012a		
338	82	NE
245	70	SE
270	80	S
255	70	S
335	90	
234	76	S
318	90	
236	72	SE
326	90	
257	86	S
247	90	
134	75	SW

346	90	
354	90	
324	65	S
322	85	SW
336	90	
298	90	
270	90	
303	90	
305	90	
012b		
330	75	SE
9	90	
342	90	
92	90	
355	90	
71	85	NW
320	90	
338	90	
222	90	
234	90	
239	90	
274	90	
258	90	
324	75	SW
264	90	
351	90	
260	90	
307	90	
315	79	SW
325	90	
255	90	
321	90	
216	90	
296	90	
202	90	
255	90	
012b Chert		
224	90	
238	90	

229	90	
225	90	
230	90	
258	90	
229	90	
334	90	
343	90	
347	90	
316	90	
322	90	
315	90	
013a		
333	78	NE
327	90	
355	90	
346	85	E
326	85	SW
314	90	
219	90	
11	90	
241	90	
240	90	
339	90	
013b		
212	90	
4	90	
57	82	SE
84	90	
290	75	SW
309	90	
304	90	
276	76	S
294	74	N
347	90	
2	90	
355	90	
240	80	NW
234	90	
322	85	SW

321	85	SW
329	86	SW
337	87	SW
325	85	SW
325	85	SW
317	79	SW
336	79	SW
317	80	SW
318	82	SW
314	75	SW
340	82	SW
345	75	SW
195	90	
242	90	
245	70	N
300	66	SW
305	76	SW
322	80	SW
335	77	SW
300	88	SW
301	72	SW
233	90	
350	90	
235	90	
239	85	SE
013c		
226	90	
342	90	
238	90	
337	75	SW
335	90	
350	85	NE
356	85	NE
357	85	NE
349	87	NE
331	90	
344	90	
2	90	
285	90	

273	90	
0	90	
1	90	
340	90	
351	90	
4	90	
36	90	
359	90	
1	90	
345	90	
014a		
76	90	
84	80	S
95	76	N
23	72	SE
95	78	S
129	82	S
34	80	SE
26	75	SE
98	75	NE
89	76	N
72	90	
88	60	N
33	86	SE
97	90	
29	80	SE
77	88	S
29	76	SE
81	84	N
30	80	E
84	90	
45	85	E
46	75	SE
350	90	
56	90	
71	54	NW
014b		
69	78	SE
22	56	NW

107	79	NE
12	67	NW
106	90	
69	90	
10	63	NW
102	90	
56	90	
19	90	
56	90	
26	90	
71	90	
45	90	
71	90	
016c		
318	90	
331	90	
4	90	
336	90	
327	80	NE
1	90	
339	90	
325	70	E
311	90	
307	90	
310	90	
302	90	
318	90	
305	90	

APPENDIX B

FRACTURE STEREONETS

OZ 001a

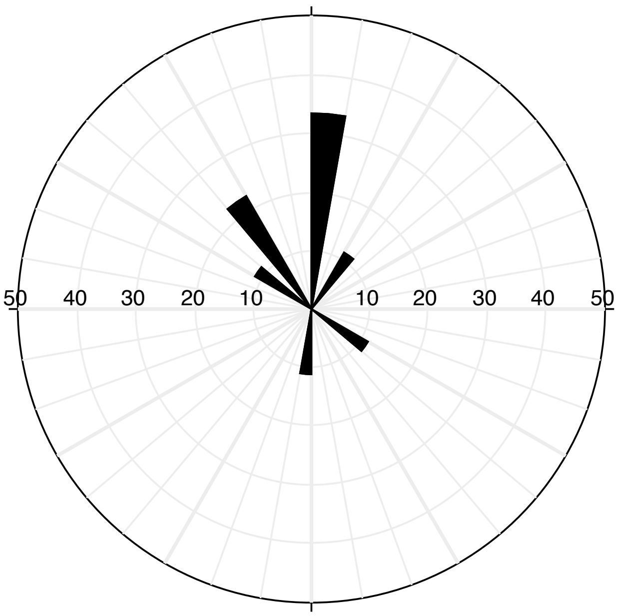

OZ 001b

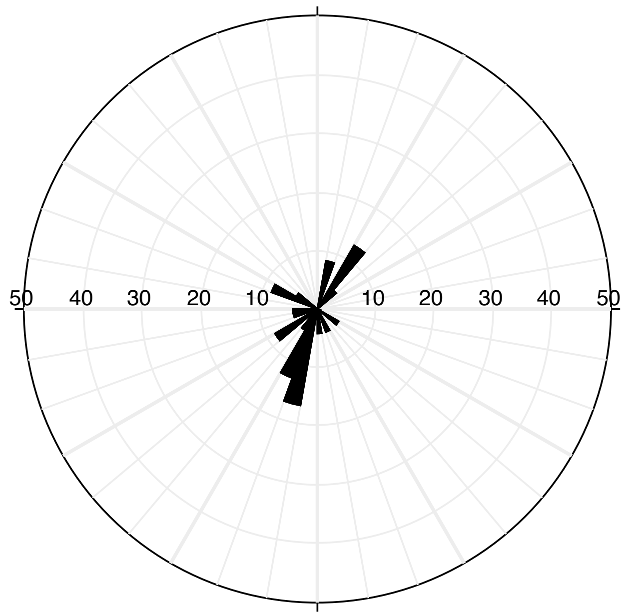

OZ 001c

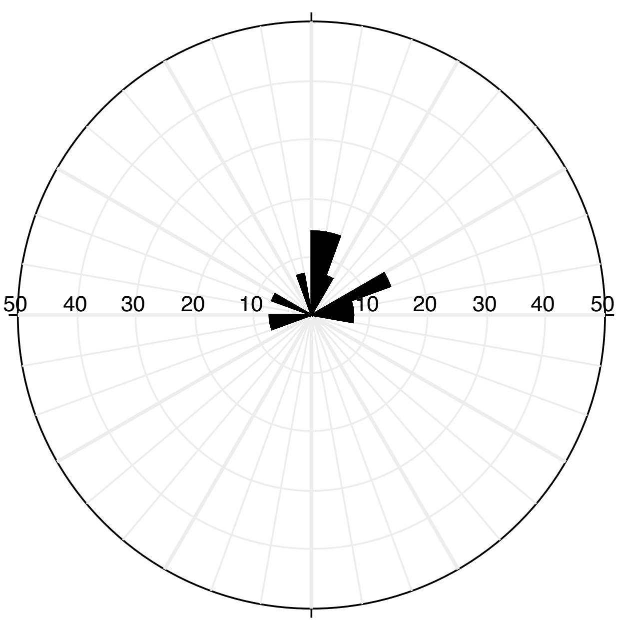

OZ 002a

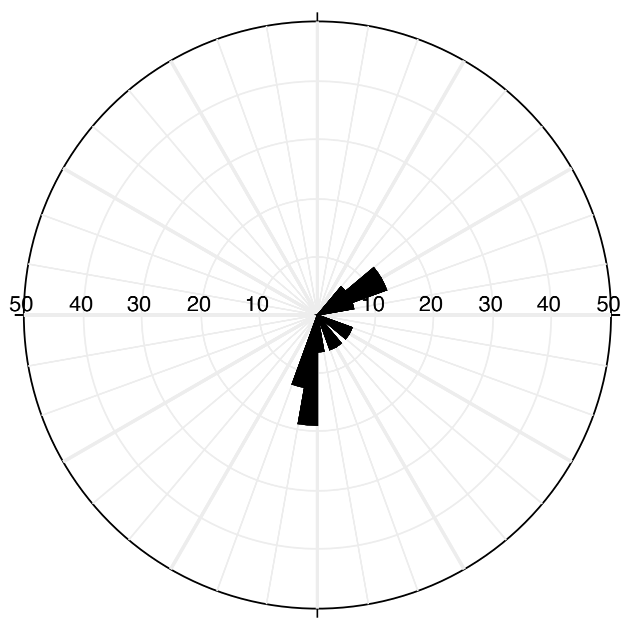

OZ 002b

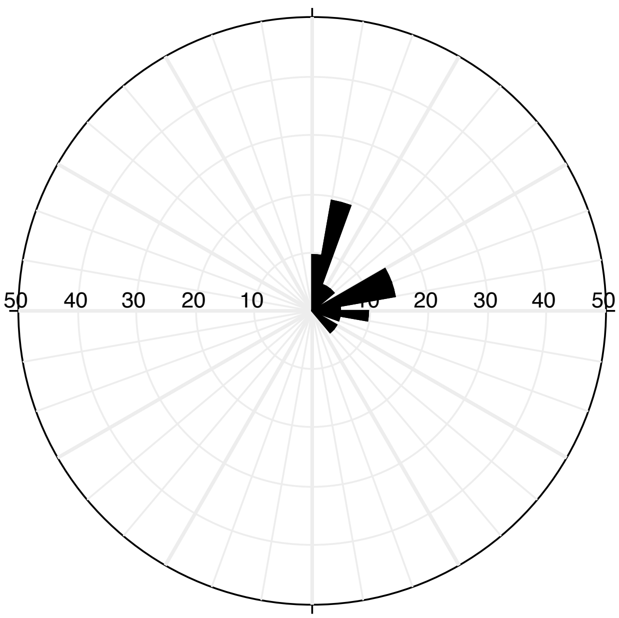

OZ 002c

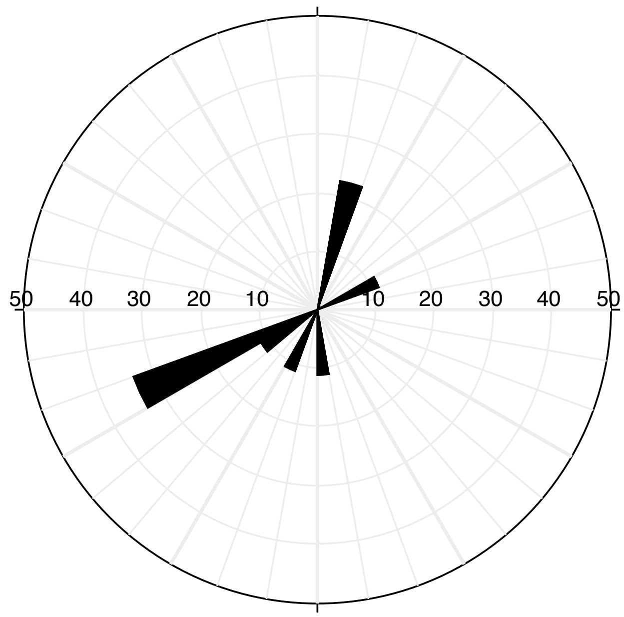

OZ 002d

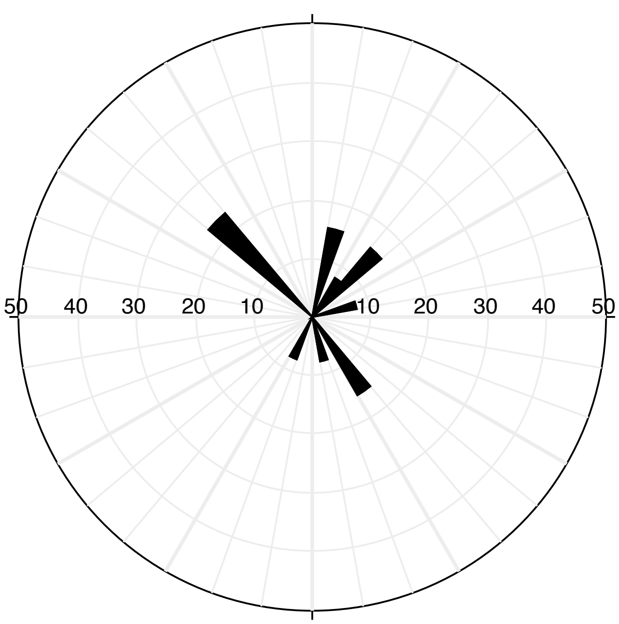

OZ 002e

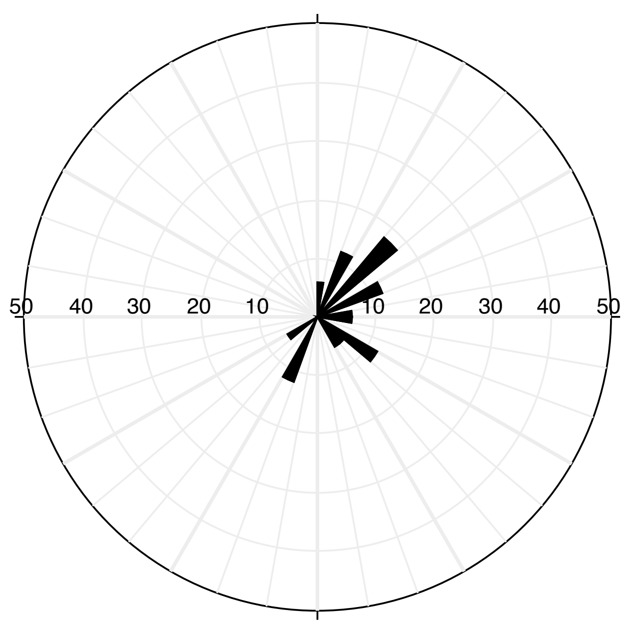

OZ 002f

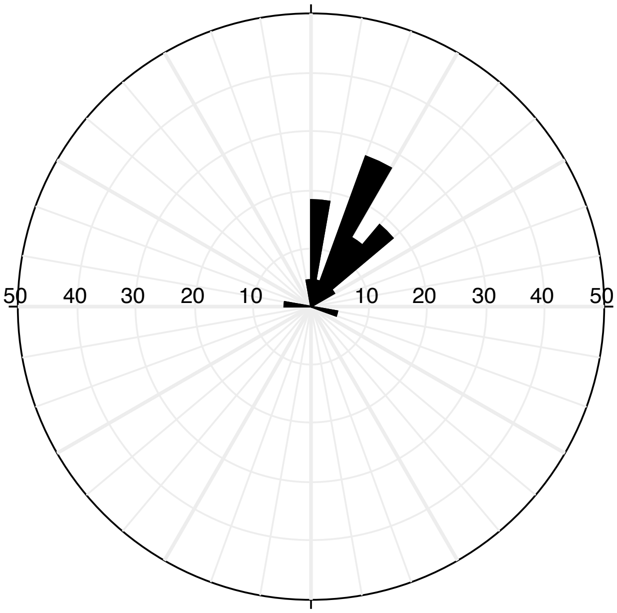

OZ 003a

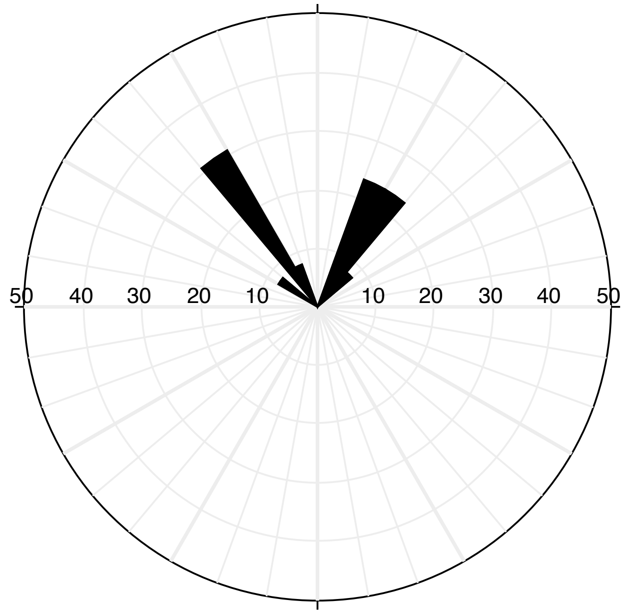

OZ 004a

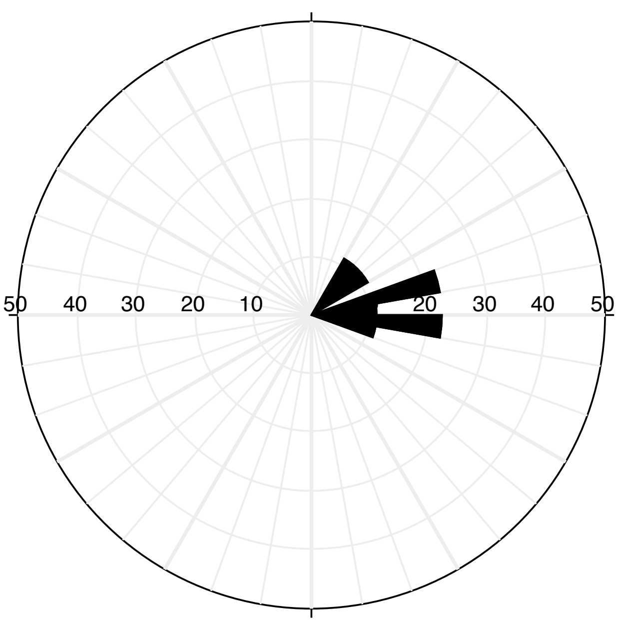

OZ 004b

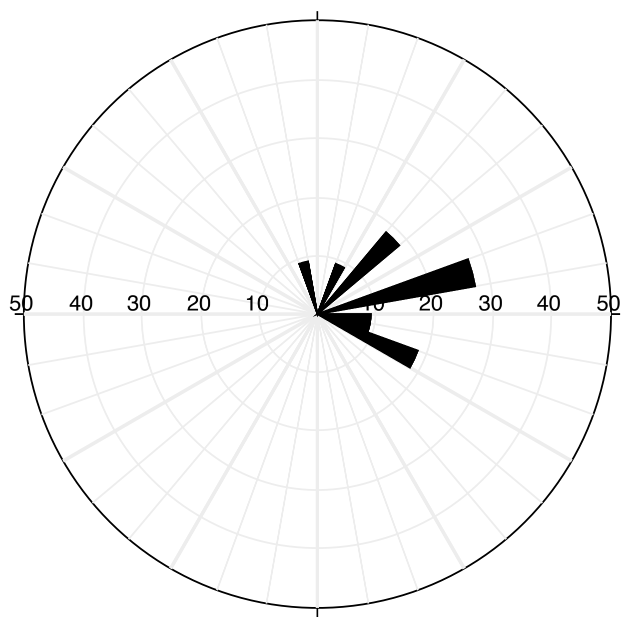

OZ 004d

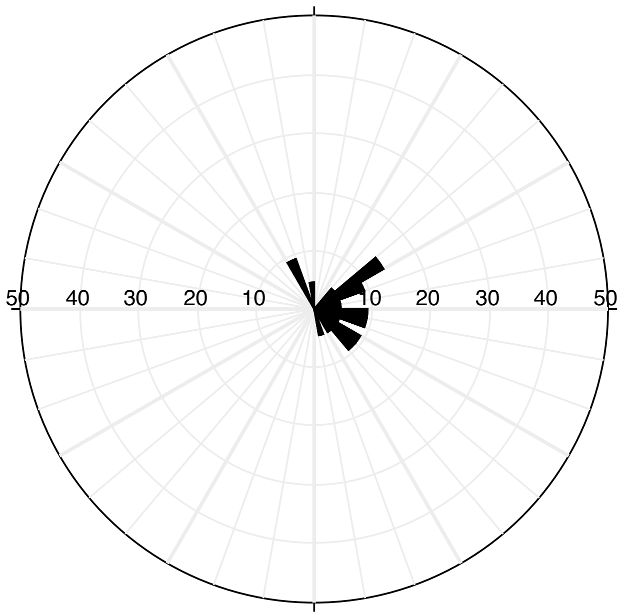

OZ 004e

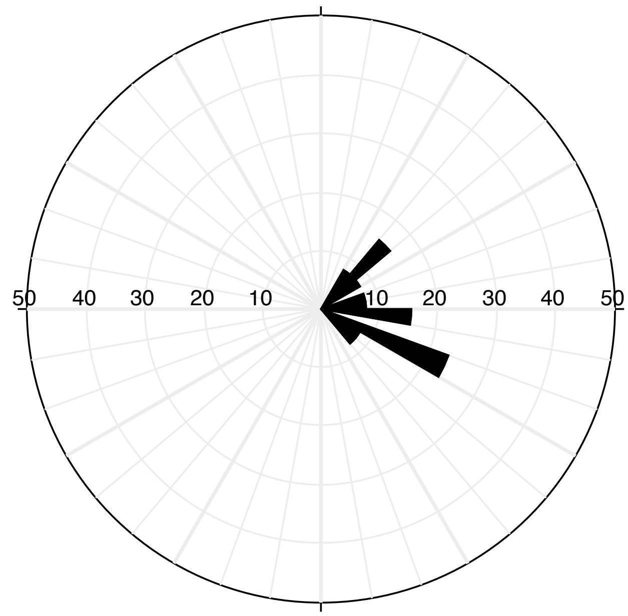

OZ 006a

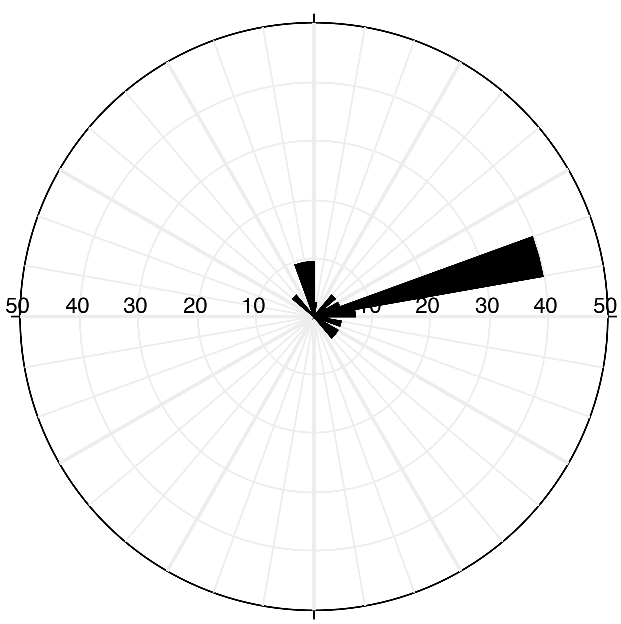

OZ 006b

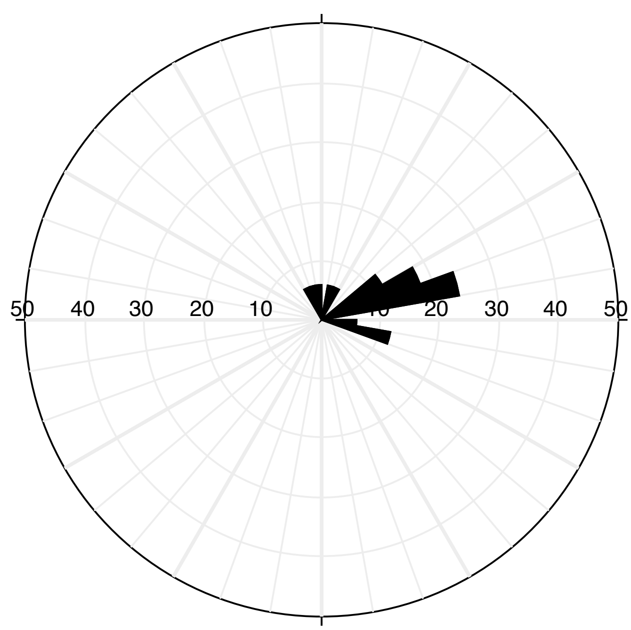

OZ 006c

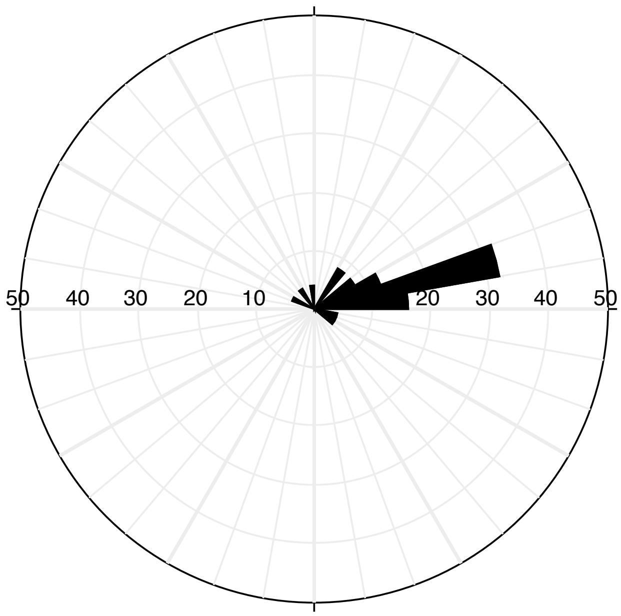

OZ 006d

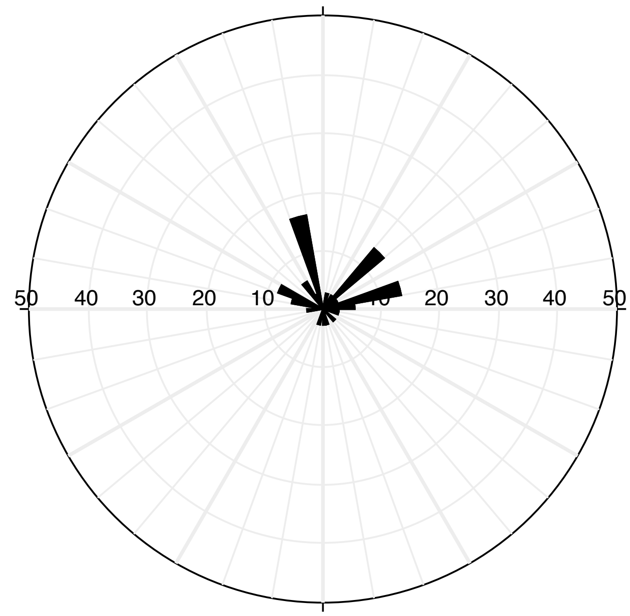

OZ 007a

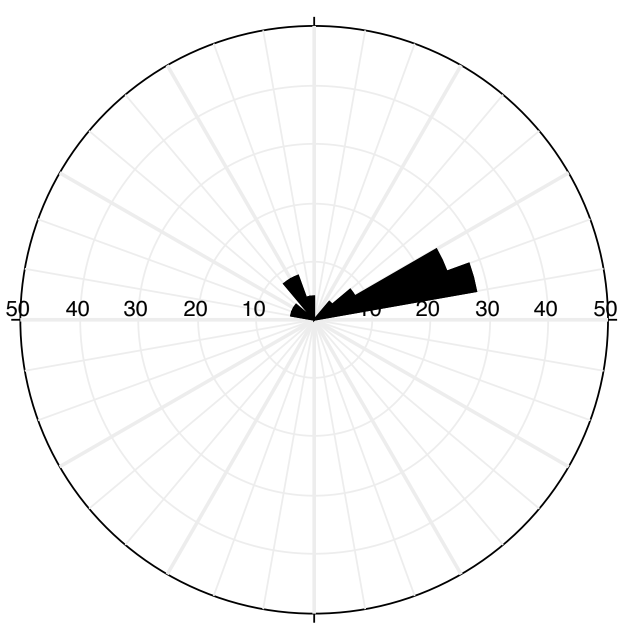

OZ 008a

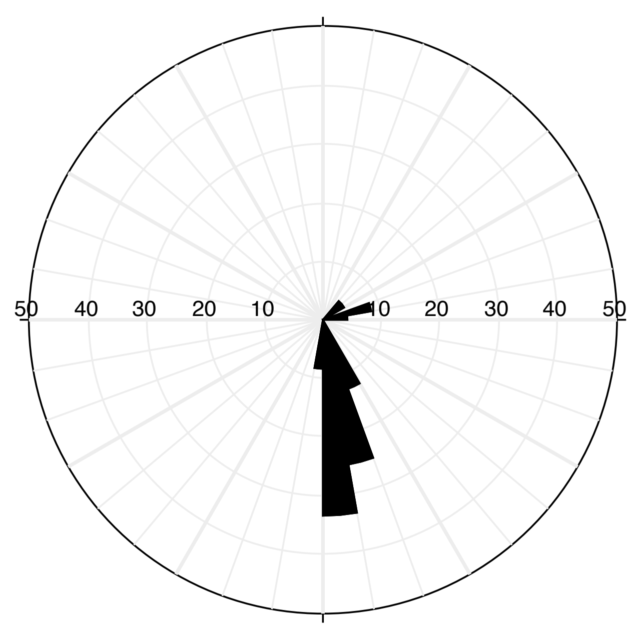

OZ 008b

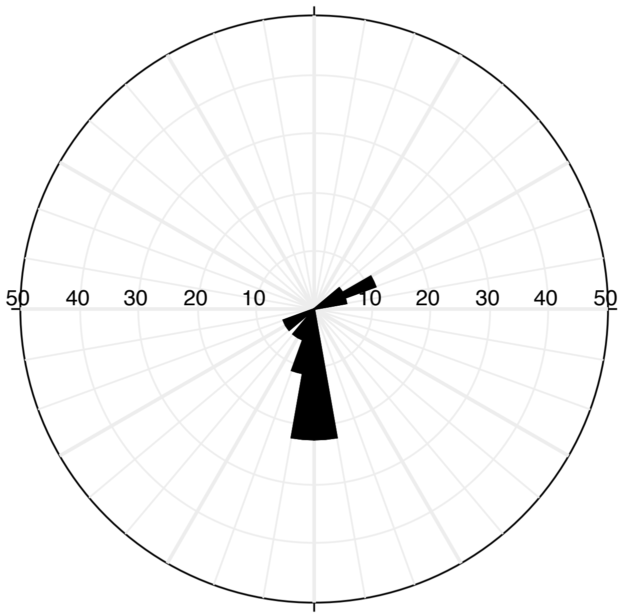

OZ 008c

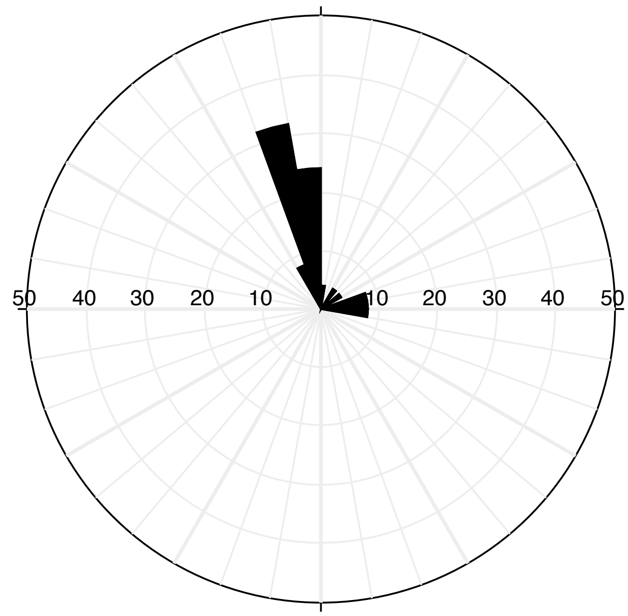

OZ 009a

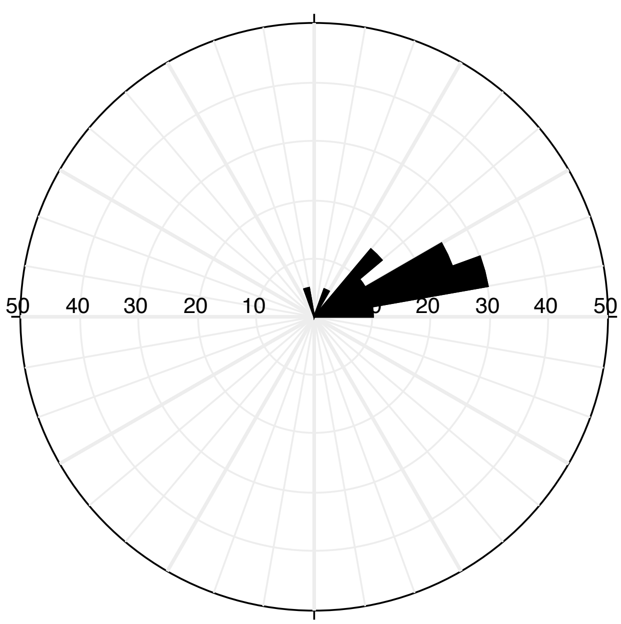

OZ 009c

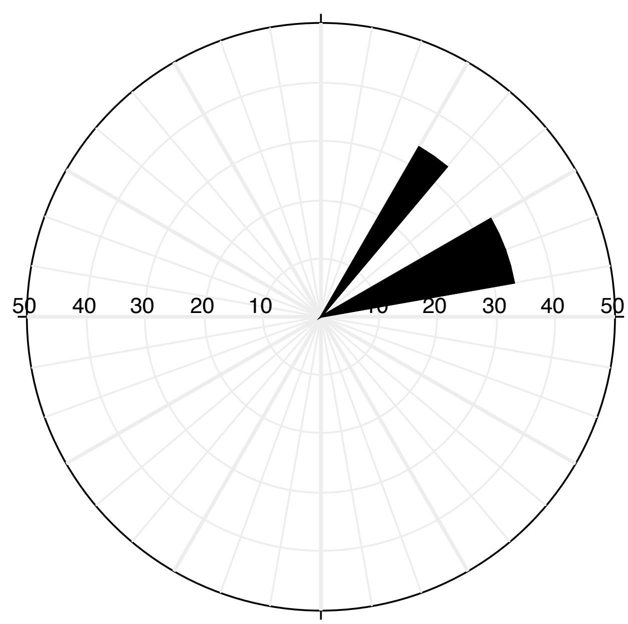

OZ 010c

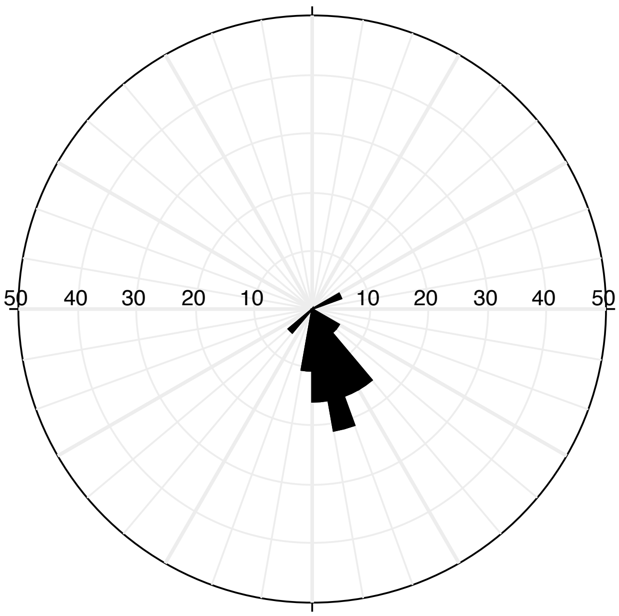

OZ 010d

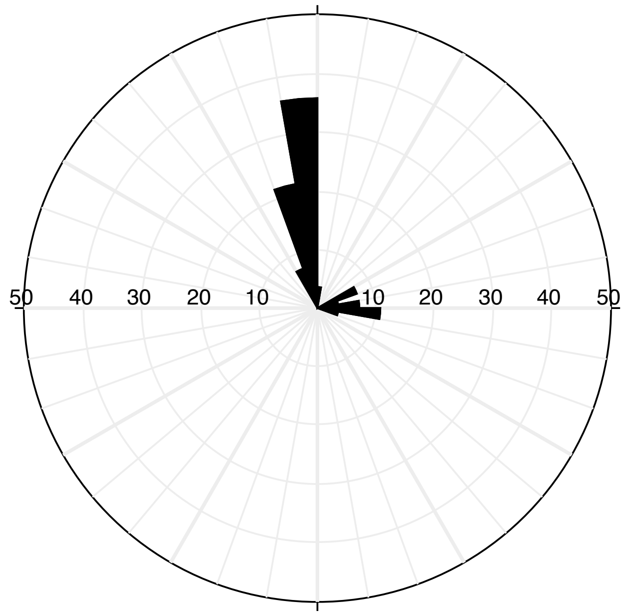

OZ 011a

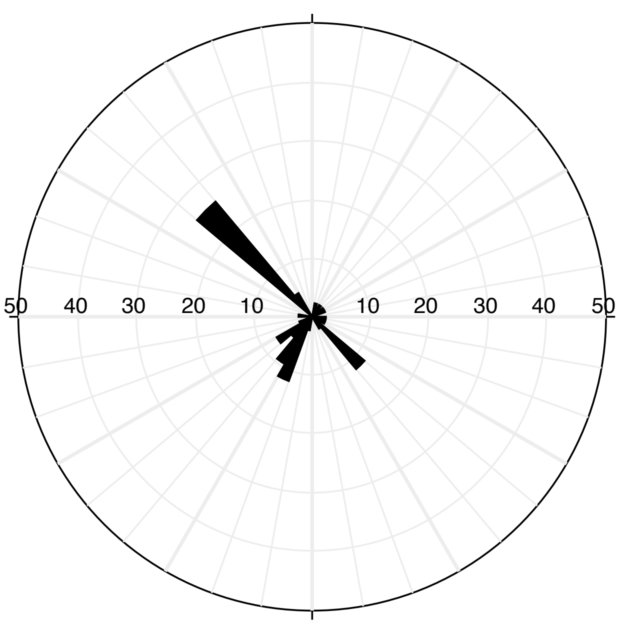

OZ 012a

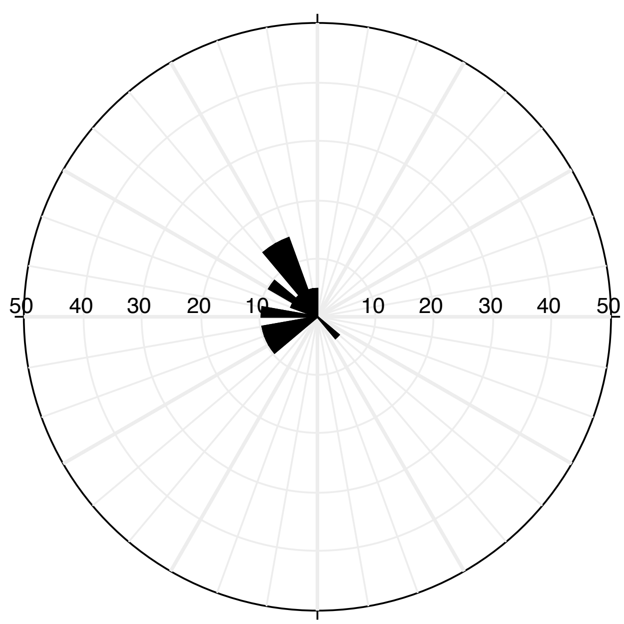

OZ 012b

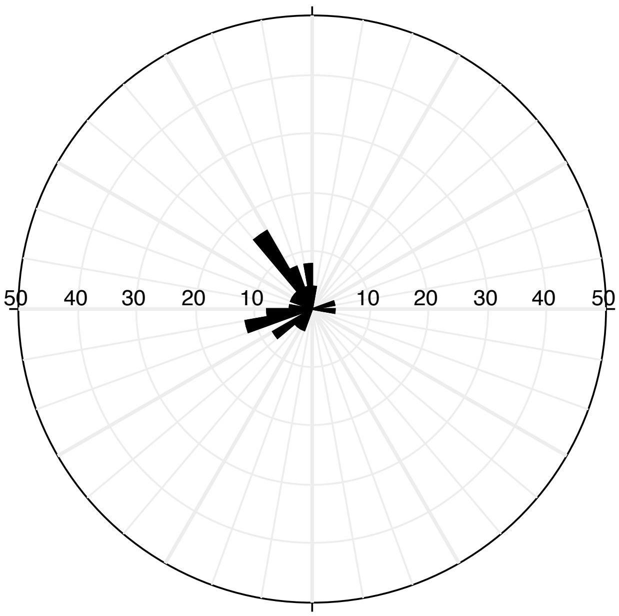

OZ 012b CHERT

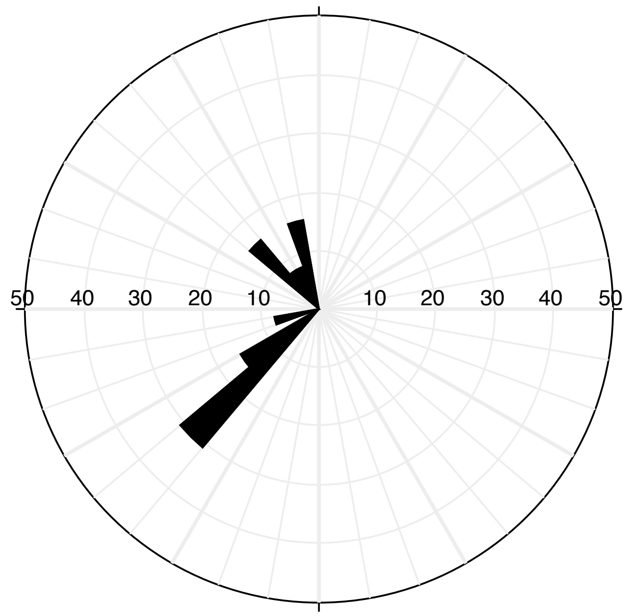

OZ 013a

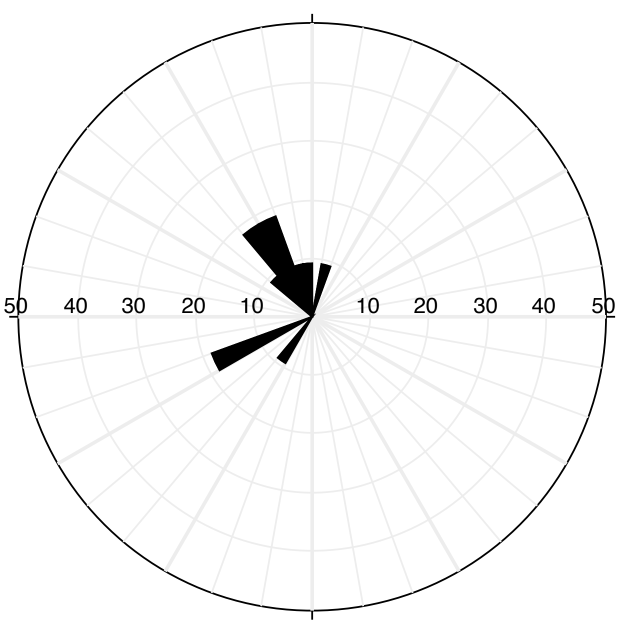

OZ 013b

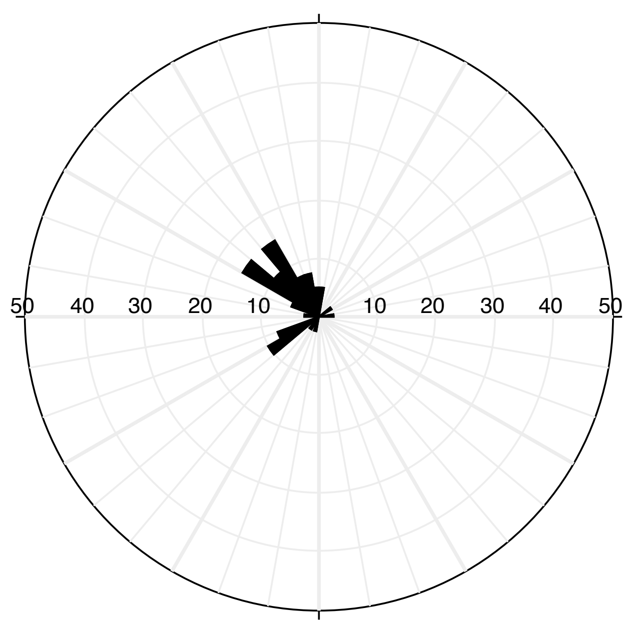

OZ 013c

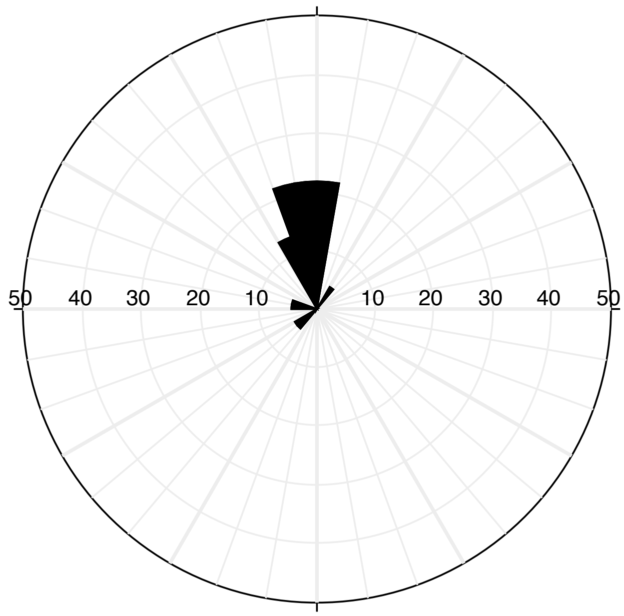

OZ 014a

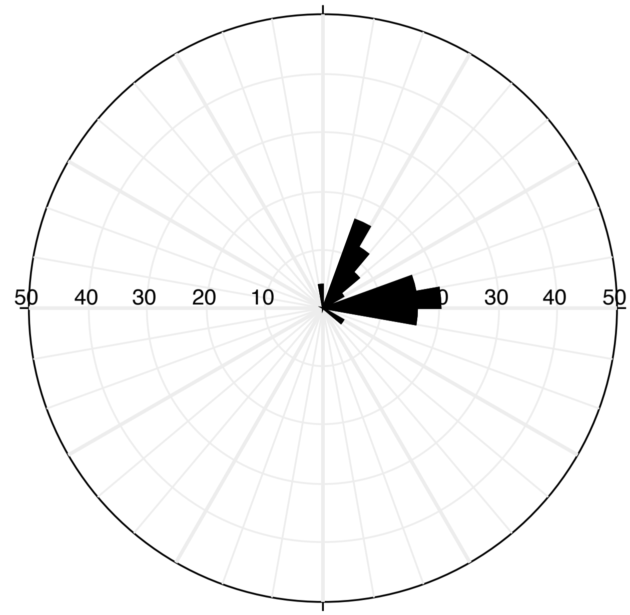

OZ 014b

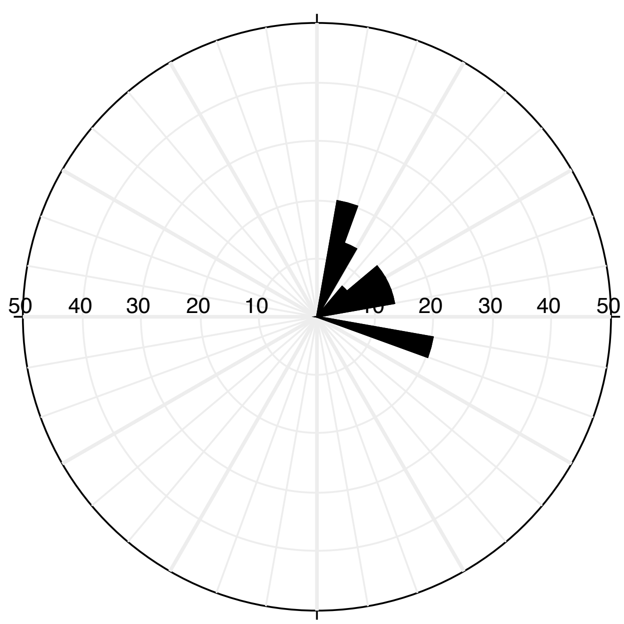

OZ 016c

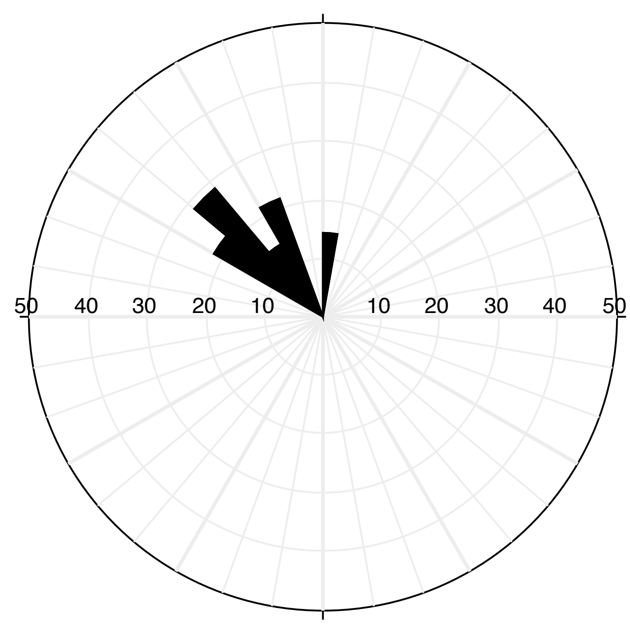

APPENDIX C

Q VALUE SERIES MEASUREMENTS

001a

Impact counter	Name	Date & Time	Mean value	Averaging mode	Upper outliers	Lower outliers	Valid/Total	Std dev.	Conv. curve	Form factor	Carbonation factor
615		03/10/2003 5:41 AM	43.3 Q	Mean	0	0	10/10	7.6 Q	Curve EU	Cube 150mm (100%)	1.00

Q-Values diagram [measurement order]

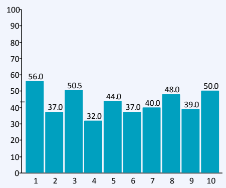

Q-Values

56.0
37.0
50.5
32.0
44.0
37.0
40.0
48.0
39.0
50.0

Statistics

Measurements	N = 10
Invalid measurements	Ni = 0 (0%)
Mean value	f = 43.3 Q
Standard deviation	s = 7.6 Q

Settings

Averaging mode	Mean
Conversion curve	Curve EU
Form factor	Cube 150mm (100%)
Carbonation factor	1.00
Unit	Q
Serial number	SH01-006-0084
Spring type	SilverSchmidt N

Comment

[Add]

001b

Impact counter	Name	Date & Time	Mean value	Averaging mode	Upper outliers	Lower outliers	Valid/Total	Std dev.	Conv. curve	Form factor	Carbonation factor
625		03/10/2003 5:46 AM	57.6 Q	Mean	0	0	10/10	5.5 Q	Curve EU	Cube 150mm (100%)	1.00

Q-Values diagram [ordered by value]

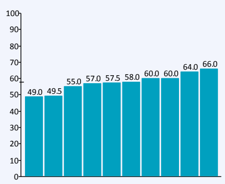

Q-Values

49.0
57.0
60.0
49.5
66.0
58.0
60.0
55.0
64.0
57.5

Statistics

Measurements	N = 10
Invalid measurements	Ni = 0 (0%)
Mean value	f = 57.6 Q
Standard deviation	s = 5.5 Q

Settings

Averaging mode	Mean
Conversion curve	Curve EU
Form factor	Cube 150mm (100%)
Carbonation factor	1.00
Unit	Q
Serial number	SH01-006-0084
Spring type	SilverSchmidt N

Comment

[Add]

001c

Impact counter	Name	Date & Time	Mean value	Averaging mode	Upper outliers	Lower outliers	Valid/Total	Std dev.	Conv. curve	Form factor	Carbonation factor
635		03/10/2003 5:47 AM	43.4 Q	Mean	0	0	10/10	8.5 Q	Curve EU	Cube 150mm (100%)	1.00

Q-Values diagram [measurement order]

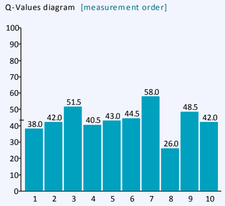

Q-Values

38.0
42.0
51.5
40.5
43.0
44.5
58.0
26.0
48.5
42.0

Statistics

Measurements	N = 10
Invalid measurements	Ni = 0 (0%)
Mean value	f = 43.4 Q
Standard deviation	s = 8.5 Q

Settings

Averaging mode	Mean
Conversion curve	Curve EU
Form factor	Cube 150mm (100%)
Carbonation factor	1.00
Unit	Q
Serial number	SH01-006-0084
Spring type	SilverSchmidt N

Comment

[Add]

001c (2)

Impact counter	Name	Date & Time	Mean value	Averaging mode	Upper outliers	Lower outliers	Valid/Total	Std dev.	Conv. curve	Form factor	Carbonation factor
655		03/10/2003 5:51 AM	39.5 Q	Mean	0	0	10/10	7.5 Q	Curve EU	Cube 150mm (100%)	1.00

Q-Values diagram [measurement order]

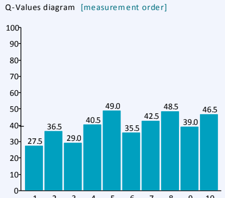

Q-Values

27.5
36.5
29.0
40.5
49.0
35.5
42.5
48.5
39.0
46.5

Statistics

Measurements	N = 10
Invalid measurements	Ni = 0 (0%)
Mean value	f = 39.5 Q
Standard deviation	s = 7.5 Q

Settings

Averaging mode	Mean
Conversion curve	Curve EU
Form factor	Cube 150mm (100%)
Carbonation factor	1.00
Unit	Q
Serial number	SH01-006-0084
Spring type	SilverSchmidt N

Comment

[Add]

002a

Impact counter	Name	Date & Time	Mean value	Averaging mode	Upper outliers	Lower outliers	Valid/Total	Std dev.	Conv. curve	Form factor	Carbonation factor
676		03/10/2003 9:11 AM	47.0 Q	Mean	0	0	10/10	9.5 Q	Curve EU	Cube 150mm (100%)	1.00

Q-Values diagram [measurement order]

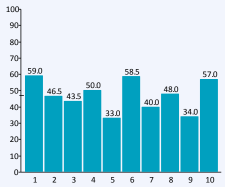

Q-Values
59.0
46.5
43.5
50.0
33.0
58.5
40.0
48.0
34.0
57.0

Statistics

Measurements	N = 10
Invalid measurements	Ni = 0 (0%)
Mean value	f = 47.0 Q
Standard deviation	s = 9.5 Q

Settings

Averaging mode	Mean
Conversion curve	Curve EU
Form factor	Cube 150mm (100%)
Carbonation factor	1.00
Unit	Q
Serial number	SH01-006-0084
Spring type	SilverSchmidt N

Comment
[Add]

002b

Impact counter	Name	Date & Time	Mean value	Averaging mode	Upper outliers	Lower outliers	Valid/Total	Std dev.	Conv. curve	Form factor	Carbonation factor
686		03/10/2003 9:12 AM	53.2 Q	Mean	0	0	10/10	14.4 Q	Curve EU	Cube 150mm (100%)	1.00

Q-Values diagram [measurement order]

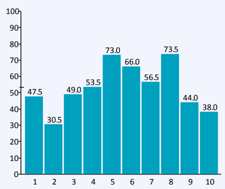

Q-Values
47.5
30.5
49.0
53.5
73.0
66.0
56.5
73.5
44.0
38.0

Statistics

Measurements	N = 10
Invalid measurements	Ni = 0 (0%)
Mean value	f = 53.2 Q
Standard deviation	s = 14.4 Q

Settings

Averaging mode	Mean
Conversion curve	Curve EU
Form factor	Cube 150mm (100%)
Carbonation factor	1.00
Unit	Q
Serial number	SH01-006-0084
Spring type	SilverSchmidt N

Comment
[Add]

002c

Impact counter	Name	Date & Time	Mean value	Averaging mode	Upper outliers	Lower outliers	Valid/Total	Std dev.	Conv. curve	Form factor	Carbonation factor
722		03/10/2003 9:17 AM	58.7 Q	Mean	0	0	10/10	8.3 Q	Curve EU	Cube 150mm (100%)	1.00

Q-Values diagram [measurement order]

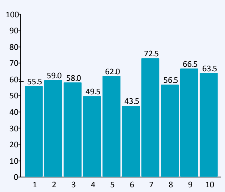

Q-Values
55.5
59.0
58.0
49.5
62.0
43.5
72.5
56.5
66.5
63.5

Statistics

Measurements	N = 10
Invalid measurements	Ni = 0 (0%)
Mean value	f = 58.7 Q
Standard deviation	s = 8.3 Q

Settings

Averaging mode	Mean
Conversion curve	Curve EU
Form factor	Cube 150mm (100%)
Carbonation factor	1.00
Unit	Q
Serial number	SH01-006-0084
Spring type	SilverSchmidt N

Comment
[Add]

002d

Impact counter	Name	Date & Time	Mean value	Averaging mode	Upper outliers	Lower outliers	Valid/Total	Std dev.	Conv. curve	Form factor	Carbonation factor
732		03/10/2003 9:18 AM	61.7 Q	Mean	0	0	10/10	7.4 Q	Curve EU	Cube 150mm (100%)	1.00

Q-Values diagram [measurement order]

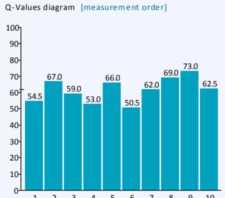

Q-Values
54.5
67.0
59.0
53.0
66.0
50.5
62.0
69.0
73.0
62.5

Statistics

Measurements	N = 10
Invalid measurements	Ni = 0 (0%)
Mean value	f = 61.7 Q
Standard deviation	s = 7.4 Q

Settings

Averaging mode	Mean
Conversion curve	Curve EU
Form factor	Cube 150mm (100%)
Carbonation factor	1.00
Unit	Q
Serial number	SH01-006-0084
Spring type	SilverSchmidt N

Comment
[Add]

002e

Impact counter	Name	Date & Time	Mean value	Averaging mode	Upper outliers	Lower outliers	Valid/Total	Std dev.	Conv. curve	Form factor	Carbonation factor
752		03/10/2003 9:20 AM	49.0 Q	Mean	0	0	10/10	10.4 Q	Curve EU	Cube 150mm (100%)	1.00

Q-Values diagram [measurement order]

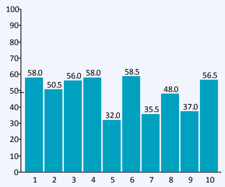

Q-Values
58.0
50.5
56.0
58.0
32.0
58.5
35.5
48.0
37.0
56.5

Statistics

Measurements	N = 10
Invalid measurements	Ni= 0 (0%)
Mean value	f = 49.0 Q
Standard deviation	s = 10.4 Q

Settings

Averaging mode	Mean
Conversion curve	Curve EU
Form factor	Cube 150mm (100%)
Carbonation factor	1.00
Unit	Q
Serial number	SH01-006-0084
Spring type	SilverSchmidt N

Comment
[Add]

002f (1)

Impact counter	Name	Date & Time	Mean value	Averaging mode	Upper outliers	Lower outliers	Valid/Total	Std dev.	Conv. curve	Form factor	Carbonation factor
762		03/10/2003 9:24 AM	46.6 Q	Mean	0	0	10/10	9.8 Q	Curve EU	Cube 150mm (100%)	1.00

Q-Values diagram [measurement order]

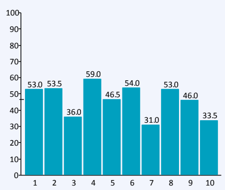

Q-Values
53.0
53.5
36.0
59.0
46.5
54.0
31.0
53.0
46.0
33.5

Statistics

Measurements	N = 10
Invalid measurements	Ni= 0 (0%)
Mean value	f = 46.6 Q
Standard deviation	s = 9.8 Q

Settings

Averaging mode	Mean
Conversion curve	Curve EU
Form factor	Cube 150mm (100%)
Carbonation factor	1.00
Unit	Q
Serial number	SH01-006-0084
Spring type	SilverSchmidt N

Comment
[Add]

002f (2)

Impact counter	Name	Date & Time	Mean value	Averaging mode	Upper outliers	Lower outliers	Valid/Total	Std dev.	Conv. curve	Form factor	Carbonation factor
772		03/10/2003 9:25 AM	47.4 Q	Mean	0	0	10/10	6.3 Q	Curve EU	Cube 150mm (100%)	1.00

Q-Values diagram [measurement order]

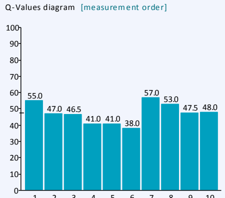

Q-Values
55.0
47.0
46.5
41.0
41.0
38.0
57.0
53.0
47.5
48.0

Statistics

Measurements	N = 10
Invalid measurements	Ni= 0 (0%)
Mean value	f = 47.4 Q
Standard deviation	s = 6.3 Q

Settings

Averaging mode	Mean
Conversion curve	Curve EU
Form factor	Cube 150mm (100%)
Carbonation factor	1.00
Unit	Q
Serial number	SH01-006-0084
Spring type	SilverSchmidt N

Comment
[Add]

002f (3)

Impact counter	Name	Date & Time	Mean value	Averaging mode	Upper outliers	Lower outliers	Valid/Total	Std dev.	Conv. curve	Form factor	Carbonation factor
782		03/10/2003 9:26 AM	55.3 Q	Mean	0	0	10/10	7.9 Q	Curve EU	Cube 150mm (100%)	1.00

Q-Values diagram [measurement order]

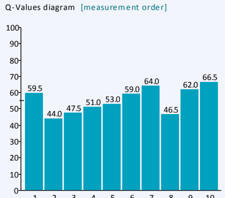

Q-Values
59.5
44.0
47.5
51.0
53.0
59.0
64.0
46.5
62.0
66.5

Statistics

Measurements	N = 10
Invalid measurements	Ni= 0 (0%)
Mean value	f = 55.3 Q
Standard deviation	s = 7.9 Q

Settings

Averaging mode	Mean
Conversion curve	Curve EU
Form factor	Cube 150mm (100%)
Carbonation factor	1.00
Unit	Q
Serial number	SH01-006-0084
Spring type	SilverSchmidt N

Comment
[Add]

002f (4)

Impact counter	Name	Date & Time	Mean value	Averaging mode	Upper outliers	Lower outliers	Valid/Total	Std dev.	Conv. curve	Form factor	Carbonation factor
792		03/10/2003 9:28 AM	51.5 Q	Mean	0	0	10/10	7.4 Q	Curve EU	Cube 150mm (100%)	1.00

Q-Values diagram [measurement order]

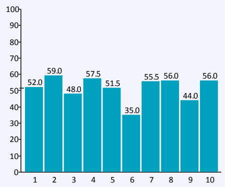

Q-Values
52.0
59.0
48.0
57.5
51.5
35.0
55.5
56.0
44.0
56.0

Statistics

Measurements	N = 10
Invalid measurements	Ni = 0 (0%)
Mean value	f = 51.5 Q
Standard deviation	s = 7.4 Q

Settings

Averaging mode	Mean
Conversion curve	Curve EU
Form factor	Cube 150mm (100%)
Carbonation factor	1.00
Unit	Q
Serial number	SH01-006-0084
Spring type	SilverSchmidt N

Comment
[Add]

003a

Impact counter	Name	Date & Time	Mean value	Averaging mode	Upper outliers	Lower outliers	Valid/Total	Std dev.	Conv. curve	Form factor	Carbonation factor
802		03/10/2003 10:11 AM	70.8 Q	Mean	0	0	10/10	9.9 Q	Curve EU	Cube 150mm (100%)	1.00

Q-Values diagram [measurement order]

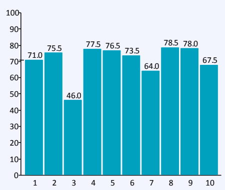

Q-Values
71.0
75.5
46.0
77.5
76.5
73.5
64.0
78.5
78.0
67.5

Statistics

Measurements	N = 10
Invalid measurements	Ni = 0 (0%)
Mean value	f = 70.8 Q
Standard deviation	s = 9.9 Q

Settings

Averaging mode	Mean
Conversion curve	Curve EU
Form factor	Cube 150mm (100%)
Carbonation factor	1.00
Unit	Q
Serial number	SH01-006-0084
Spring type	SilverSchmidt N

Comment
[Add]

004a

Impact counter	Name	Date & Time	Mean value	Averaging mode	Upper outliers	Lower outliers	Valid/Total	Std dev.	Conv. curve	Form factor	Carbonation factor
1279		03/20/2003 10:32 AM	40.2 Q	Mean	0	0	10/10	4.7 Q	Curve EU	Cube 150mm (100%)	1.00

Q-Values diagram [measurement order]

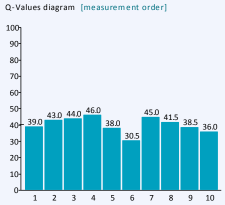

Q-Values
39.0
43.0
44.0
46.0
38.0
30.5
45.0
41.5
38.5
36.0

Statistics

Measurements	N = 10
Invalid measurements	Ni = 0 (0%)
Mean value	f = 40.2 Q
Standard deviation	s = 4.7 Q

Settings

Averaging mode	Mean
Conversion curve	Curve EU
Form factor	Cube 150mm (100%)
Carbonation factor	1.00
Unit	Q
Serial number	SH01-006-0084
Spring type	SilverSchmidt N

Comment
[Add]

004b

Impact counter	Name	Date & Time	Mean value	Averaging mode	Upper outliers	Lower outliers	Valid/Total	Std dev.	Conv. curve	Form factor	Carbonation factor
924		03/13/2003 8:23 AM	56.5 Q	Mean	0	0	10/10	11.4 Q	Curve EU	Cube 150mm (100%)	1.00

Q-Values diagram [measurement order]

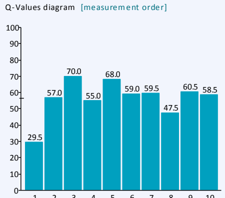

Q-Values
29.5
57.0
70.0
55.0
68.0
59.0
59.5
47.5
60.5
58.5

Statistics

Measurements	N = 10
Invalid measurements	Ni = 0 (0%)
Mean value	f = 56.5 Q
Standard deviation	s = 11.4 Q

Settings

Averaging mode	Mean
Conversion curve	Curve EU
Form factor	Cube 150mm (100%)
Carbonation factor	1.00
Unit	Q
Serial number	SH01-006-0084
Spring type	SilverSchmidt N

Comment
[Add]

004d

Impact counter	Name	Date & Time	Mean value	Averaging mode	Upper outliers	Lower outliers	Valid/Total	Std dev.	Conv. curve	Form factor	Carbonation factor
1301		03/20/2003 10:35 AM	51.5 Q	Mean	0	0	10/10	7.4 Q	Curve EU	Cube 150mm (100%)	1.00

Q-Values diagram [measurement order]

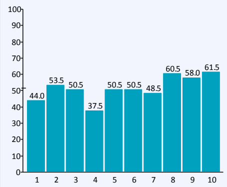

Q-Values
44.0
53.5
50.5
37.5
50.5
50.5
48.5
60.5
58.0
61.5

Statistics

Measurements	N = 10
Invalid measurements	Ni = 0 (0%)
Mean value	f = 51.5 Q
Standard deviation	s = 7.4 Q

Settings

Averaging mode	Mean
Conversion curve	Curve EU
Form factor	Cube 150mm (100%)
Carbonation factor	1.00
Unit	Q
Serial number	SH01-006-0084
Spring type	SilverSchmidt N

Comment
[Add]

004d (2)

Impact counter	Name	Date & Time	Mean value	Averaging mode	Upper outliers	Lower outliers	Valid/Total	Std dev.	Conv. curve	Form factor	Carbonation factor
645		03/10/2003 5:49 AM	51.1 Q	Mean	0	0	10/10	8.3 Q	Curve EU	Cube 150mm (100%)	1.00

Q-Values diagram [measurement order]

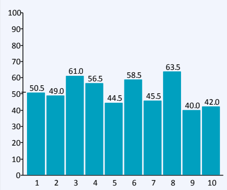

Q-Values
50.5
49.0
61.0
56.5
44.5
58.5
45.5
63.5
40.0
42.0

Statistics

Measurements	N = 10
Invalid measurements	Ni = 0 (0%)
Mean value	f = 51.1 Q
Standard deviation	s = 8.3 Q

Settings

Averaging mode	Mean
Conversion curve	Curve EU
Form factor	Cube 150mm (100%)
Carbonation factor	1.00
Unit	Q
Serial number	SH01-006-0084
Spring type	SilverSchmidt N

Comment
[Add]

004e

Impact counter	Name	Date & Time	Mean value	Averaging mode	Upper outliers	Lower outliers	Valid/Total	Std dev.	Conv. curve	Form factor	Carbonation factor
844		03/12/2003 7:57 AM	28.4 Q	Mean	0	0	10/10	8.8 Q	Curve EU	Cube 150mm (100%)	1.00

Q-Values diagram [measurement order]

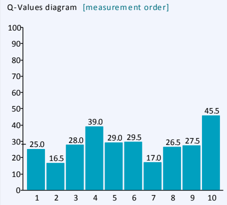

Q-Values
25.0
16.5
28.0
39.0
29.0
29.5
17.0
26.5
27.5
45.5

Statistics

Measurements	N = 10
Invalid measurements	Ni = 0 (0%)
Mean value	f = 28.4 Q
Standard deviation	s = 8.8 Q

Settings

Averaging mode	Mean
Conversion curve	Curve EU
Form factor	Cube 150mm (100%)
Carbonation factor	1.00
Unit	Q
Serial number	SH01-006-0084
Spring type	SilverSchmidt N

Comment
[Add]

006a

Impact counter	Name	Date & Time	Mean value	Averaging mode	Upper outliers	Lower outliers	Valid/Total	Std dev.	Conv. curve	Form factor	Carbonation factor
812		03/11/2003 11:38 AM	12.0 Q	Mean	0	0	10/10	2.2 Q	Curve EU	Cube 150mm (100%)	1.00

Q-Values diagram [measurement order]

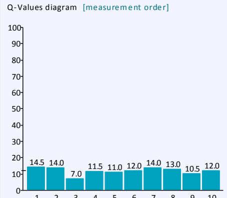

Q-Values
14.5
14.0
7.0
11.5
11.0
12.0
14.0
13.0
10.5
12.0

Statistics

Measurements	N = 10
Invalid measurements	Ni = 0 (0%)
Mean value	f = 12.0 Q
Standard deviation	s = 2.2 Q

Settings

Averaging mode	Mean
Conversion curve	Curve EU
Form factor	Cube 150mm (100%)
Carbonation factor	1.00
Unit	Q
Serial number	SH01-006-0084
Spring type	SilverSchmidt N

Comment
[Add]

006b

Impact counter	Name	Date & Time	Mean value	Averaging mode	Upper outliers	Lower outliers	Valid/Total	Std dev.	Conv. curve	Form factor	Carbonation factor
822		03/11/2003 12:04 PM	55.5 Q	Mean	0	0	10/10	5.4 Q	Curve EU	Cube 150mm (100%)	1.00

Q-Values diagram [measurement order]

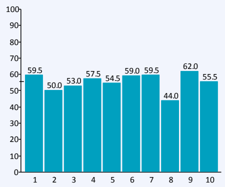

Q-Values
59.5
50.0
53.0
57.5
54.5
59.0
59.5
44.0
62.0
55.5

Statistics

Measurements	N = 10
Invalid measurements	Ni = 0 (0%)
Mean value	f = 55.5 Q
Standard deviation	s = 5.4 Q

Settings

Averaging mode	Mean
Conversion curve	Curve EU
Form factor	Cube 150mm (100%)
Carbonation factor	1.00
Unit	Q
Serial number	SH01-006-0084
Spring type	SilverSchmidt N

Comment
[Add]

006c

Impact counter	Name	Date & Time	Mean value	Averaging mode	Upper outliers	Lower outliers	Valid/Total	Std dev.	Conv. curve	Form factor	Carbonation factor
854		03/12/2003 7:58 AM	31.8 Q	Mean	0	0	10/10	12.0 Q	Curve EU	Cube 150mm (100%)	1.00

Q-Values diagram [measurement order]

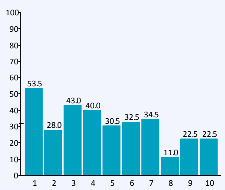

Q-Values
53.5
28.0
43.0
40.0
30.5
32.5
34.5
11.0
22.5
22.5

Statistics

Measurements	N = 10
Invalid measurements	Ni = 0 (0%)
Mean value	f = 31.8 Q
Standard deviation	s = 12.0 Q

Settings

Averaging mode	Mean
Conversion curve	Curve EU
Form factor	Cube 150mm (100%)
Carbonation factor	1.00
Unit	Q
Serial number	SH01-006-0084
Spring type	SilverSchmidt N

Comment
[Add]

006c (2)

Impact counter	Name	Date & Time	Mean value	Averaging mode	Upper outliers	Lower outliers	Valid/Total	Std dev.	Conv. curve	Form factor	Carbonation factor
864		03/12/2003 7:59 AM	38.5 Q	Mean	0	0	10/10	8.9 Q	Curve EU	Cube 150mm (100%)	1.00

Q-Values diagram [measurement order]

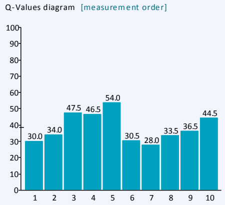

Q-Values
30.0
34.0
47.5
46.5
54.0
30.5
28.0
33.5
36.5
44.5

Statistics

Measurements	N = 10
Invalid measurements	Ni = 0 (0%)
Mean value	f = 38.5 Q
Standard deviation	s = 8.9 Q

Settings

Averaging mode	Mean
Conversion curve	Curve EU
Form factor	Cube 150mm (100%)
Carbonation factor	1.00
Unit	Q
Serial number	SH01-006-0084
Spring type	SilverSchmidt N

Comment
[Add]

006c (3)

Impact counter	Name	Date & Time	Mean value	Averaging mode	Upper outliers	Lower outliers	Valid/Total	Std dev.	Conv. curve	Form factor	Carbonation factor
874		03/12/2003 8:00 AM	18.3 Q	Mean	0	0	10/10	6.3 Q	Curve EU	Cube 150mm (100%)	1.00

Q-Values diagram [measurement order]

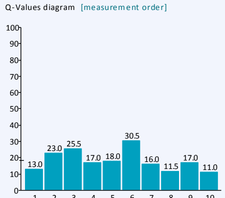

Q-Values
13.0
23.0
25.5
17.0
18.0
30.5
16.0
11.5
17.0
11.0

Statistics

Measurements	N = 10
Invalid measurements	Ni = 0 (0%)
Mean value	f = 18.3 Q
Standard deviation	s = 6.3 Q

Settings

Averaging mode	Mean
Conversion curve	Curve EU
Form factor	Cube 150mm (100%)
Carbonation factor	1.00
Unit	Q
Serial number	SH01-006-0084
Spring type	SilverSchmidt N

Comment
[Add]

006c (4)

Impact counter	Name	Date & Time	Mean value	Averaging mode	Upper outliers	Lower outliers	Valid/Total	Std dev.	Conv. curve	Form factor	Carbonation factor
884		03/12/2003 8:01 AM	42.0 Q	Mean	0	0	10/10	9.5 Q	Curve EU	Cube 150mm (100%)	1.00

Q-Values diagram [measurement order]

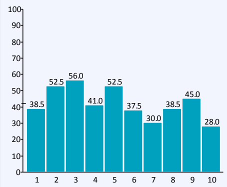

Q-Values
38.5
52.5
56.0
41.0
52.5
37.5
30.0
38.5
45.0
28.0

Statistics

Measurements N = 10
Invalid measurements Ni = 0 (0%)
Mean value f = 42.0 Q
Standard deviation s = 9.5 Q

Settings

Averaging mode Mean
Conversion curve Curve EU
Form factor Cube 150mm (100%)
Carbonation factor 1.00
Unit Q
Serial number SH01-006-0084
Spring type SilverSchmidt N

Comment
[Add]

006d

Impact counter	Name	Date & Time	Mean value	Averaging mode	Upper outliers	Lower outliers	Valid/Total	Std dev.	Conv. curve	Form factor	Carbonation factor
834		03/12/2003 7:35 AM	63.6 Q	Mean	0	0	10/10	5.7 Q	Curve EU	Cube 150mm (100%)	1.00

Q-Values diagram [measurement order]

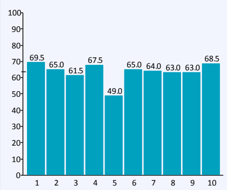

Q-Values
69.5
65.0
61.5
67.5
49.0
65.0
64.0
63.0
63.0
68.5

Statistics

Measurements N = 10
Invalid measurements Ni = 0 (0%)
Mean value f = 63.6 Q
Standard deviation s = 5.7 Q

Settings

Averaging mode Mean
Conversion curve Curve EU
Form factor Cube 150mm (100%)
Carbonation factor 1.00
Unit Q
Serial number SH01-006-0084
Spring type SilverSchmidt N

Comment
[Add]

007a

Impact counter	Name	Date & Time	Mean value	Averaging mode	Upper outliers	Lower outliers	Valid/Total	Std dev.	Conv. curve	Form factor	Carbonation factor
894		03/12/2003 9:56 AM	12.5 Q	Mean	0	0	10/10	2.8 Q	Curve EU	Cube 150mm (100%)	1.00

Q-Values diagram [measurement order]

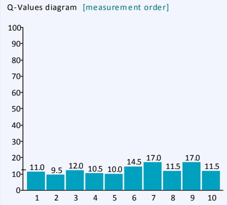

Q-Values
11.0
9.5
12.0
10.5
10.0
14.5
17.0
11.5
17.0
11.5

Statistics

Measurements N = 10
Invalid measurements Ni = 0 (0%)
Mean value f = 12.5 Q
Standard deviation s = 2.8 Q

Settings

Averaging mode Mean
Conversion curve Curve EU
Form factor Cube 150mm (100%)
Carbonation factor 1.00
Unit Q
Serial number SH01-006-0084
Spring type SilverSchmidt N

Comment
[Add]

008a

Impact counter	Name	Date & Time	Mean value	Averaging mode	Upper outliers	Lower outliers	Valid/Total	Std dev.	Conv. curve	Form factor	Carbonation factor
955		03/13/2003 10:00 AM	54.7 Q	Mean	0	0	10/10	8.9 Q	Curve EU	Cube 150mm (100%)	1.00

Q-Values diagram [measurement order]

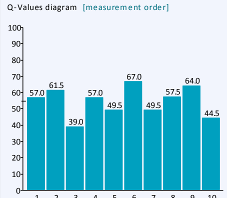

Q-Values
57.0
61.5
39.0
57.0
49.5
67.0
49.5
57.5
64.0
44.5

Statistics

Measurements N = 10
Invalid measurements Ni = 0 (0%)
Mean value f = 54.7 Q
Standard deviation s = 8.9 Q

Settings

Averaging mode Mean
Conversion curve Curve EU
Form factor Cube 150mm (100%)
Carbonation factor 1.00
Unit Q
Serial number SH01-006-0084
Spring type SilverSchmidt N

Comment
[Add]

008a (2)

Impact counter	Name	Date & Time	Mean value	Averaging mode	Upper outliers	Lower outliers	Valid/Total	Std dev.	Conv. curve	Form factor	Carbonation factor
967		03/13/2003 10:01 AM	54.4 Q	Mean	0	0	10/10	7.3 Q	Curve EU	Cube 150mm (100%)	1.00

Q-Values diagram [measurement order]

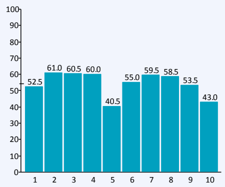

Q-Values
52.5
61.0
60.5
60.0
40.5
55.0
59.5
58.5
53.5
43.0

Statistics
Measurements N = 10
Invalid measurements Ni= 0 (0%)
Mean value f = 54.4 Q
Standard deviation s = 7.3 Q

Settings
Averaging mode Mean
Conversion curve Curve EU
Form factor Cube 150mm (100%)
Carbonation factor 1.00
Unit Q
Serial number SH01-006-0084
Spring type SilverSchmidt N

Comment
[Add]

008b

Impact counter	Name	Date & Time	Mean value	Averaging mode	Upper outliers	Lower outliers	Valid/Total	Std dev.	Conv. curve	Form factor	Carbonation factor
978		03/13/2003 10:16 AM	41.6 Q	Mean	0	0	10/10	18.0 Q	Curve EU	Cube 150mm (100%)	1.00

Q-Values diagram [measurement order]

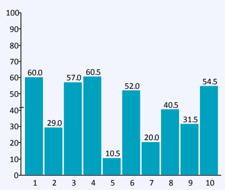

Q-Values
60.0
29.0
57.0
60.5
10.5
52.0
20.0
40.5
31.5
54.5

Statistics
Measurements N = 10
Invalid measurements Ni= 0 (0%)
Mean value f = 41.6 Q
Standard deviation s = 18.0 Q

Settings
Averaging mode Mean
Conversion curve Curve EU
Form factor Cube 150mm (100%)
Carbonation factor 1.00
Unit Q
Serial number SH01-006-0084
Spring type SilverSchmidt N

Comment
[Add]

008b (2)

Impact counter	Name	Date & Time	Mean value	Averaging mode	Upper outliers	Lower outliers	Valid/Total	Std dev.	Conv. curve	Form factor	Carbonation factor
988		03/13/2003 10:17 AM	36.7 Q	Mean	0	0	11/11	18.6 Q	Curve EU	Cube 150mm (100%)	1.00

Q-Values diagram [measurement order]

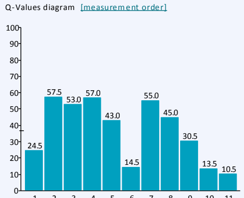

Q-Values
24.5
57.5
53.0
57.0
43.0
14.5
55.0
45.0
30.5
13.5
10.5

Statistics
Measurements N = 11
Invalid measurements Ni= 0 (0%)
Mean value f = 36.7 Q
Standard deviation s = 18.6 Q

Settings
Averaging mode Mean
Conversion curve Curve EU
Form factor Cube 150mm (100%)
Carbonation factor 1.00
Unit Q
Serial number SH01-006-0084
Spring type SilverSchmidt N

Comment
[Add]

008c

Impact counter	Name	Date & Time	Mean value	Averaging mode	Upper outliers	Lower outliers	Valid/Total	Std dev.	Conv. curve	Form factor	Carbonation factor
904		03/12/2003 10:47 AM	46.8 Q	Mean	0	0	10/10	8.1 Q	Curve EU	Cube 150mm (100%)	1.00

Q-Values diagram [measurement order]

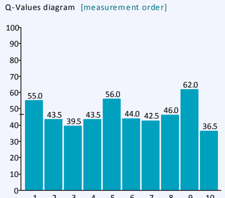

Q-Values
55.0
43.5
39.5
43.5
56.0
44.0
42.5
46.0
62.0
36.5

Statistics
Measurements N = 10
Invalid measurements Ni= 0 (0%)
Mean value f = 46.8 Q
Standard deviation s = 8.1 Q

Settings
Averaging mode Mean
Conversion curve Curve EU
Form factor Cube 150mm (100%)
Carbonation factor 1.00
Unit Q
Serial number SH01-006-0084
Spring type SilverSchmidt N

Comment
[Add]

010c

Impact counter	Name	Date & Time	Mean value	Averaging mode	Upper outliers	Lower outliers	Valid/Total	Std dev.	Conv. curve	Form factor	Carbonation factor
935		03/13/2003 8:27 AM	60.9 Q	Mean	0	0	10/10	6.4 Q	Curve EU	Cube 150mm (100%)	1.00

Q-Values diagram [measurement order]

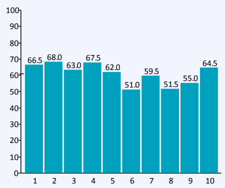

Q-Values
66.5
68.0
63.0
67.5
62.0
51.0
59.5
51.5
55.0
64.5

Statistics

Measurements	N = 10
Invalid measurements	Ni = 0 (0%)
Mean value	f = 60.9 Q
Standard deviation	s = 6.4 Q

Settings

Averaging mode	Mean
Conversion curve	Curve EU
Form factor	Cube 150mm (100%)
Carbonation factor	1.00
Unit	Q
Serial number	SH01-006-0084
Spring type	SilverSchmidt N

Comment
[Add]

010c (2)

Impact counter	Name	Date & Time	Mean value	Averaging mode	Upper outliers	Lower outliers	Valid/Total	Std dev.	Conv. curve	Form factor	Carbonation factor
945		03/13/2003 8:28 AM	57.8 Q	Mean	0	0	10/10	9.9 Q	Curve EU	Cube 150mm (100%)	1.00

Q-Values diagram [measurement order]

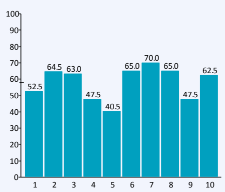

Q-Values
52.5
64.5
63.0
47.5
40.5
65.0
70.0
65.0
47.5
62.5

Statistics

Measurements	N = 10
Invalid measurements	Ni = 0 (0%)
Mean value	f = 57.8 Q
Standard deviation	s = 9.9 Q

Settings

Averaging mode	Mean
Conversion curve	Curve EU
Form factor	Cube 150mm (100%)
Carbonation factor	1.00
Unit	Q
Serial number	SH01-006-0084
Spring type	SilverSchmidt N

Comment
[Add]

010d

Impact counter	Name	Date & Time	Mean value	Averaging mode	Upper outliers	Lower outliers	Valid/Total	Std dev.	Conv. curve	Form factor	Carbonation factor
914		03/13/2003 8:19 AM	61.0 Q	Mean	0	0	10/10	3.6 Q	Curve EU	Cube 150mm (100%)	1.00

Q-Values diagram [measurement order]

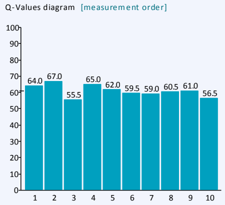

Q-Values
64.0
67.0
55.5
65.0
62.0
59.5
59.0
60.5
61.0
56.5

Statistics

Measurements	N = 10
Invalid measurements	Ni = 0 (0%)
Mean value	f = 61.0 Q
Standard deviation	s = 3.6 Q

Settings

Averaging mode	Mean
Conversion curve	Curve EU
Form factor	Cube 150mm (100%)
Carbonation factor	1.00
Unit	Q
Serial number	SH01-006-0084
Spring type	SilverSchmidt N

Comment
[Add]

011a

Impact counter	Name	Date & Time	Mean value	Averaging mode	Upper outliers	Lower outliers	Valid/Total	Std dev.	Conv. curve	Form factor	Carbonation factor
999		03/13/2003 11:14 AM	10.8 Q	Mean	0	0	10/10	1.7 Q	Curve EU	Cube 150mm (100%)	1.00

Q-Values diagram [measurement order]

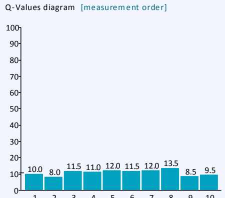

Q-Values
10.0
8.0
11.5
11.0
12.0
11.5
12.0
13.5
8.5
9.5

Statistics

Measurements	N = 10
Invalid measurements	Ni = 0 (0%)
Mean value	f = 10.8 Q
Standard deviation	s = 1.7 Q

Settings

Averaging mode	Mean
Conversion curve	Curve EU
Form factor	Cube 150mm (100%)
Carbonation factor	1.00
Unit	Q
Serial number	SH01-006-0084
Spring type	SilverSchmidt N

Comment
[Add]

012a

Impact counter	Name	Date & Time	Mean value	Averaging mode	Upper outliers	Lower outliers	Valid/Total	Std dev.	Conv. curve	Form factor	Carbonation factor
1009		03/14/2003 7:41 AM	55.9 Q	Mean	0	0	10/10	8.7 Q	Curve EU	Cube 150mm (100%)	1.00

Q-Values diagram [measurement order]

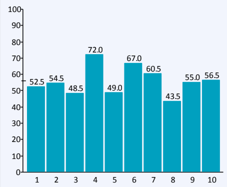

Q-Values
52.5
54.5
48.5
72.0
49.0
67.0
60.5
43.5
55.0
56.5

Statistics

Measurements	N = 10
Invalid measurements	Ni= 0 (0%)
Mean value	f = 55.9 Q
Standard deviation	s = 8.7 Q

Settings

Averaging mode	Mean
Conversion curve	Curve EU
Form factor	Cube 150mm (100%)
Carbonation factor	1.00
Unit	Q
Serial number	SH01-006-0084
Spring type	SilverSchmidt N

Comment
[Add]

012a (2)

Impact counter	Name	Date & Time	Mean value	Averaging mode	Upper outliers	Lower outliers	Valid/Total	Std dev.	Conv. curve	Form factor	Carbonation factor
1019		03/14/2003 7:42 AM	59.1 Q	Mean	0	0	10/10	8.9 Q	Curve EU	Cube 150mm (100%)	1.00

Q-Values diagram [measurement order]

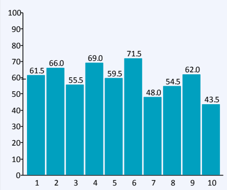

Q-Values
61.5
66.0
55.5
69.0
59.5
71.5
48.0
54.5
62.0
43.5

Statistics

Measurements	N = 10
Invalid measurements	Ni= 0 (0%)
Mean value	f = 59.1 Q
Standard deviation	s = 8.9 Q

Settings

Averaging mode	Mean
Conversion curve	Curve EU
Form factor	Cube 150mm (100%)
Carbonation factor	1.00
Unit	Q
Serial number	SH01-006-0084
Spring type	SilverSchmidt N

Comment
[Add]

012a (3)

Impact counter	Name	Date & Time	Mean value	Averaging mode	Upper outliers	Lower outliers	Valid/Total	Std dev.	Conv. curve	Form factor	Carbonation factor
1029		03/14/2003 7:45 AM	59.4 Q	Mean	0	0	10/10	9.5 Q	Curve EU	Cube 150mm (100%)	1.00

Q-Values diagram [measurement order]

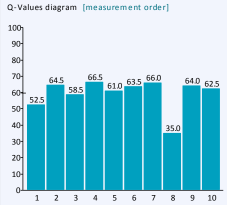

Q-Values
52.5
64.5
58.5
66.5
61.0
63.5
66.0
35.0
64.0
62.5

Statistics

Measurements	N = 10
Invalid measurements	Ni= 0 (0%)
Mean value	f = 59.4 Q
Standard deviation	s = 9.5 Q

Settings

Averaging mode	Mean
Conversion curve	Curve EU
Form factor	Cube 150mm (100%)
Carbonation factor	1.00
Unit	Q
Serial number	SH01-006-0084
Spring type	SilverSchmidt N

Comment
[Add]

012b

Impact counter	Name	Date & Time	Mean value	Averaging mode	Upper outliers	Lower outliers	Valid/Total	Std dev.	Conv. curve	Form factor	Carbonation factor
1226		03/14/2003 10:22 AM	54.6 Q	Mean	0	0	10/10	7.3 Q	Curve EU	Cube 150mm (100%)	1.00

Q-Values diagram [measurement order]

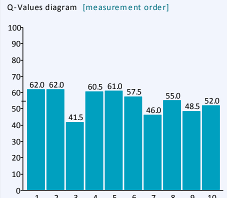

Q-Values
62.0
62.0
41.5
60.5
61.0
57.5
46.0
55.0
48.5
52.0

Statistics

Measurements	N = 10
Invalid measurements	Ni= 0 (0%)
Mean value	f = 54.6 Q
Standard deviation	s = 7.3 Q

Settings

Averaging mode	Mean
Conversion curve	Curve EU
Form factor	Cube 150mm (100%)
Carbonation factor	1.00
Unit	Q
Serial number	SH01-006-0084
Spring type	SilverSchmidt N

Comment
[Add]

013a

Impact counter	Name	Date & Time	Mean value	Averaging mode	Upper outliers	Lower outliers	Valid/Total	Std dev.	Conv. curve	Form factor	Carbonation factor
1214		03/14/2003 10:19 AM	56.3 Q	Mean	0	0	10/10	9.0 Q	Curve EU	Cube 150mm (100%)	1.00

Q-Values diagram [measurement order]

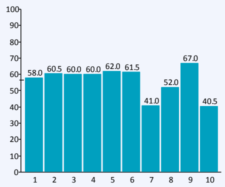

Q-Values
58.0
60.5
60.0
60.0
62.0
61.5
41.0
52.0
67.0
40.5

Statistics

Measurements	N = 10
Invalid measurements	Ni= 0 (0%)
Mean value	f = 56.3 Q
Standard deviation	s = 9.0 Q

Settings

Averaging mode	Mean
Conversion curve	Curve EU
Form factor	Cube 150mm (100%)
Carbonation factor	1.00
Unit	Q
Serial number	SH01-006-0084
Spring type	SilverSchmidt N

Comment
[Add]

013b

Impact counter	Name	Date & Time	Mean value	Averaging mode	Upper outliers	Lower outliers	Valid/Total	Std dev.	Conv. curve	Form factor	Carbonation factor
1188		03/14/2003 10:11 AM	25.3 Q	Mean	0	0	10/10	2.7 Q	Curve EU	Cube 150mm (100%)	1.00

Q-Values diagram [measurement order]

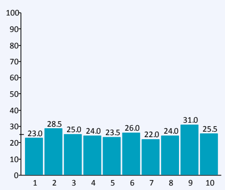

Q-Values
23.0
28.5
25.0
24.0
23.5
26.0
22.0
24.0
31.0
25.5

Statistics

Measurements	N = 10
Invalid measurements	Ni= 0 (0%)
Mean value	f = 25.3 Q
Standard deviation	s = 2.7 Q

Settings

Averaging mode	Mean
Conversion curve	Curve EU
Form factor	Cube 150mm (100%)
Carbonation factor	1.00
Unit	Q
Serial number	SH01-006-0084
Spring type	SilverSchmidt N

Comment
[Add]

013c

Impact counter	Name	Date & Time	Mean value	Averaging mode	Upper outliers	Lower outliers	Valid/Total	Std dev.	Conv. curve	Form factor	Carbonation factor
1178		03/14/2003 10:08 AM	47.4 Q	Mean	0	0	10/10	10.2 Q	Curve EU	Cube 150mm (100%)	1.00

Q-Values diagram [measurement order]

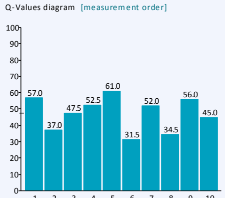

Q-Values
57.0
37.0
47.5
52.5
61.0
31.5
52.0
34.5
56.0
45.0

Statistics

Measurements	N = 10
Invalid measurements	Ni= 0 (0%)
Mean value	f = 47.4 Q
Standard deviation	s = 10.2 Q

Settings

Averaging mode	Mean
Conversion curve	Curve EU
Form factor	Cube 150mm (100%)
Carbonation factor	1.00
Unit	Q
Serial number	SH01-006-0084
Spring type	SilverSchmidt N

Comment
[Add]

013c (2)

Impact counter	Name	Date & Time	Mean value	Averaging mode	Upper outliers	Lower outliers	Valid/Total	Std dev.	Conv. curve	Form factor	Carbonation factor
1198		03/14/2003 10:18 AM	47.5 Q	Mean	0	0	10/10	10.5 Q	Curve EU	Cube 150mm (100%)	1.00

Q-Values diagram [measurement order]

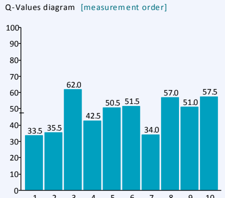

Q-Values
33.5
35.5
62.0
42.5
50.5
51.5
34.0
57.0
51.0
57.5

Statistics

Measurements	N = 10
Invalid measurements	Ni= 0 (0%)
Mean value	f = 47.5 Q
Standard deviation	s = 10.5 Q

Settings

Averaging mode	Mean
Conversion curve	Curve EU
Form factor	Cube 150mm (100%)
Carbonation factor	1.00
Unit	Q
Serial number	SH01-006-0084
Spring type	SilverSchmidt N

Comment
[Add]

014a

Impact counter	Name	Date & Time	Mean value	Averaging mode	Upper outliers	Lower outliers	Valid/Total	Std dev.	Conv. curve	Form factor	Carbonation factor
1237		03/16/2003 8:15 AM	16.0 Q	Mean	0	0	10/10	2.5 Q	Curve EU	Cube 150mm (100%)	1.00

Q-Values diagram [measurement order]

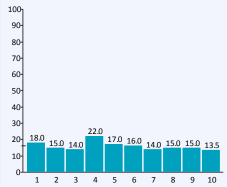

Q-Values
18.0
15.0
14.0
22.0
17.0
16.0
14.0
15.0
15.0
13.5

Statistics

Measurements N = 10
Invalid measurements Ni = 0 (0%)
Mean value f = 16.0 Q
Standard deviation s = 2.5 Q

Settings

Averaging mode Mean
Conversion curve Curve EU
Form factor Cube 150mm (100%)
Carbonation factor 1.00
Unit Q
Serial number SH01-006-0084
Spring type SilverSchmidt N

Comment
[Add]

014a (2)

Impact counter	Name	Date & Time	Mean value	Averaging mode	Upper outliers	Lower outliers	Valid/Total	Std dev.	Conv. curve	Form factor	Carbonation factor
1249		03/16/2003 8:19 AM	14.5 Q	Mean	0	0	10/10	2.7 Q	Curve EU	Cube 150mm (100%)	1.00

Q-Values diagram [measurement order]

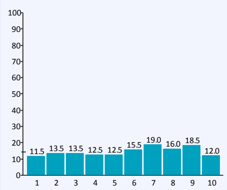

Q-Values
11.5
13.5
13.5
12.5
12.5
15.5
19.0
16.0
18.5
12.0

Statistics

Measurements N = 10
Invalid measurements Ni = 0 (0%)
Mean value f = 14.5 Q
Standard deviation s = 2.7 Q

Settings

Averaging mode Mean
Conversion curve Curve EU
Form factor Cube 150mm (100%)
Carbonation factor 1.00
Unit Q
Serial number SH01-006-0084
Spring type SilverSchmidt N

Comment
[Add]

016c

Impact counter	Name	Date & Time	Mean value	Averaging mode	Upper outliers	Lower outliers	Valid/Total	Std dev.	Conv. curve	Form factor	Carbonation factor
1259		03/17/2003 9:10 AM	25.4 Q	Mean	0	0	10/10	8.7 Q	Curve EU	Cube 150mm (100%)	1.00

Q-Values diagram [measurement order]

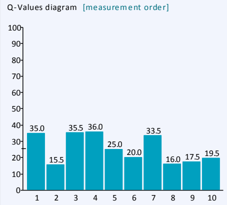

Q-Values
35.0
15.5
35.5
36.0
25.0
20.0
33.5
16.0
17.5
19.5

Statistics

Measurements N = 10
Invalid measurements Ni = 0 (0%)
Mean value f = 25.4 Q
Standard deviation s = 8.7 Q

Settings

Averaging mode Mean
Conversion curve Curve EU
Form factor Cube 150mm (100%)
Carbonation factor 1.00
Unit Q
Serial number SH01-006-0084
Spring type SilverSchmidt N

Comment
[Add]

016a (c)

Impact counter	Name	Date & Time	Mean value	Averaging mode	Upper outliers	Lower outliers	Valid/Total	Std dev.	Conv. curve	Form factor	Carbonation factor
1269		03/17/2003 9:11 AM	28.5 Q	Mean	0	0	10/10	9.6 Q	Curve EU	Cube 150mm (100%)	1.00

Q-Values diagram [measurement order]

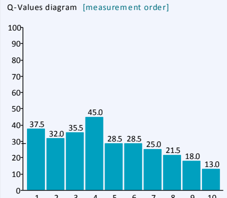

Q-Values
37.5
32.0
35.5
45.0
28.5
28.5
25.0
21.5
18.0
13.0

Statistics

Measurements N = 10
Invalid measurements Ni = 0 (0%)
Mean value f = 28.5 Q
Standard deviation s = 9.6 Q

Settings

Averaging mode Mean
Conversion curve Curve EU
Form factor Cube 150mm (100%)
Carbonation factor 1.00
Unit Q
Serial number SH01-006-0084
Spring type SilverSchmidt N

Comment
[Add]